Water transport in multilayer coatings

Document Version:
Publisher's PDF, also known as Version of Record (includes final page, issue and volume numbers)

Please check the document version of this publication:

• A submitted manuscript is the version of the article upon submission and before peer-review. There can be important differences between the submitted version and the official published version of record. People interested in the research are advised to contact the author for the final version of the publication, or visit the DOI to the publisher's website.
• The final author version and the galley proof are versions of the publication after peer review.
• The final published version features the final layout of the paper including the volume, issue and page numbers.

[Link to publication](#)

Water Transport in Multilayer Coatings

PROEFSCHRIFT

ter verkrijging van de graad van doctor aan de
Technische Universiteit Eindhoven, op gezag van de
rector magnificus, prof.dr.ir. C.J. van Duijn, voor een
commissie aangewezen door het College voor
Promoties in het openbaar te verdedigen
op maandag 5 maart 2012 om 16.00 uur

door

Viktor Baukh

geboren te Komsomolsk aan de Amoer, Rusland

Dit proefschrift is goedgekeurd door de promotoren:

prof.dr.ir. O.C.G. Adan
en
prof.dr. P.J. McDonald (University of Surrey)

Copromotor:
dr.ir. H.P. Huinink

to my beloved wife Gyulnara,
my mother and my grandparents.

Contents

1. Introduction

1.1 The context

Paints and coatings are a common way to protect and decorate objects. Various industries use coatings to enhance the properties of their products: building, automotive, marine, aerospace industries, etc. Annually the coating industry produces more than 30 billion kg of coatings and presently has a revenue of ca. 100 billion USD per year.

      History. Coatings have been used since ancient times, starting from decoration of caves by their dwellers. These ancient paints were composed of a variety of natural pigments dispersed in water and primitive binders. Ancient Greeks and Romans (600 BC-
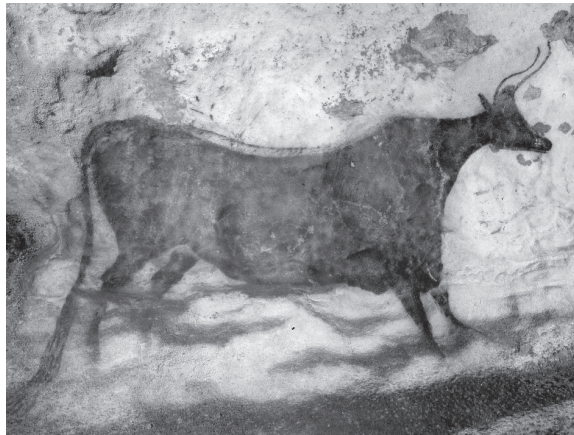
Fig. 1.1: A cave painting from Paleolithic period (ca. 17000 year before present), Lascaux, France.

400 AD) already knew that the preservation of objects is an additional function and and added value of paints. In the same period, varnishes were used for protective purposes in India, China and Japan. Between the 5th and 9th century AD, Indian and Chinese artists used oil based paints. Later on, the application of oil-based paints moved westward, gaining popularity during the Renaissance period and became the principal medium for artworks. The Renaissance is also the period, in which multilayer application of paints

was widely used. Many painters first applied a ground layer, and then other layers were added to create color and image. Finally, a varnish finish was frequently applied on top of the layers to provide protection.

Fig. 1.2: An oil painting 'The Tower of Babel' of Pieter Bruegel the Elder, 1563.

Deliberate Seek. Scientific discoveries had triggered a deliberate seeking of new pigments, paint formulations and color ranges since 18th century. Further, the increase of use of iron and steel for construction and engineering, initiated by the industrial revolution, resulted in a steep increase in demand for anti-corrosive coatings to prevent oxidation, rusting and corrosion. The 20th century introduced a wide range of substrates to be decorated and to be protected by coatings. It became common that the most of human made objects are decorated and protected by coatings.

Concerns. At the beginning of 20th century the first health and environmental concerns about paint were raised. Lead, cadmium and other metals used in pigments appeared to be hazardous to health and environment [1, 2, 3, 4, 5]. Next to metallic pigments, most solvents were identified as unhealthy and as perils to the environment. Health related problems refer to exposures of painters and end-users during solvent emission from drying coatings [5]. The environmental concern is related to the ability of volatile organic solvents to potentially contribute to photochemical smog [6, 7], ozone pollution [6, 8], ozone layer depletion and greenhouse effect [8]. Additionally, the flammability of the most solvents raises a safety concern about their use.

Safety, health and environmental concerns have initiated restrictive legislations in Europe and United States. At present, directives and regulations of The European Parliament and of The Council of The European Union [9, 10] restrict the use of hazardous pigments and volatile organic components. The necessity to meet these and similar restrictions was the main driver for the development of paint and coating technology in 20th

Fig. 1.3: Coatings and some their applications.

century.

While many pigments were replaced by less hazardous, many of these alternatives were used for dual purposes, e.g. for providing color and anti-corrosive properties. The reduction of solvents in coating compositions triggered the development of a variety of new coating systems: high solid coatings, powder coatings, radiation cured and water-borne coatings [11]. Each of these new technologies has its pros and cons and their development is still in progress.

Present. Presently, coatings are required to provide a wide range of added properties to objects, such as opacity, color, gloss, smoothness, adhesion, specific mechanical properties, chemical resistance, corrosion protection and durability. In addition, legislative demands have to be met. To meet all these requirements, multilayer application of coatings is frequently used, where each layer is designed to provide a specific functionality to a desired film performance. As a result, present coatings are complex systems, composed of several layers with different compositions and functionalities. An example of such system is an automotive coating (Figure 1.4), where the primer provides corrosion protection and adhesion, the filler removes surface irregularities of the substrate, the base coat gives color and the top coat provides a glossy appearance and protection against the environment.

Sustainable coating performance refers to a long term functionality in terms of protection and delivering the desired aesthetic appearance. Understanding the factors that contribute to performance failure is critical for coating development. A number of factors are recognized to be responsible for coating failure, like mechanical damage, UV radiation, thermal stresses, moisture and exposure to chemicals. Mechanical damage dis-
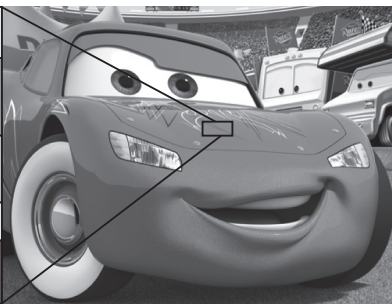
Fig. 1.4: Schematic picture of a typical structure of an automotive paint, as an example
of multilayer coatings. The primer usually provides adhesion and the filler hides
irregularities of the substrate. The base coat delivers color, whereas the top coat
serves as a barrier layer, protecting the system from the environment. The typical
thicknesses of the layers are indicated in the figure.

rupts the integrity of the coating. UV radiation causes photodegradation of a coating and
thermal stresses promote physical ageing. Exposure of paint to moisture and chemicals
is a common reason for failure of the coating. The penetration of moisture is known to

Fig. 1.5: Blisters under coatings as a typical damage by water.

promote deterioration of coatings and their substrates. Water can cause blister forma-
tion, freeze-thaw damage and hygroscopic stresses. Furthermore, water may act as an
electrolyte, promoting corrosion of metal substrates. Additionally, coatings can appear in
contact with various liquids, such as cleaning fluid, fuels, de-icing fluids and hydraulic
liquids. Frequently these substances contain chemicals, which may cause degradation of

a coating.

   Understanding the penetration of moisture and organic solvents into coatings is essential for further development of coating technology in terms of coating resistance to penetrants. Transport in single layer coatings is addressed in numerous studies, e.g. reviewed in [12, 13, 14]. However, only a few published studies address water transport in multilayer coatings [15, 16, 17, 18, 19, 20].

   Questions. There are many open questions about water transport in multilayer coatings, which have to be answered for profound understanding of the process of deterioration. How does water redistribute inside a multilayer coating? What is the state of water and its mobility in layers and how does this influence water transport? Are there interactions between layers, which affect the water transport? How does temperature affect the kinetics? What are the mechanisms of multilayer coating failures due to water uptake? How does the composition of the layers affect water transport? How do such systems respond to humidity and temperature fluctuations? How does lateral redistribution in the layers influence the transport?

1.2   Goals and Outline

This thesis presents the results of a study that aimed to understand water transport in multilayer coatings. This investigation was performed in two ways: experimentally with high resolution NMR imaging, combined with relaxometry and theoretically with an introduction and verification of a model for water transport.

   The thesis starts with a concise overview of knowledge about water in coatings in Chapter 2 and a description of NMR principles in Chapter 3. The results of the study are presented in Chapters 4-8. Chapter 9 summarizes the main conclusions and outlines follow-up.

   The key Chapters 4 to 8 are outlined as follows.

   First, water uptake in two-layered coatings, consisting of hydrophilic base coats and hydrophobic top coats, is studied with high resolution NMR imaging in Chapter 4. The objective of this chapter is to quantify water in the coating during the uptake, to estimate the sample swelling and to understand how water redistribution in the layers limits the rate of water transport.

   Further, the study aims to evaluate water-polymer interactions in the polymer matrix of the base coats. This is done by assessing with relaxation analysis of the NMR signal of the mobility of water and its interplay with the polymer phases in the base coat in Chapter 5.

   The next goal of the study is to find an exact relationship between the water transport kinetics in base coat/top coat systems and the layer properties. This is done by introducing and verifying a theoretical model for water transport in Chapter 6.

   In addition, Chapter 7 uses this theoretical model to understand how the water

content of the base coat/top coat systems respond to humidity fluctuations.

Finally, Chapter 8 aims to understand the penetration of plasticizer into a highly crosslinked top coat. This is done by imaging plasticizer profiles in the coating during uptake with high resolution NMR imaging and analysis of the penetration kinetics.

2. Water in Organic Coatings

2.1   Introduction

Penetration of water is an important process for the performance of organic coatings, since water can promote degradation of a coating and the substrate and can be a reason for failure of the decorative or protective function of the coating. Understanding water transport in multilayer coatings requires an insight in of how water is present and diffuses in individual layers.

Individual layers of multilayer organic coatings consist mostly of a polymeric binder, fillers, pigments and various additives. Since pigments and fillers are usually impermeable or insoluble materials, the transport of water mainly takes place through polymeric binder. Thus, this requires understanding of how water is present and migrates in polymeric materials.

The goal of this chapter is to give a concise overview of the state of the art knowledge on sorption and transport in polymeric coatings. First, equilibrium sorption in polymeric materials is discussed. Second, the kinetics of water transport is addressed. Finally, the chapter concludes with a brief overview of published studies about water in multilayer coatings.

2.2   Equilibrium Sorption in Coatings

The aim of this section is to give an overview of the state of the art of equilibrium sorption in polymeric materials. It addresses typical sorption isotherms of polymers and discusses the physical backgrounds.

The leading classification of equilibrium sorption isotherms, developed by Brunauer, Emmett and Teller [21] for porous materials, was adopted for moisture sorption in polymers by Barrie [22]. The commonly observed isotherms for polymers are linear isotherms, Type II and Type III, according to the BET classification (Figure 2.1). Linear isotherms are usually observed for hydrophobic polymers. Type II isotherms are usually observed for hydrophilic polymers [23, 24, 25, 26, 27], whereas Type III isotherms are typical for less hydrophilic polymers [23, 28, 29].

Generally, the shape of the isotherm reflects how water is present in the polymer matrix. In polymers water may be present as dispersed and isolated molecules, as
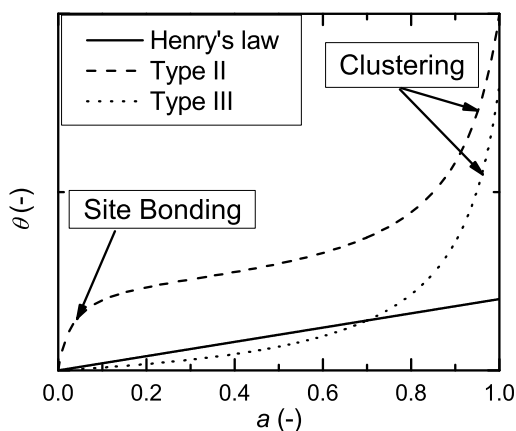
Fig. 2.1: Sorption isotherms, typically observed for polymers. The linear isotherm, de-
scribed by Henry's law is typical for hydrophobic polymers. Type II and Type
III isotherms (according to the BET classification [21]) are usually observed for
hydrophilic and less hydrophilic polymers, respectively. The initial increase in
the Type II isotherm is due to strong bonding of water to the hydrophilic sites in
the polymer. The steep increase in the slope of Type II and Type III isotherms at
high water activities is usually attributed to clustering of the penetrant.

molecules that are bonded to hydrophilic sites, or as clusters.

When a hydrophobic polymer is considered, only low concentrations of water in
a polymer are possible. Therefore, water is diluted and is present as single molecules,
which are dispersed in the polymer matrix. This means that interactions between water
molecules are negligible. In this case the water in the polymer behaves as an ideal system
and Henry's law holds, resulting in a linear sorption isotherm (Figure 2.1).

In case the polymer has a number of hydrophilic sites, such as polar groups, water
bind to these sites. In this case the sorption isotherm increases at low activities. With an
increase of the water activity, the water molecules occupy the sites, excluding them for
subsequently absorbed molecules. As a result, the sorption isotherm has a plateau region,
which is typical for Type II isotherms at low water activities (Figure 2.1). The Type II
isotherm at low activities can be described by localized sorption models of Brunauer,
Teller and Emmett (BET) [21] and of Guggenheim, Anderson and de Boer (GAB) [14,
22].

At higher water activities water is attracted by already absorbed water molecules,
which become sorption sites themselves. This results in absorption of new molecules,
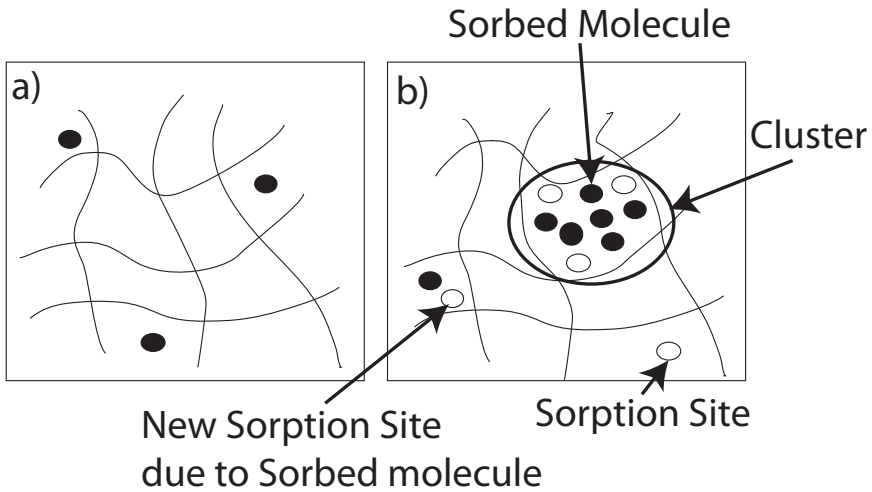
Fig. 2.2: Presence of absorbed molecules in polymer matrix of hydrophobic polymers (a), when penetrant concentrations are low and in hydrophilic polymers (b). The solid circles denote penetrant molecules and open circles are hydrophilic sorption sites in polymer. The sorbed molecules may attract the subsequent penetrant molecules, thus creating new sorption sites. This may result in cluster formation.

which subsequently become attractors for new water molecules too. As a result, clusters of water are formed and the isotherm shows a steep increase at high water activities. This behavior is observed in Type II and Type III isotherms at high water activities (Figure 2.1).

Clustering of water can be described by dissolution models, modified by Perrin et al. [30] by taking into account the difference between water-polymer and water-water interactions. This model has succeeded to describe some Type III isotherms for entire activity range. Another approach is chosen by localized sorption models, i.e. BET or GAB models, which describe cluster formation as multilayer adsorption. The BET model assume that water in clusters is the same as liquid water, whereas GAB model consider that the polymer exerts force on water clusters, limiting their size. The GAB model has been successful in describing of Type II and Type III isotherms for activities between 0 and 0.95 [14], which is not the case for the BET model. In the GAB models the difference between bonded water and water in clusters determine if the isotherm of Type II or Type III. If water molecules are bonded to hydrophilic sites stronger than in clusters, Type II isotherm will be observed. Otherwise the model will describe Type III isotherm.

The previous overview [14, 22] of types of sorption isotherm of polymeric material and their theoretical models for them shows the relationship between the state of water in

the polymer and the sorption isotherm. Linear isotherms suggest negligible water-water interactions and usually are observed for hydrophobic polymers with a low absorption capacity. Type II isotherm indicate that some water is bonded by hydrophilic sites at low activities, i.e. polar groups, with a subsequent formation of water clusters at higher activities. Type III isotherms indicate that sorption is mainly due to formation of water clusters in the polymer.

2.3   Kinetics of Diffusion in Coatings

The goal of this section is to give an overview of typically observed diffusion types and their physical background.

The simpliest case of diffusion is Fickian diffusion. For Fickian diffusion it is characteristic that the redistribution of water occurs in a way that the concentration of water is a unique function of $x/\sqrt{t}$, where x is a distance from film/penetrant interface[1]. In this cases diffusion is driven purely by the concentration gradient and there is a local equilibrium at the sample surface. The total amount of water initially increases proportionally to $\sqrt{t}$ [31]. When the diffusion coefficient steeply increases with water concentration, a clear front develops that separatew the dry coating regions from regions of the coating with water. The front progresses linearly with $\sqrt{t}$. In such cases small amounts of penetrant cause plasticization of the polymer matrix, resulting in a higher diffusivity value, which in its turn allows quick penetrant redistribution behind the front.

Mostly, deviations from Fickian diffusion occur due to relaxation processes in the polymer, e.g. caused by plasticizing penetrants. Such deviations become significant, when the timescale of relaxation becomes comparable with the diffusion timescale. The ratio of the relaxation timescale to the diffusion timescale is in fact the so-called Deborah number *De*, first introduced for sorption in polymers by Vrentas et al. [32]. Diffusion in glassy polymer systems typically occurs, when $De \gg 1$, whereas diffusion in rubbery systems is characterized by $De \ll 1$. In both cases diffusion will have Fickian kinetics. When the Deborah number becomes close to 1, the relaxation processes influence the transport kinetics and deviation from the typical behavior can be observed. The cases, when front progression rate departs from being linear with $\sqrt{t}$ and being linear with t, diffusion is usually classified as anomalous diffusion [33].

A well known extreme case when relaxation processes participate in the driving force of the diffusion is Case II diffusion [34]. It is characterized by sharp concentration profiles, with a front, which progresses linearly with time. This was explained by diffusivity concentration dependency and relaxation processes by Thomas and Windle [34].

---

[1] This holds as long as penetrant has not reached the interface, opposite to water/coating interface

2.4 Water in Multilayer Coatings

Presently, only few studies have been dedicated to water uptake in multilayer films [15, 16, 18]. Carbonini et al. [15] studied the effects of the chemical composition of the constituent layers on the water uptake in a multilayer system with electroimpedance spectroscopy. Park et al. [16] investigated multilayer coatings degradation and substrate corrosion during water sorption/desorption cycling. They showed that water absorption and degradation of multilayered systems depend on the chemical characteristics of each layer and on the layer position in the system. Allahar et al. [18] studied water transport in both single and multilayer epoxy/urethane coatings. They showed that despite observed Fickian diffusion in each single layer, the Fickian diffusion is not sufficient to describe the process in the two-layered epoxy/urethane system.

3. Nuclear Magnetic Resonance

3.1 Introduction

Investigation of water transport in multilayer organic coatings requires knowledge of water distributions in the layers and assessment of water polymer interactions.

Various techniques are used to probe water in organic coatings, such as gravimetry [35], electrochemical impedance spectroscopy [15, 16, 18, 36], Fourier transform infrared spectroscopy (FTIR) [37, 38, 39], fluorescent spectroscopy [40] and high resolution nuclear magnetic resonance (NMR) imaging [41]. Except for NMR imaging and FTIR, these techniques only measure the total amount of water and do not probe interactions between water and polymer. While FTIR is able to evaluate water-polymer interactions [42], it can probe water distributions only in the direction, parallel to the coating plane [38, 39]. From the listed techniques, NMR imaging is the only technique, which is capable to measure with a high spatial resolution in the direction perpendicular to the coating plane.

The GARField approach for NMR imaging, introduced by Glover et al. [43], enables imaging with a high resolution of about $5\,\mu$m. It was successfully used to obtain water distributions in drying films [44, 45, 46, 47, 48]. Additionally, NMR relaxation analysis was used to evaluate mobility of polymer chains during crosslinking reactions [49], crosslinking fronts in drying alkyd films [48] and to estimate diffusivity of water in water-swollen cellophane [41]. Consequently, the combination of high resolution NMR imaging with NMR relaxometry can provide information about mobility of the polymer chains, water diffusivity and water content as a function of the position in the sample. Thus, this is a promising combination for studying water transport in multilayer coatings.

The aim of this chapter is to give an overview of NMR principles. For the detailed information about NMR we refer to the book "Principles of Magnetic Resonance" [50].

3.2 NMR Principles

3.2.1 Magnetic Resonance

NMR is based on behavior of nuclei in magnetic fields. When a nuclear magnetic moment $\vec{\mu}$ is located in a static magnetic field $\vec{B}_0$, it precesses around the field direction with a

Larmor frequency ω_0 [rad/s]

$$\omega_0 = \gamma |\vec{B}_0|,, \tag{3.1}$$

where γ is the gyromagnetic ratio of the nucleus. The gyromagnetic ratio has unique values for each type of nuclei, e.g. for ^{1}H $\gamma = 42.58\,\text{MHz/T}$. In this thesis we always place the static magnetic field $\vec{B}_0$ aligned along z-axis.

   Nuclei in a magnetic field can be excited by a radio-frequency field $\vec{B}_1$, which is oriented perpendicular to the static static magnetic field. The RF-field has an angular frequency ω_{RF}. Further in this chapter we will discuss the motions in a reference frame, which rotates around the z-axis with an angular frequency equal to the radio-frequency ω_{RF}. In this rotating frame the RF-field is static and is described by

$$\vec{B}_1 = (B_1 \cos\phi, B_1 \sin\phi, 0) . \tag{3.2}$$

where B_1 is the RF-field intensity and ϕ is the phase of the field.

   The excitation occurs at a resonance frequency, which matches the Larmor frequency, i.e. when $\omega_{RF} = \omega_0$. For simplicity we consider the amplitude of the RF-field B_1 to be constant, when the RF-field is applied.

   It is important to note that in the rotating frame the magnetic moments precess with the angular velocity $\vec{\Omega}$, which is described by[50]

$$\vec{\Omega}(t) = (\omega_1(t)\cos\phi, \omega_1(t)\sin\phi, \omega_0 - \omega_{RF}) \tag{3.3}$$

In the absence of the RF-field, the precession occurs only around the z-axis with the frequency $\omega_0 - \omega_{RF}$

3.2.2 Macroscopic Behavior

In NMR experiments magnetization $\vec{M}$ of the sample is measured. The magnetization vector $\vec{M}$ equals the sum of expectation values of nuclear magnetic moments $\langle \vec{\mu}_i \rangle$ in the sample

$$\vec{M} = \sum_i \langle \vec{\mu}_i \rangle , \tag{3.4}$$

In an equilibrium with the static field $\vec{B}_0$ the magnetization is aligned along z-axis, $\vec{M} = (0, 0, M_0)$. The magnetization dynamics is described by Bloch's equations[50, 51]

$$\frac{dM_x}{dt} = (\vec{\Omega} \times \vec{M})_x - \frac{M_x}{T_2}$$

$$\frac{dM_y}{dt} = (\vec{\Omega} \times \vec{M})_y - \frac{M_y}{T_2} \tag{3.5}$$

$$\frac{dM_z}{dt} = (\vec{\Omega} \times \vec{M})_z - \frac{M_z - M_0}{T_1}$$

The first terms in the right side of the equations describes the precession of the magnetization in the rotating frame due to the external magnetic fields. The second terms describe relaxation of the magnetization. The relaxation of the longitudinal component M_z is called T_1 relaxation or longitudinal relaxation, whereas the relaxation of transverse components M_x and M_y is referred to as transverse relaxation or T_2 relaxation. The nature of T_1 and T_2 relaxation is discussed later in Section 3.3 and Section 3.4, respectively.

When the magnetization has non-zero transversal components, $M_t = \sqrt{M_x^2 + M_y^2} > 0$, the magnetization will precess in the laboratory frame around z-axis with Larmor frequency ω_0 and will generate a RF-field with this frequency. The NMR signals are obtained by recording this field.

3.2.3 Spatial Resolution

In order to enable imaging with a spatial resolution, magnetic fields gradients have to be applied. To achieve high resolution one has to generate an inhomogeneous magnetic field. The mobile universal surface explorer (MOUSE) [52], Stray field magnetic resonance imaging [53] and Gradient-At-Right-angles-to-Field (GARField) [43] are examples, where high static magnetic field gradients are generated. In the present study, the GARField approach was used, which can operate with a spatial resolution of ca. $5\,\mu$m. Since in this study GARField approach is used, we discuss only static gradients of the magnetic field.

If the applied static field is position dependent, the Larmor frequency becomes position dependent

$$\omega_0(\vec{r}) = \gamma |B_0(\vec{r})|. \tag{3.6}$$

Since nuclei will resonate at position dependent frequencies, measurements with spatial resolution become possible. In the excited sample, the local magnetization $\vec{M}(\vec{r})$ generates RF signal with the intensity, proportional to the local transverse magnetization and the angular frequency $\omega_0(\vec{r})$.

The GARField approach utilizes special shaped magnetic poles to generate a gradient in the magnetic field. The magnetic poles are designed to create a gradient of $G \simeq 40\,\text{T/m}$. To excite the sample hort pulses with a pulse duration of ca. $1\,\mu s$ are used. The use of short pulses results in a broad spectrum, with a width of about $1\,\text{MHz}$, which corresponds to approximately $500\,\mu$m at the used gradient. As a result, such pulses excite nuclei in the whole coating, which usually has a thickness of $\sim 100\,\mu$m. Since the field of view, provided by the pulse spectral width, is directly related to the pulse duration, all the pulses in the pulse sequence should have the same pulse duration.
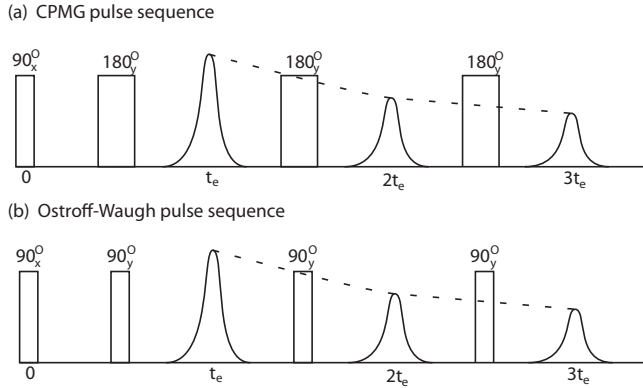
(a) CPMG pulse sequence

90^O_x 180^O_y 180^O_y 180^O_y

0   t_e $2t_e$ $3t_e$

(b) Ostroff-Waugh pulse sequence

90^O_x 90^O_y 90^O_y 90^O_y

0   t_e $2t_e$ $3t_e$

Fig. 3.1: A classical CPMG pulse sequence (a) and Ostroff-Waugh (OW) pulse sequence (b), which are used in NMR measurements. First, a 90°_x pulse with *x*-phase is used. Further, refocusing 180°_y-pulses (CPMG) or 90°_y-pulses (OW) are applied. The time between the first 90°_x-pulse and the second pulse is $t_e/2$, whereas subsequent pulses are separated by t_e. The spin-echoes are obtained between the refocusing pulses. Their intensity decays with the T_2 relaxation time. The decay is denoted by the dashed line.

3.2.4 Excitation

In NMR experiments pulse sequences are commonly used to excite samples. Series of RF-field pulses are applied. During the pulse the magnetization precesses around the RF-field direction and rotates on a certain angle. Further, this angle is referred as flipping angle. The pulses are characterized by a flipping angle α_ϕ and the ϕ of the $\vec{B}_1$ RF-field, which determines the direction of RF-field in the rotating frame during the pulse

$$\alpha_\phi = \gamma |B_1| t_p \tag{3.7}$$

where t_p ms is the pulse duration.

A classical example is CPMG (Carr-Purcell-Meiboom-Gill) pulse sequence, see Figure 3.1a. It starts with a 90°_x-pulse, followed by a train of 180°_y-pulses. The time between the 90°_x-pulse and the first 180°_y-pulse is $t_e/2$ and time between 180°_y-pulses equals t_e. The time t_e is called the inter-echo or inter-pulse time. The first pulse brings the magnetization along *y*-axis, resulting in magnetization lying in *xy*-plane. As a result, signal can be recorded. This signal rapidly decays due to nuclear spins dephasing, which is the result of magnetic field inhomogeneities. The subsequent 180°_y-pulses are applied to refocus the nuclear spins, and the spins are refocused between the pulses. The resulting peak in the signal is called a spin-echo, which can be recorded. Still, the total intensity of

the signals of the recorded spin-echoes will decrease in time due to T_2 relaxation.

According to Eq. 3.7, the product of the intensity and the pulse duration should be twice bigger for 180°-pulses than for 90°-pulses. This can be achieved by tuning the pulse duration t_p or by adjusting the RF-field intensity $|B_1|$. As imaging with the GARField approach requires the same pulse duration, using CPMG is possible only if the intensity of the RF-field can be increased twice. When this is not possible due to equipment limitations, an Ostroff-Waugh (OW) pulse sequence is used[54], see Figure 3.1b. The OW-pulse sequence is similar to CPMG pulse sequence, with the only difference that in the OW-pulse sequence 90_y°-pulses are used instead of 180_y°-pulses. Therefore, when OW-pulse sequence is used, all pulses have the same durations and intensities.

Still, even when the pulses are tuned to be 90°, only in a single slice of the sample magnetization will be flipped 90° degrees. This is because of the intensity of the RF-field is position dependent due to the shape of the pulse spectrum. The field intensity varies with the frequency and the position. As a result, significant part of the magnetization will be flipped with angles different than 90°.

3.3 T_1 Relaxation

T_1 relaxation of the longitudinal component of the magnetization M_z occurs due to dissipation of the energy absorbed by the nuclei to the lattice of the sample. This results in a return to the equilibrium state, where the magnetization is completely aligned along z-axis and and has its maximal value M_0.

Longitudinal or T_1 relaxation plays an important role in the choice of repetition time in NMR measurements. The NMR signal during the experiments is measured multiple times with subsequent averaging. Subsequent measurements are separated by a repetition time t_r ms. When $t_r \gg T_1$, the magnetization restores to equilibrium after the previous measurement. Otherwise, the NMR signal will be depressed, due to lower value of the sample magnetization. Note, that if several types of nuclei are measured, than it is important that repetition time is bigger than their T_1 relaxation time. Thus, T_1 of the samples should be determined.

Usually, the inversion recovery method [55] or saturation recovery method [56] are used. In this study T_1 values of the samples were measured with the saturation recovery method. Several short pulses were applied to saturated the nuclear spins in the sample and then magnetization recovery was probed.

3.4 T_2 Relaxometry

The relaxation of the transversal magnetization occurs due to loss of coherence by the nuclear spins due to spin-spin interactions or diffusion of the measured protons in a magnetic

field gradient. T_2 relaxation time characterizes the local molecular motions [57, 58, 59] and self-diffusion [60, 61] of the measured species.

When both self-diffusion and local molecular motions contribute to the relaxation process, the measured T_2 time reads

$$T_2^{-1} = T_{2D}^{-1} + T_{2S}^{-1}, \tag{3.8}$$

where T_{2D} [s] is the relaxation due to diffusion and T_{2S} [s] describes relaxation associated with the mobility of the measured species.

The general expression for signal attenuation of protons diffusing in a gradient of the magnetic field was presented by Hurlimann [61]. Due to an inhomogeneous excitation, pathways have unique parameters for each position in the sample. The attenuation of the signal of the diffusing species reads[61]

$$S(t) \sim \sum_{\{q_k\}} M_{\{q_k\}} \exp\left[-\alpha_{\{q_k\}}\gamma^2 G^2 D t_e^2 t\right], \tag{3.9}$$

where $\{q_k\}$ defines a coherent pathway, $M_{\{q_k\}}$ is a weighing factor for a coherent pathway and $\phi_{\{q_k\}}$ is the phase accumulation during diffusion. D [m^2/s] is the self-diffusion coefficient and $N \equiv t/t_e$ is the number of pulses. The parameter

$$\alpha_{\{q_k\}} = \left(\frac{1}{3}\sum_k^N q_k^2 + \sum_k^N q_k \sum_l^N q_l(l-1) + \sum_k^N q_k(k-1)\sum_k^N q_l\right)/N$$

includes the coherence pathway contributions.

It can be concluded that every coherent pathway evolves as a function of a rescaled time $\gamma^2 G^2 D t_e^2 t$ and the overall signal $S(t)$ will always be a function of $\gamma^2 G^2 D t_e^2 t$. If the measured signal of diffusing species decays monoexponentially as $\exp\left(-t/T_{2D}\right)$, the decay time can be described as

$$T_{2D}^{-1} = \alpha\gamma^2 G^2 D t_e^2. \tag{3.10}$$

The parameter α is a constant, which is defined by the evolution of coherent pathways for a given pulse sequence.

It is known that for Ostroff-Waugh-like pulse sequences, the relaxation time determined by the correlation time τ_c associated with molecular motions as follows[57, 59]

$$T_{2S}^{-1} = \langle\omega^2\rangle\tau_c\left[1 - \frac{\tanh\left(t_e/\tau_c\right)}{t_e/\tau_c}\right], \tag{3.11}$$

where $\langle\omega^2\rangle$ is the second moment associated with residual interactions[62].

The dependency of T_2 on the echo-time is shown in Figure 3.2 for $\tau_c = 60\,\mu s$, $\langle\omega^2\rangle = 12.7\,\mathrm{ms}^{-2}$ and $\alpha\gamma^2 G^2 D = 1.5\,\mathrm{ms}^{-3}$. The dotted line shows the relaxation time T_{2D} purely

determined by diffusion, whereas the dashed line shows the behavior of the T_{2S}. The dashed-dot line shows the total T_2 time when T_{2S} equals the plateau $\langle \omega^2 \rangle \tau_c$, whereas total T_2 is shown by the solid line. Given that $t_e/\tau_c \gg 1$ the slope of the curve is proportional to the self-diffusion coefficient of the measured species. The switch to the linear mode as well as the value of the plateau $\langle \omega^2 \rangle \tau_c$ characterizes the mobility of the nuclei. Higher plateau values and later transition times indicate a lower mobility of the nuclei, showing that they are more tightly bonded. Lower plateau values and shorter transition times indicate weaker bonding of the measured nuclei.
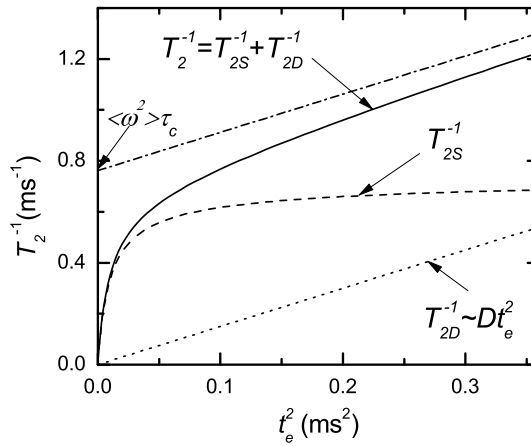
Fig. 3.2: Typical behavior of the T_2 relaxation time as a function of t_e^2 for a system, completely dominated by diffusion in the field gradient (dotted line), dipolar interactions of the nuclei (no diffusion, dashed line). The solid line refers to the relaxation behavior governed by both dipolar interactions and diffusion. The dashed-dotted line shows the behavior when $\tau_c \ll t_e$.

3.5 NMR Signal

When the pulse sequence is used a train of spin-echoes is recorded. Generally, a sample can contain a number of ^1H pools with distinct relaxation time. In the case of N distinct ^{1}H pools the signal of the n-th spin echo read

$$S_n(x,t) = P_n(x) \sum_{k=1}^{N} \rho_k(x) \left[1 - \exp(-t_r/T_{1k}(x)) \right] \exp(-nt_e/T_{2k}(x)), \qquad (3.12)$$

where k refers to a number of a specific ^{1}H pool, ρ_k [mol/m^3] is the density of ^{1}H nuclei of the k-th specific pool. The k-th pool has longitudinal relaxation time T_{1k}[s] and transversal relaxation time T_{2k}[s]. Note that the mentioned parameters reflect properties of a sample. In contrast, the repetition time t_r[s] and inter-echo (inter-pulse) time t_e[s] are settings in the measurements. The function $P_n(x)$ is a weighing factor for the n-th echo. It combines effects of the excitation and coil sensitivity profiles and evolution of coherent pathways in the used pulse sequences [61] and does not contain information about the measured sample.

4. Water Uptake Visualization

4.1 Introduction

Visualizing the transient water distribution in multilayer coating systems is the contribution of individual layers to water uptake, kinetics and to determine influence of water on the layers.

The investigation of water transport in multilayer coatings requires knowledge of how water distributes in the sample and its individual layers. This knowledge is crucial for understanding the contribution of individual layers to water uptake, to understand uptake kinetics and influence of water on the layers.

High resolution NMR imaging based on the GARField approach features proton distribution measurement in the sample. However, during water uptake both protons of water and protons of the coating will be probed. Thus, the NMR study of water uptake meets the challenge to distinguish the contributions of water to the NMR signal. This requires proper calibration of the signal as related to the amount of water in samples.

The aim of this chapter is to visualize and analyze transient water distributions in two-layered coatings during uptake on the basis high resolution NMR imaging. The considered coatings consist of a hydrophobic top coat and a hydrophilic base coat. The chapter starts with a determination of the relation between NMR signal profiles during uptake and water distributions. Furthermore, the consequences of water uptake in terms of swelling of the constituent layers is addressed. The chapter concludes with a discussion of the observed water distributions during uptake and the overall water uptake process by the considered systems.

4.2 Samples Description

Since this thesis is dedicated to investigation of water transport in multilayer coatings, samples, which may represent multilayer coatings, have to be chosen. As such systems two-layered base coat/top coat (BC/TC) systems were chosen. The considered top coats are solventborne crosslinked systems whereas the base coats are waterborne physically dries layers. This choice of layers provides significant contrast between them, therefore this type of two-layered systems can be considered as a valid representative of multilayered coatings. Additionally, the chosen base coats contain multiple polymeric phases due

to their waterborne nature. Thus, the chosen systems a valid candidate as a sample for studying water transport in multilayer coatings.

The base coats consist of 40% w/w acrylic particles, 20% w/w polyurethane (PUR) particles, 30% w/w DPP (di-keto-pyrrolo-pyrrole) pigment particles and 10% w/w polymeric dispersant in the sample, see Figure 4.1.
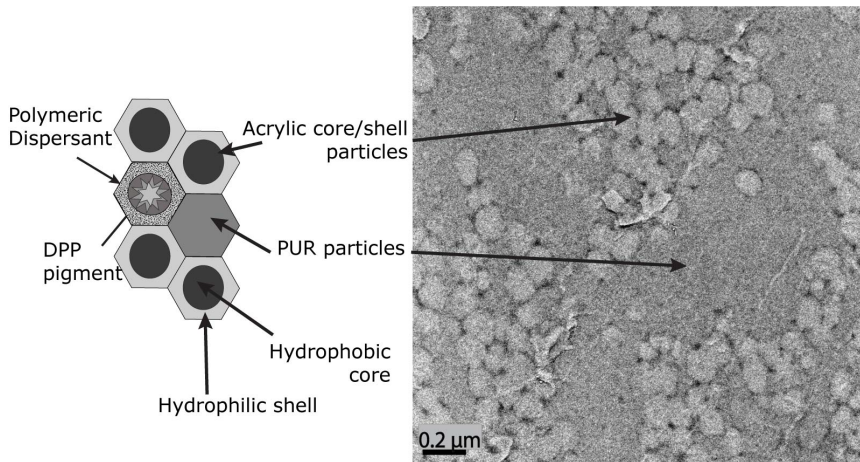

Fig. 4.1: Schematic presentation of the polymer matrix of the base coat and TEM image of an unpigmented base coat (acrylic and PUR particles only).

The ingredients of the base coat material are as follows [63]. The acrylic particles are synthesized by emulsion polymerization and have a core/shell structure. The core consists of BA (butylacrylate), BMA (butylmethacrylate) and HEMA (hydroxyethyl methacrylate). The shell is made from BA, MMA (methyl methacrylate) and MAA (methacrylic acid) and neutralized with DMEA (dimethylethanolamine). The shell/core volume ratio equals approximately 1:7 and their glass transition temperature T_g is about $25\,^{\circ}$C. The PUR particles consist of hydroxyl functional carbonate and DMPA (2,2'-bis-hydroxymethyl propoionic acid) chain extended with isocyanate and neutralized with DMEA [64]. The T_g of the PUR particles is approximately equal to $0\,^{\circ}$C. The polymeric dispersant is nonionic comb-polymer with a backbone of styrene and maleic anhydride of and hydrophilic hairs of PEO (polyethyleneoxide) and PPO (polypropyleneoxide). The total hydroxyl, acid and amine numbers for the basecoat are respectively 0.15, 0.25 and 0.15 meq/g basecoat.

The top coat is a 2-component solvent borne polyurethane coating which comprises polyacrylic polyol, polyester polyol and an isocyanate crosslinker. A glass transition temperature of the top coat equals approximately $60\,^{\circ}$C. Since experiments were performed at $25\,^{\circ}$C, the top coat was still in the glassy state, the acrylic core/shell particles of the

base coat were at transition between rubbery and glassy state and PUR particles were at the rubbery state.

These 2-layered films were applied on glass cover slides with an area of 18 x 18 mm^2 and a glass thickness of $150\,\mu$m. First, base coats were applied by spraying an aqueous dispersion on the glass slides. After spraying, the base coat was dried at 60 °C for 1 hour. The top coat was sprayed on top of the base coat and then cured at 60 °C for approximately 20 minutes. To ensure that the samples were fully cured before using them, the samples were stored for at least 4 weeks at room temperature. The base coat and top coat thicknesses are varied to investigate their influence on water transport. The base coat thicknesses were measured with a laser displacement sensor and the top coat thicknesses were measured with a micrometer, see Table 4.1.

Sample	BC thickness, (μm)	TC thickness, (μm)
BC25TC57	25	57
BC50TC23	50	23
BC50TC64	50	64
BC50TC73	50	73
BC50TC102	50	102

Tab. 4.1: The list of samples used in experiments. The letters BC and TC refer to the base coat and top coat, respectively. The numbers added to BC and TC represent the thickness of the layers in μm

To place liquid in contact with samples, a glass tube was glued on top of the coating/film, see Figure 4.2. A marker at the bottom of the substrate allowed to trace deflections of the substrate and fluctuations of the setup due to instabilities. The sample was positioned above the coil and aligned perpendicularly to the magnetic field.

4.3 NMR Equipment

The used NMR setup comprised an electromagnet with homebuilt magnet poles according to GARField approach [43]. The electromagnet generated a magnetic field of 1.5 T and the magnet poles have created the magnetic field gradient of 41 T/m. The sample is excited with a home made surface coil with a diameter of 3 mm. The same coil is used to record a signal. Home-built NMR equipment was used with acquisition systems described by Kopinga and Pel [65]. The NMR signal was sampled with a frequency of 5 MHz at a receiver bandwidth of 1.5 MHz. All pulses had the duration of 1 μs with rise and fall times of ca. 0.25 μs, yielding an excitation profile with a width of 1 MHz. Since the effective field of view (FOV) is determined by both the receiver bandwidth and pulse excitation profile, the resulting FOV was about 1 MHz.
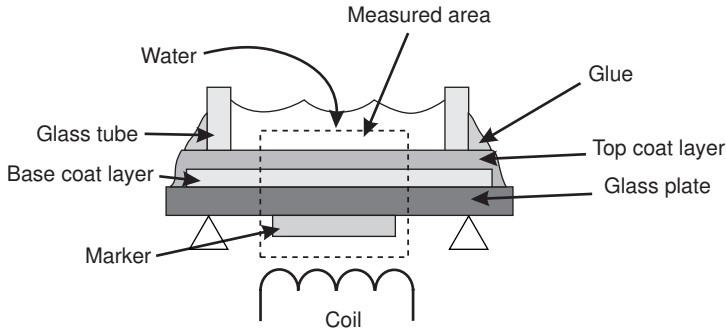
Fig. 4.2: Schematic representation of the experimental set-up used for water uptake ex-
         periments. The glass tube is fixed on the sample to place water on top of it. The
         marker is used to trace the substrate position displacements.

4.4   NMR Imaging Procedure

Profiles were measured by using an Ostroff-Waugh pulse sequence $\beta_x - t_e/2 - [\beta_y - t_e/2 - echo - t_e/2]_n$ with β nominally equal to 90° [54]. This pulse sequence was chosen because same β is required for each pulse, which is possible only with same pulse duration and pulse excitation profile.

        The duration of a single pulse equals 1 μs. To obtain the distribution of water, signal profiles were measured with $t_e = 100\,\mu$s and an acquisition window of 90 μs, correspond-ing to a resolution of 6 μm. For imaging, the first echo was used. The whole sample was excited by a short pulse and then Fourier transformation was applied to the recorded signal to retrieve the signal profiles.

        Signal profiles were averaged 2048 times and the time between two subsequent measurements has been set to $t_r = 0.5\,$s. A measurement of a single profile measurement took 20 minutes.

        The recorded profiles combine proton density distributions, T_1 and T_2 factors and the effects of the coil and receiver sensitivities and flipping angle distributions. Figure 4.3 shows the signal profile of the column of an aqueous $CuSO_4$ solution. Additionally it shows the signal profiles of the dry and wet base coat/top coat sample (solid lines). The density of the protons, T_1 and T_2 values in the solution should not vary with position, thus the variation of the signal is due to sensitivity of NMR equipment and pulse excitation profile.

        The obtained signal should be a product of proton density, T_1, T_2 factors and the factor due to pulse excitation profiles and equipment sensitivity. In order to remove the effects of the pulse excitation profile and equipment sensitivity, the measured signal pro-files are divided by signal profile of the reference sample. As a reference sample aqueous
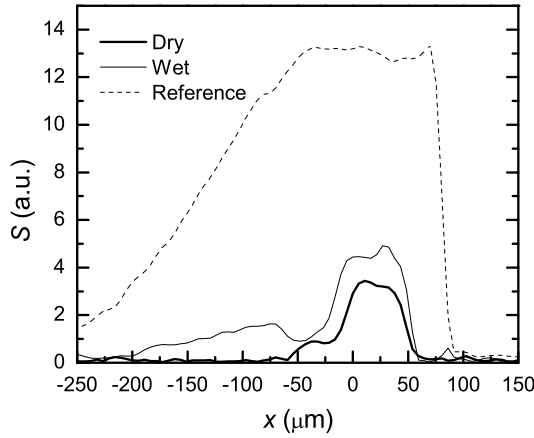
Fig. 4.3: Signal profile of the dry (bold line), wet sample and the reference (an aqueous 0.01 M CuSO$_4$ solution, dashed line). The reference signal profile reflects how the combination of the excitation profile of the pulses and coil sensitivity result the NMR signal of a homogeneous sample. The reference signal is used to eliminate this mapping from the NMR signal of the samples.

0.01 M CuSO$_4$ solution is used. It has a T_1 value of about 70 ms and $T_2 = 2.3$ ms. For the used settings there is limited signal loss due to longitudinal and transverse relaxation. Thus, for the reference T_1 and T_2 factors are neglected and the corrected signals of the first echoes read:

$$S_n(x) = \frac{\rho(x)}{\rho_w} \left[1 - \exp(-t_r/T_1)\right] \exp(-nt_e/T_2), \qquad (4.1)$$

where $\rho \, [\text{mol/m}^3]$ is actual density of probed ^{1}H nuclei, $\rho_w \, [\text{mol/m}^3]$ is the density of ^{1}H nuclei in liquid water (since it is the same in the reference sample), $t_r \, [\text{s}]$ is the repetition time, $T_1 \, [\text{s}]$ is the longitudinal relaxation time, $t_e \, [\text{s}]$ is the echo time, $T_2 \, [\text{s}]$ is the transversal relaxation time and n is the number of spin-echo.

4.5   Results

4.5.1   Visualization and quantification of water uptake in multilayer coatings

This section focuses on the relationship between the NMR signal profiles and the distribution of water in a coating.
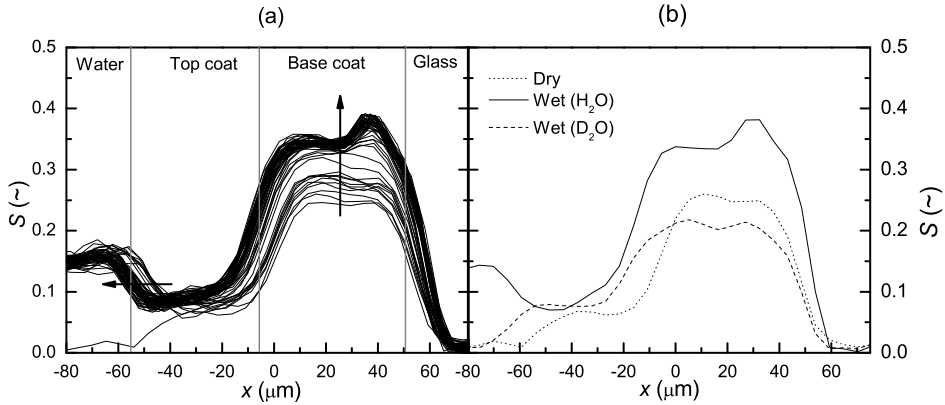
Fig. 4.4: NMR signal profiles in the sample BC50TC64 during water uptake (a) and in dry (dashed line), saturated with water (solid line) and heavy water (dotted line) states (b). The time between subsequent profiles during uptake (a) is 20 minutes and 6 hours for the first ten and the rest of the profiles, respectively. The vertical lines refer to the positions of the interfaces. The vertical arrow denotes the signal increase in the base coat and the horizontal arrow denote swelling.

The signal profiles of the sample BC50/TC64 are presented in Figure 4.4a. The profiles as shown were corrected with the marker data, i.e. the profiles were corrected for any displacement (bending) of the glass slide. In Figure 4.4a, therefore, the lower side of the base coat, i.e. the interface between glass and base coat is a real, fixed reference position. The different signal levels in the base coat and the top coat are due to signal loss, which can be explained with the help of Eq. 4.1.

Figure 4.4a shows the profiles during a water uptake experiment. The time between two subsequent profiles is 20 minutes for the first 10 profiles and 6 hours for the later ones. The measurement time of a single profile is 20 minutes. The signal of the water on top of the coating is lower than the signal in the base coat, which is due to the fact that the T_1 of pure water is much longer than the chosen repetition time, (see Eq. 4.1).

During water uptake, a signal increase is observed in the base coat layer. Since T_1 values are the same for dry and wet base coat, (see Table 4.2), there is no change in T_1 weighing of the signal during water uptake. Therefore, the signal increase can be attributed to an ingress of water into the coating and to an increase of the coating background signal (i.e. signal of the polymer of the coating). An increase of the background signal can be caused by an increase of the T_2 of the polymer matrix due to mobilization of the polymer.

To detect changes in the background signal of the coating water on top of the sample

Layer/state	T_1 [ms]
Base coat/dry	200
Base coat/wet	200
Top coat/dry	350
Water	3000

Tab. 4.2: T_1 values of the the polymer systems and water.

was replaced by heavy water. Since deuterium is not probed, only the background signal from the coating is measured. While the exchange between deuterons of heavy water and protons of the polymer is possible, the number of exchangeable protons is negligible (Section 4.2). There are only few differences between heavy water and water, like slightly higher density and slightly stronger hydrogen bonding. It is known that in polymers heavy water transport is similar to water transport [66, 67] and is used instead of water in studies of water transport. The measured signal profiles for the dry sample and sample saturated with water and heavy water are presented in Figure 4.4b. The signal level of the base coat filled with D_2O is lower than signal level of the dry base coat. Due to the swelling of the coating the hydrogen density of the polymeric material slightly decreases resulting in lower signal level. Since a signal increase is not observed, it is concluded that during water uptake the observed signal increase is only due to an increase of the amount of water in the base coat layer.
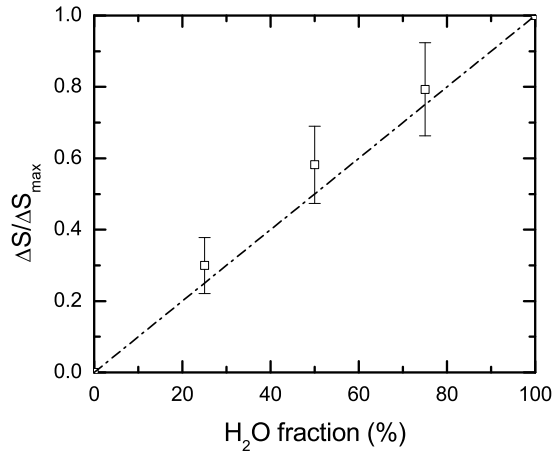

Fig. 4.5: The normalized signal increase in the wet base coat layer as a function of the volume percentage of water in the H_2O/D_2O mixture on top of the sample.

The water on top of the wetted sample was replaced by various D_2O/H_2O mixtures in order to find a relation between the signal increase and the amount of water in the base coat. The signal was integrated from the base coat/glass interface to the top coat/water interface. In Figure 4.5 the NMR signal is plotted against the fraction of water in the mixture on top of the sample. The normalized integrated signal change is calculated according to $\triangle S/\triangle S_{max} = [S_{mix} - S_{D_2O}]/[S_{H_2O} - S_{D_2O}]$, where S_{mix}, S_{H_2O} and S_{D_2O} are the levels of the integrated signal of the base coat layer in the case of exposure to a D_2O/H_2O mixture, pure water or pure heavy water, respectively. A linear relation between the signal and the amount of water in the mixture is observed. It can be concluded that signal increase $\triangle S$ is proportional to the mass of water in the coating $\triangle m\,[\text{mg}]$, $\triangle S = k\triangle m$, where $k\,[\text{mg}^{-1}]$ is a proportionality coefficient.

To quantify the signal increase $\triangle S$ in terms of the amount of absorbed water $\triangle m\,[\text{mg}]$ the coefficient k should be found. The expression for k can be derived by the integration of Eq. 4.1

$$k = \frac{1}{\rho_w A}\left[1 - \exp(-t_r/T_1)\right]\exp(-t_e/T_2) \qquad (4.2)$$

where $\rho_w\,[\text{mg/cm}^3]$ is the density of liquid water and $A\,[\text{m}^2]$ is the area of the base coat, $T_1\,[\text{s}]$ is the longitudinal relaxation time and $T_2\,[\text{s}]$ is transversal relaxation time of water. The signal loss in the wet base coat due to the T_1 relaxation is equal to 8% with $t_r = 0.5\,\text{s}$. To estimate the signal loss of water due to T_2 relaxation, the signal decay of the whole base coat saturated with D_2O was subtracted from the signal decay of the wet base coat, see Figure 4.6. The T_2 value of water in the base coat appears to be 6 ms. Therefore, only 2% of the signal is lost due to T_2 relaxation, since with used echo time $t_e = 100\,\mu\text{s}$. Since the signal loss due to relaxation processes is limited, Eq. 4.2 can be approximated by

$$k \approx \frac{1}{\rho_w A}. \qquad (4.3)$$

4.5.2 The water uptake process

Now the origin of the signal has been established, the water uptake process itself can be investigated. The uptake and the resulting mechanical response of the whole system will be discussed in this section.

Shortly after exposure to water, profiles show that the water is visible near the glass/base coat layer interface, see Figure 4.4. This means that redistribution of water inside the base coat layer is faster than a single profile measurement. Moreover, it also implies that that the water uptake rate is only limited by the penetration through the top coat layer. As a consequence, the total amount of water in the base coat layer is the main variable, which should be considered to characterize water uptake.
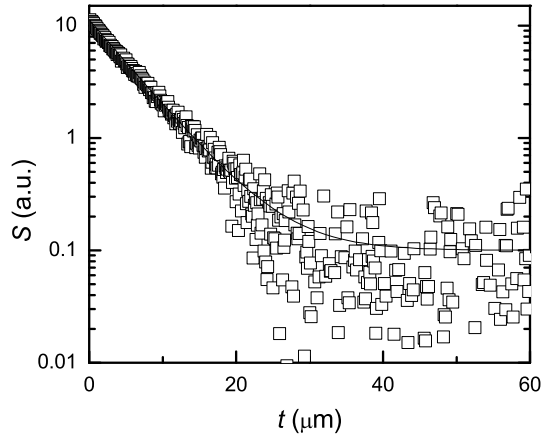
Fig. 4.6: The signal decay of water in the base coat. The value of the T_2 relaxation time is 6 ca. ms. This value means that at used setting only 2% of the signal of water in the base coat is lost due to T_2 relaxation.

The total amount of water $m(t)$ inside the base coat layer is obtained via integrating the profiles from the BC/glass to the TC/water interface as the top layer hardly absorbs any water. The swelling $\Delta H(t)$ is obtained as the change in distance between the top coat/water interface and the marker from the second echo profiles, as they provide better contrast between water and top coat. Since the top coat absorbs only a small amount of water, the swelling is attributed to the base coat layer. The amount of water in the base coat layer is shown as functions of time in Figure 4.7.

The relation between the amount of water in the base coat and its swelling of the sample is presented in Figure 4.8, showing that the thickness varies linearly with the mass. Since the volume change of the base coat can be approximated with $\Delta V = A\Delta H$ (A is the area of the base coat layer), it can be concluded that the molar volume of water in the base coat layer is constant. A linear fit gives a slope of ca. $A\Delta H/\Delta m \simeq 1.1 \pm 0.1\,\mathrm{cm}^3/\mathrm{g}$. With the area of the base coat, obtained in the previous section, the molar volume of water $v = MA\Delta H/\Delta m$ in the base coat is estimated to be $18 \pm 2\,\mathrm{cm}^3/\mathrm{mol}$. This value is similar to the molar volume of liquid water. This may indicate that the most of absorbed water results in volume increase, i.e swelling of the base coat.

The non-zero intercept of the data is an artifact of the procedure, introduced by use of the first value of distance between the water/top coat interface and the marker as zero-point for swelling. The distance between the interface and the marker for the dry sample cannot be used as the zero-point due to poor accuracy of the interface in the
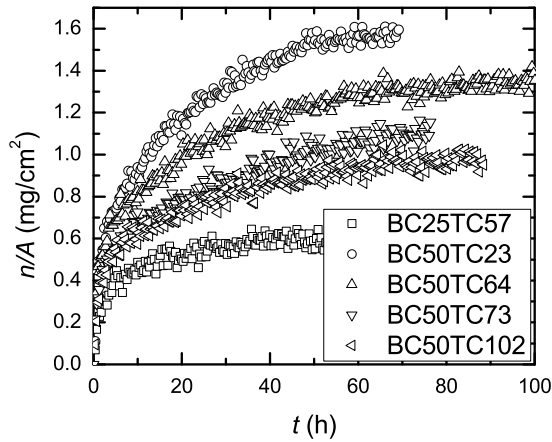
Fig. 4.7: The amount of water in the base coat as a function of time during water uptake
as obtained with NMR. The whole uptake lasts several days, with an initial rapid
stage, where about half of total amount of absorbed water is taken up at first few
hours.
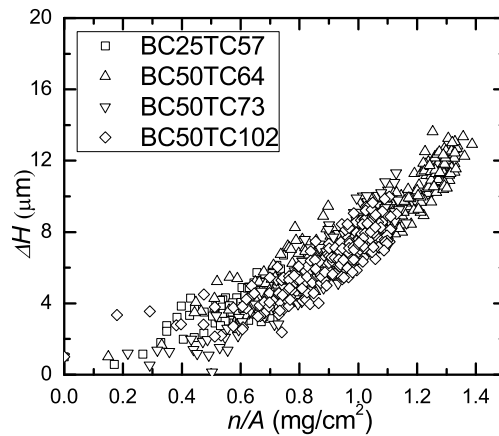
Fig. 4.8: The swelling of the base coat (i.e. thickness change) as a function of the amount
of water in the base coat during water uptake. The linear relation indicates that
the molar volume of water inside the base coat layer is constant.

absence of water. Another possible physical explanation could be that initial some water, i.e. $\sim 0.2\,\mathrm{mg/cm^2}$ is adsorbed by the base coat with no volume change. However, it is not possible to assess this on the basis of the swelling data.

4.6   Conclusions

The application of high resolution NMR imaging based on GARField approach showed that it is an appropriate experimental technique for measuring water uptake in multilayer coatings. The considered samples were two-layered coatings of a waterborne physically dried base coat and a solventborne crosslinked top coat. Water distributions and swelling could be simultaneously monitored during uptake.

The measurements of water uptake showed that the rate of water uptake is limited by the penetration through the protective top coat layer. The penetrated water causes swelling, which appears to be linear with the total amount of absorbed water. This implies that the molar volume of water in the polymer matrix of the base coat is constant and has a value, which is close to the molar volume of liquid water. This also means that water transport in such type of systems is accompanied by swelling stresses in the base coats.

5. Water-Polymer Interactions During Uptake

5.1   Introduction

The previous chapter has brought insight into water redistribution in two-layered coatings. The studied systems consisted of a waterborne physically dried base coat and a solvent-borne crosslinked top coat. The next step in this study is evaluation of state and mobility of water in the considered base coat/top coat systems, as it brings insight into how water present in the coating. As the base coat is the main reservoir for water, the main focus in this chapter is on investigation of water in the state of water in the base coat and its influence on the polymer matrix.

A proper interpretation of NMR transverse relaxation times should form the backbone for such investigation. The contribution of water to the relaxation can be evaluated by using heavy water. Additionally, there is an opportunity to identify contributions of the various polymer phases of the base coat to the NMR signal decay, given a significant difference between polymer chains mobilities in these phases. Furthermore, the relaxation time of water contains information about self-diffusion coefficient and local molecular motions in the sample. The polymer relaxation time depends on chains mobility of the polymer. Understanding these parameters is a key to get an insight of how water is present in the base coat and what is the effect of water on the polymer matrix. Combined with NMR imaging, NMR relaxometry has the potential to evaluate interactions within specific layers of multilayer coatings.

The goal of this chapter is to investigate the interplay between water and polymer of the base coat during uptake in the considered base coat/top coat systems. The base coat is a waterborne physically dried system, which consists of acrylic, polyurethane and pigment particles and includes a polymeric dispersant for the pigment. NMR relaxometry is used to identify water and polymer phases of the base coat. Furthermore, it is evaluated, whether water is highly mobile in the base coat and what is the influence of water on the polymer phases.

5.2   Experimental Details

5.2.1   Sample Description

The studied samples are two-layered base coat/top coat coatings. Here we give a brief information about the samples and for more detailed sample composition we refer to Section 4.2. The base coats consist of 40% w/w acrylic particles, 20% w/w polyurethane (PUR) particles, 30% w/w DPP (di-keto-pyrrolo-pyrrole) pigment particles and 10% w/w polymeric dispersant in the sample. The acrylic particles are core/shell particles with a glass transition temperature of about 25 °C. The PUR particles have a glass transition temperature of about 0 °C. The dispersant is a comb polymer with a hydrophobic backbone and water-soluble side chains.

The top coat is a solvent borne highly crosslinked system with a glass transition ca. 60 °C.

To place liquid in contact with samples, a glass tube was glued on top of the coating, see Figure 4.2.

5.2.2   Data Processing

The obtained signals can be described by Eq. 3.12. To extract relaxation spectra, the values of $P_n(x)$ have to be known. To determine the values of $P_n(x)$ a 0.01 molal CuSO$_4$ aqueous solution was used as a reference. As the signal of this solution decays monoexponentially, the values of $P_n(x)$ can be determined using Eq. 3.12:

$$S_{n,ref}(x) = \rho_{ref} P_n(x) \exp\left(-\frac{nt_e}{T_2^{ref}}\right),\tag{5.1}$$

where ρ_{ref} [mol/m^3] is the density of ^{1}H nuclei in the CuSO$_4$ solution and $S_{n,ref}$ [a.u.] is the intensity of the n-th echo. The echo trains $S_n(x)$ of the studied samples, described by equation Eq. 3.12, can be divided by correction factors obtained from CuSO$_4$ solution data, see Eq. 5.1. The corrected signal I_n becomes a simple multi-exponential decay and is described in the following equation

$$I_n(x) \equiv \frac{S_n(x)}{S_{n,ref}(x)\exp\left(nt_e/T_2^{ref}\right)} = \sum_k \frac{\rho_k(x)}{\rho_{ref}} \exp\left(-nt_e/T_{2k}(x)\right).\tag{5.2}$$

Each exponent represents a specific ^{1}H pool with distinct T_2 value. Note that amplitudes of the exponents are relative densities of ^{1}H nuclei with respect to the density of the ^{1}H nuclei in water. Consequently, the factors before each exponent are proportional to concentrations of ^{1}H nuclei.

Considering the main objective of the present study, each of these pools should be identified, their T_2 values should be evaluated and be expressed in terms of ^{1}H quantities

n_k. Therefore, measured signal decays were fitted with a regularized inverse Laplace transform algorithm (RILT) as proposed by Venkataramanan et al. [68], which resulted in T_2 spectra containing a number of peaks. The peaks refer to ^{1}H pools, with a position corresponding to the T_2 values of ^{1}H in the specific pool. The intensities of the peaks reflect the densities ρ_k and the total amount n_k of ^{1}H nuclei if profiles or total signals are treated, respectively. The robustness of the fitting procedure is discussed in Appendix B.

5.2.3 Measurements

In this study we are interested in identifying the contributions of water and polymer to the NMR signal and investigating the state of water in the polymer. For identification of the contributions of water and polymer phases to the signal measurements of the sample in dry, H_2O-wet and D_2O-wet situations were done. They were performed with $t_e = 0.1$ ms and 8192 averages. The identification experiments were performed with primary and acrylic BC/TC samples and with pure PUR films.

Experiments, dedicated to study the state and mobility of water in the polymer were performed with t_e ranging from 0.1 ms to 0.6 ms and with 8192 averages. The primary BC/TC sample was studied in partially and fully saturated states, which were achieved by equilibrating the sample with an aqueous solution of polyethylene glycol (PEG) and liquid water, respectively. The aqueous solution of PEG had a water activity equal to 0.9. This water activity was obtained by tuning the PEG concentration in the solution[69].

Water uptake in the primary BC/TC sample was measured with $t_e = 0.1$ ms and 2048 averages. Measurements were performed with a repetition time of $t_r = 0.5$ s, resulting in temporal resolution of 20 min. The acquisition time was $t_{acq} = 90\,\mu$s.

The parameter α in Eq. 3.10 was estimated from the signal decay of an 0.01 M aqueous $CuSO_4$ solution. Water in this solution has a $T_2 \simeq 2.6$ ms. The self-diffusion coefficient of water in the $CuSO_4$ solution is equal to $2.5 \times 10^{-9}\,m^2/s$, which is equal to diffusivity of pure water[70]. Using this value and the fact that for $CuSO_4$ solution $T_{2S} \gg T_{2D}$ in our experiments, we obtain that $\alpha = 5$.

5.3 Results

5.3.1 Distinguishing Water and Polymer

T_2 Relaxation Spectra

A prerequisite for understanding the interplay of water and the polymer matrix during uptake is that the signals of water and polymeric material can be distinguished. This section focuses on identifying the NMR signal components and assigning them to water and polymeric components (acrylic, PUR and dispersant), respectively.

With the help of the RILT fitting procedure relaxation spectra were obtained for

each position in the base coat of the primary BC/TC sample. Four T_2 spectral components were detected at each position in the base coat. The average T_2 values for each component is shown in Figure 5.1. The dashed line represents the original signal profile $I_n(x)$. The T_2 values are nearly constant as a function of position. Consequently, the properties of each ^{1}H pool, which are reflected by the T_2 value, can be considered as homogeneous in the studied base coat. Concerning the homogeneity, further analysis in our study is based on the total signals of the base coat of the primary BC/TC sample.
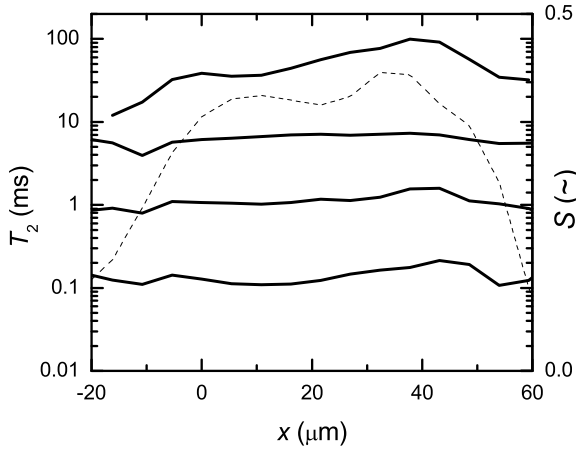

Fig. 5.1: The average T_2 value of each spectral component in the wet base coat of the primary sample as a function of the position. The dashed line represents the signal intensity of the first echo of the coating.

The total signal was obtained by integrating the corrected signal in Eq. 5.2. As a result, the expression for the total signal I_n^t of the base coat reads

$$I_n^t = \sum_k A_k \exp\left(-nt_e/T_{2k}\right),\tag{5.3}$$

where $A_k \equiv \rho_{ref}^{-1} \int_{BC} \rho_k dx\,[\mu m]$ reflect a total amount of ^{1}H nuclei in k-th pool in the base coat. The density ^{1}H nuclei in liquid water $\rho_{ref} = 0.11\,\mathrm{mol/cm^3}$. The amount of ^{1}H nuclei $n_k\,[\mathrm{mol/m^2}]$ in k-th pool relates to A_k as follows

$$n_k = \rho_{ref} A_k.\tag{5.4}$$

The solid line in Figure 5.2a shows the relaxation spectrum obtained from the total signal of the wet base coat. Obviously, there are at least four typical ^{1}H pools that

contribute to the signal. The bars show both the average spectral position and the total intensity of the peaks. The total intensity equals the total amount of ^{1}H nuclei in the pool. The next steps in our analysis focus on the identification of the peaks, i.e. understanding the connection of the T_2 components with water and polymeric ingredients of the primary base coat.
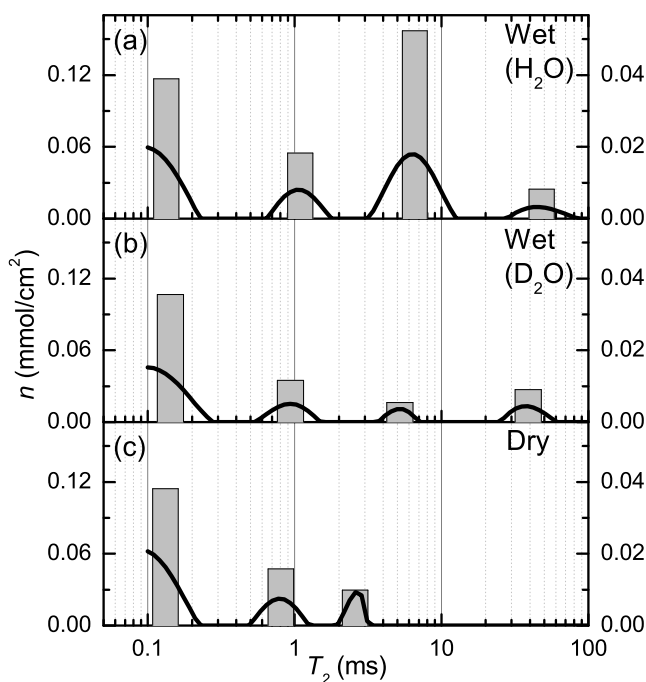
Fig. 5.2: The T_2 spectra of the base coat in wet (H_2O (a) and D_2O (b)) and dry (c) states. The bars mark the average spectral positions of the peaks and total intensity of the peaks. The bars intensities are shown by the left scale and the raw spectra intensities are shown by the right scale.

Water and Polymer

First, the signal of water in the relaxation spectrum will be identified in Figure 5.2a. Comparing the spectra of the primary base coat wetted with H_2O (Figure 5.2a) and wetted with D_2O (Figure 5.2b) only revealed a significant difference in the intensity of the spectral

component at $T_2 \simeq 6\,\text{ms}$. Whereas in the H_2O-wet spectrum a huge peak exists, this peak is small in the D_2O-wet spectrum. This implies that this spectral component represents water in the base coat (Table 5.1). The intensity of the water component corresponds to $1.41\,\text{mg/cm}^2$. This value means that the base coat has absorbed approximately 26% w/w of water. Note that the number of exchangeable protons in hydroxyl, acid and amine groups in the base coat are equivalent to 0.4% w/w of water in the base coat. Therefore, their amount can be neglected when relaxation spectra are discussed.

As a consequence, all other spectral components are from the polymeric matrix of the coating, which may be sensitive to interaction with water. To detect the influence of water on the polymer matrix, the T_2 spectra of a dry base coat and one wetted with D_2O have to be compared. The spectrum of the dry base coat contains three peaks, see Figure 5.2. The first component is at $T_2 \simeq 0.1\,\text{ms}$ and two other components are located at $T_2 \simeq 0.9\,\text{ms}$ and $T_2 \simeq 2\,\text{ms}$, respectively. The spectra of the wet (H_2O and D_2O) system contain a component at $T_2 \simeq 20-40\,\text{ms}$, which is absent in the spectrum of the dry base coat. Since the T_2 increases drastically due to an increase in polymer mobility, the component at $20-40\,\text{ms}$ is a consequence of polymer plasticized by water.

The next step in our analysis is the identification of the acrylic, PUR and dispersant ingredients among the spectral components of the polymer.

Polymeric Compounds

The pigment particles of the base coat are in a crystalline state and hydrophobic. As they have a T_2 value much less than the used interecho time t_e, pigment is not visible in relaxation spectra. Polymeric components in the relaxation spectra in Figure 5.2 should originate from acrylic core/shell particles, PUR material and the polymeric dispersant.

In order to identify the T_2 components of the polymer matrix and to determine the polymer compounds that are plasticized by water, the spectra of a base coat of a pure acrylic BC/TC system and of a PUR film are compared with the spectra of the base coat of the primary sample.

The spectra of the base coat of the acrylic BC/TC sample are presented in Figure 5.3. The spectrum of the dry acrylic base coat contains a single component at approximately 0.1 ms, see Figure 5.3c. This implies that the components observed at 0.9 ms and 2 ms in the spectrum of the dry primary base coat (Figure 5.2) belong PUR particles and the dispersant. The spectrum of the acrylic base coat wetted with D_2O is presented in Figure 5.3b. As compared to Figure 5.3a it includes a single additional component at 1 ms with negligible intensity, it is concluded that the acrylic core/shell particles are not plasticized by water. We conclude that the shell of the acrylic particles is not distinguished either due to small intensity or due to overlap with the main component at 0.1 ms.

The spectrum of the wet acrylic base coat includes two additional T_2 components, see Figure 5.3a. Since the component at 1 ms is very small and since there is no spec-
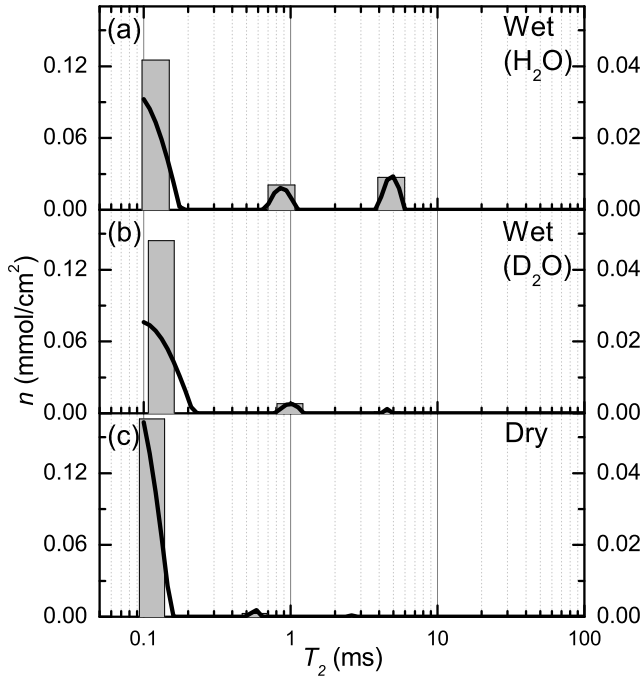
Fig. 5.3: The T_2 spectra of the acrylic core/shell base coat in the wet (H_2O (a) and D_2O (b)) and in the dry (c) states. The bars show the average spectral position and the total intensity of the peaks.

tral component at 6 ms in the spectra of dry and D_2O wetted sample, these components represent water in the pure acrylic base coat. Note that the amount of absorbed water is significantly lower than the amount of water taken up by the primary base coat. The analysis of the spectra of the acrylic sample implies that the T_2 component at $20-40$ ms observed in the wetted primary base coat (Figure 5.2) represents plasticized PUR or plasticized dispersant. In order to investigate the contributions of PUR and dispersant to the plasticized material, the PUR film was measured. The relaxation spectra of PUR films are presented in Figure 5.4. The spectrum of the dry PUR, Figure 5.4c, contains two T_2 components. Their spectral positions are at 0.8 and 2.5 ms, which are similar to the spectral positions of the non-acrylic components in the primary system, Figure 5.2c. The spectra of the wetted PUR material feature an extra but small component at 15-40 ms. This component belongs to PUR material, plasticized by water. The intensity of the plasticized
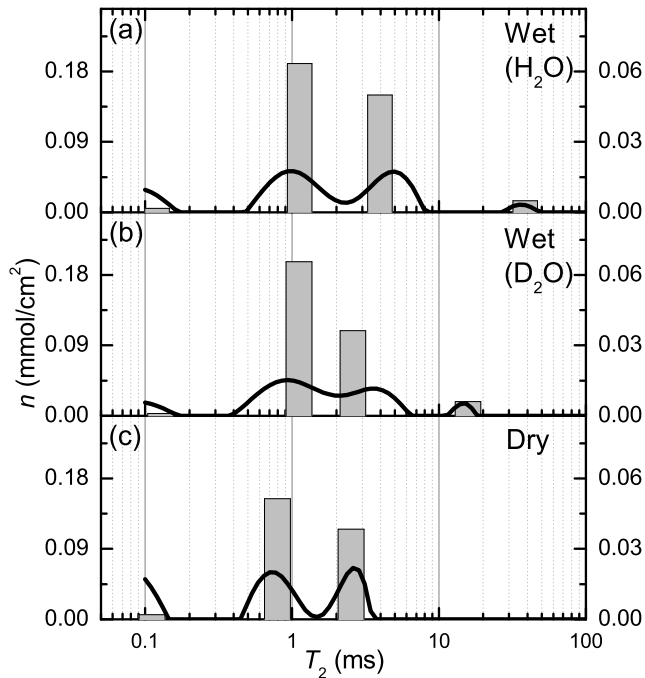
Fig. 5.4: The T_2 spectra of the PUR material in the wet (H_2O (a) and D_2O (b)) and in the dry (c) states. The bars show the average spectral position and the total intensity of the peaks.

PUR component is less than 5% of the total PUR intensity and cannot explain the intensity of the slow relaxing component in the primary sample, see Figure 5.2a and Figure 5.2b. In the primary system the intensity of the plasticized material is 32% of the non-acrylic polymeric components. Note that the mass ratio between the polymeric dispersant and PUR particles in the primary sample was approximately 1:2. This implies that in the primary system the component at 20-40 ms is mainly due to the dispersant plasticized by water. Water in the wetted PUR material is represented by component located at approximately 4 ms. This position is similar to water spectral position in the primary base coat in Figure 5.2a. The intensity of the water component equals the difference between intensity of this component and corresponding component in the spectrum of PUR saturated with heavy water Figure 5.4b. However, it is significantly lower than the intensity of water component in the primary sample.

A summary of the assignments of the T_2 components is given in Table 5.1. Thus, in the spectrum of the wet primary base coat, see Figure 5.2a, we assign the spectral component at $0.1\,\text{ms}$ to acrylic core/shell material, the components at $0.8 - 2.5\,\text{ms}$ to the PUR material and the dry dispersant. The component at $20 - 40\,\text{ms}$ mainly belongs to the plasticized dispersant with possibly a very small contribution of plasticized PUR. The spectral component at $T_2 \simeq 6\,\text{ms}$ represents mainly water. Note, that the T_2 of water has a smaller value than of the plasticized dispersant. Normally, one would expect that the plasticizer has a similar or higher T_2 value than the plasticized material. The reason may be that either diffusion of water in the field gradient dominates the T_2 relaxation of the water or that protons of water are present at least in two different environments with different mobilities. In the latter case, the measured T_2 time may be affected by a rapid exchange between these environments [71]. Whether or not diffusion explains this observation is discussed in the next section.

An important observation is that the intensity of the water components in the spectra of wet acrylic (Figure 5.3a) and wet PUR (Figure 5.4a) materials cannot explain the high intensity of water spectral component in the primary system (Figure 5.2a). Therefore we conclude that the hydrophilic PEO/PPO hairs of the polymeric dispersant absorb a significant amount of water.

Spectral position	$0.1\,\text{ms}$	$0.8 - 2.5\,\text{ms}$	$6\,\text{ms}$	$20 - 40\,\text{ms}$
Compound	Acrylic	PUR & dispersant	water	plasticized dispersant

Tab. 5.1: Identified compounds in the wet primary base coat of the primary sample and their spectral positions, for $t_e = 0.1\,\text{ms}$.

5.3.2 The diffusivity of water in the base coat

Water in the base coat is either strongly bonded to the polymer or highly mobile. The binding of water to the polymer is reflected by the T_{2S} time, whereas diffusion is described by T_{2D} in Eq. 3.8. If water molecules are highly mobile and have a high self-diffusion coefficient, then $T_{2D} \ll T_{2S}$ and $T_2 \simeq T_{2D}$. The goal of this section is to find out whether water binding to the polymer lattice or water diffusion dominates the T_2 value.

Therefore, a primary sample, in fully or partially saturated state, was measured with various echo times ranging from 0.1 to $0.6\,\text{ms}$. The relaxivity T_2^{-1} of water as a function of t_e^2 obtained from the total signal of the fully saturated base coat is shown in Figure 5.5 (squares). The inverse T_2 increases linearly with t_e^2 and has an offset. This offset seems to be the only influence of T_{2S} in this case and the echo time dependency of the water relaxation is only determined by diffusion in the field gradient. The slope of the curve of the wet system in Figure 5.5 equals $2.7 \times 10^9\,\text{s}^{-3}$, which leads to a self-diffusion constant
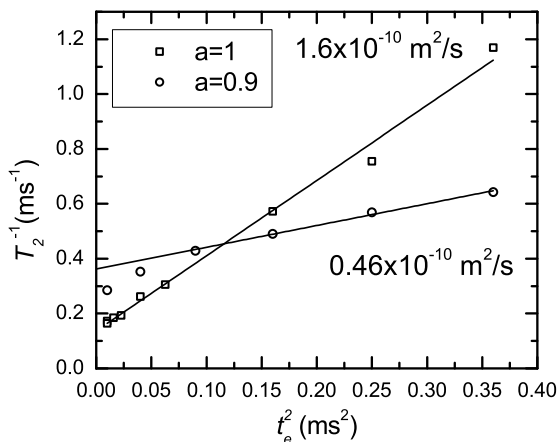
Fig. 5.5: The relaxivity of water in the base primary coat as a function of t_e^2. The base coat was fully saturated (a=1) (squares) and partially saturated (at a water activity $a = 0.9$) (circles). The dashed lines represent linear fit and fit with Eq. 3.8 for fully and partially saturated systems, respectively. Note, that the deviation of the data for $a = 1$ (circles) from the line is due to local molecular motions of water, characterized by T_{2S}, see Section 3.4.

of water of approximately $1.8 \times 10^{-10}\,\mathrm{m^2/s}$. This is only one decade less than the self-diffusion coefficient of water. This agrees with the observation in our previous study that in this particular system water very quickly redistributes in the base coat during water uptake [19]. The value $1.8 \times 10^{-10}\,\mathrm{m^2/s}$ of the self-diffusion coefficient of water in the fully wet base coat (26% w/w) is similar to values of the diffusivity of water in hydrated hydrogels (20-60% w/w) [72].

The relaxivity T_2^{-1} of water in the partially saturated base coat is shown in Figure 5.5 (circles). The relaxivity of the partially saturated system has a higher offset value. Further a linear dependency on t_e^2 is only observed for $t_e \geq 0.3\,\mathrm{ms}$. The slope of the curve in the linear regime equals $0.79 \times 10^9\,\mathrm{s^{-3}}$ and is smaller than the one of the fully saturated system. According to Eq. 3.10 this value corresponds to a self-diffusion coefficient of $0.5 \times 10^{-10}\,\mathrm{m^2/s}$, which is significantly lower than in the completely wet system. That the transition to the linear regime occurs at higher values of t_e than in the case of the completely wet system indicates that the correlation time τ_c for water molecules is longer in the partially saturated system. This is consistent with the increase in the offset.

Therefore, it is concluded that the self-diffusion coefficient of water increases with concentration of water in the polymer and that the binding of water to the polymer is

stronger at lower water concentrations. The dependency of the self-diffusion coefficient on water concentration is shown in Figure 5.6. The correlation time of the ^{1}H motions τ_c decreases with the water concentration.
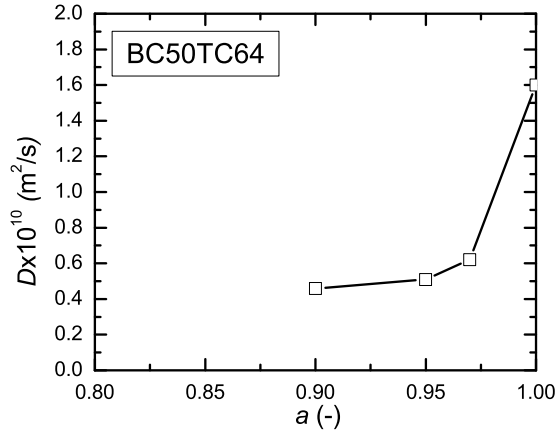

Fig. 5.6: Self-diffusion coefficient of water in the base coat (BC50TC64) as a function of water activity a in the base coat. The increase of the self-diffusion value with water activity indicate that water is highly mobile and less bonded when $a = 1$ than in the case when $a = 0.9$.

Another conclusion is that the diffusion of water in the field gradient does not explain the previously mentioned observation that T_2 time of water is lower than the T_2 time of the plasticized dispersant. Therefore, the ^{1}H nuclei of water should be present in the base coat at least in two environments, of which one has a low mobility. Further, there has to be a rapid exchange of ^{1}H between these environments. The first environment should be water in the dispersant. The possible candidates for the other environments may be exchangeable protons of the polymeric material (e.g. from hydroxyl, acid and amine groups) or of water molecules which are bounded.

5.3.3 Water and Polymer during Water Uptake

Now the spectra are understood, the evolution of the spectral components during water uptake can be analyzed. Tracking transient behavior of the water spectral component provides information about the amount of absorbed water in the base coat as a function of time. Analyzing the evolution of the spectral component of the dispersant in time gives insight in the process of plasticization during water uptake.
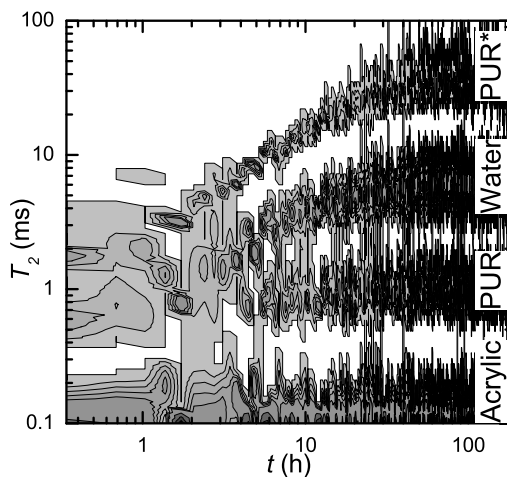
Fig. 5.7: A contour plot of the spectra of the base coat of the primary sample as a func-
tion of time during water uptake. The spectra are recorded with $t_e = 0.1$ ms.
PD abbreviation means polymeric dispersant, whereas PD* denotes plasticized
polymeric dispersant.

In Figure 5.7 T_2 spectra of the base coat are plotted as a function of time. The
contour plot starts with the spectrum of the dry sample as in Figure 5.2c, and evolves to
a 4-component spectrum characteristic for a wet sample, Figure 5.2a. Initially, several
components are overlapping in the T_2 range between 0.5 ms and 2 ms. From Figure 5.7
we conclude that T_2 values of the acrylic, PUR material and non-plasticized dispersant
do not vary, whereas the T_2 values of water and plasticized dispersant are increasing with
time.

The spectral component of water initially appears at $T_2 \sim 1$ ms. During the first 10
hours of uptake the T_2 value of water increases until it stabilizes at the spectral position
with $T_2 \simeq 6$ ms. The amount of water as a function of time was deduced from the change
in total intensity of the spectral components (Figure 5.8), since water is the only source
for new nuclei and the total number of the polymer ^{1}H nuclei is constant during uptake.
Fast initial and slow later stages of uptake are observed: half of the water is absorbed
during the first 10 hours, while an equilibrium is only reached after approximately 100
hours. The increase of T_2 indicates that the mobility of water also increases in time. Note
that these measurements were performed with a $t_e = 0.1$ ms and mainly T_{2S} is probed.

The T_2 value of the plasticized dispersant evolves in time from $T_2 \sim 1$ ms to the
value of $20 - 40$ ms during approximately 30 hours. The spectral component of plasti-
cized dispersant cannot be quantified during the first four hours due to initial overlap of
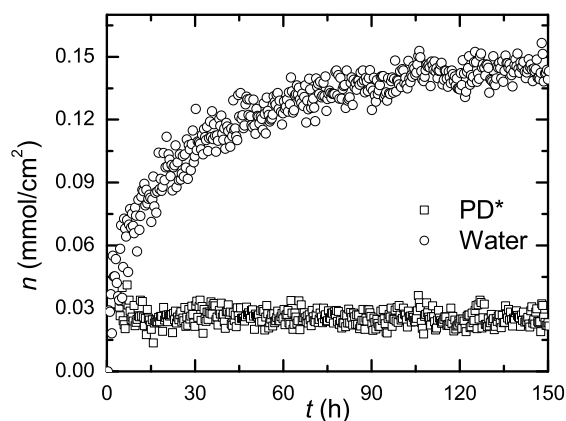
Fig. 5.8: The total intensities of water and plasticized dispersant components as a function of time during water uptake. PD* denotes plasticized polymeric dispersant. The datapoints for PD* start only after 4 hours. The fact, that it is already at the plateau means that all PD* protons are mobilized by water from the beginning.

PUR, dispersant and water spectral components. After four hours the total intensity of the plasticized dispersant is constant, see Figure 5.8. This indicates that all dispersant ^{1}H nuclei susceptible to mobilization are plasticized at low water content.

While the maximal amount of plasticized material has been reached within 4 hours, the process of mobilization of these nuclei proceeds up to 30 hours. This may be explained by the following: even small amounts of water are enough to mobilize all polymeric chains of the dispersant to a certain degree. With increasing water content the chains obtain more freedom for motions and their T_2 increases with the water content. To check, whether or not the T_2 is a unique function of the water content and there is no hysteresis, a drying sample was monitored. The drying process appears to be much faster than uptake ($t \leq 5$ h). The average T_2 values of plasticized dispersant both during uptake and drying were estimated. Figure 5.9 shows the T_2 of plasticized dispersant as a function of the amount of water both for uptake and drying. Note that there is no significant hysteresis between drying and uptake observed, indicating that there is a unique dependency of the dispersant mobility on the amount of penetrated water.
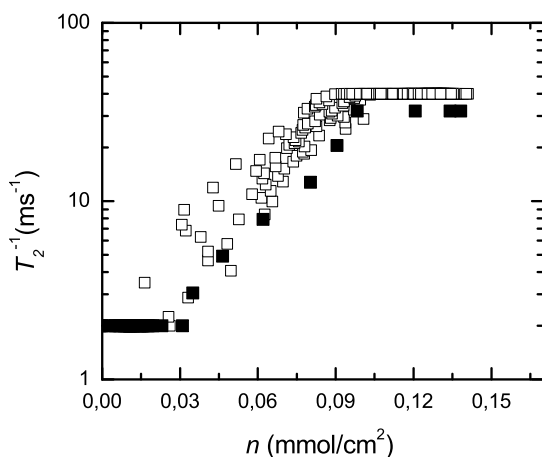
Fig. 5.9: The average relaxation time of the plasticized dispersant in the base coat as a
function of the amount of water in the base coat during uptake and drying. An
increase of the T_2 indicates an increase of the mobility of the polymeric disper-
sant.

5.4   Depicting the Uptake Process

Combining all results we suggest the following picture for the water uptake process, Fig-
ure 5.10. Water is attracted by hydrophilic areas of the polymer matrix like the shell of
the acrylic particles and the polymeric dispersant.

A large fraction the water molecules migrate into the hydrophilic PEO/PPO hairs of
the dispersant causing its plasticization. We suggest that the polymeric dispersant forms a
hydrophilic layer near the pigment surface. When water gets into the system it mobilizes
all polymeric chains in this layer. The increase of water content provides more freedom
for the polymer chains to move.

In addition, the hydrophilic dispersant is an important contributor to the water up-
take capacity of the base coat. The relaxation time of water suggests that its protons
exchange quickly between at least two environments.

5.5   Conclusions

In this chapter it has been shown that high resolution NMR imaging combined with NMR
relaxometry is a powerful technique for measuring water uptake in multilayered coatings
with multiphase polymer layers. In this particular case, water uptake in a two layer system
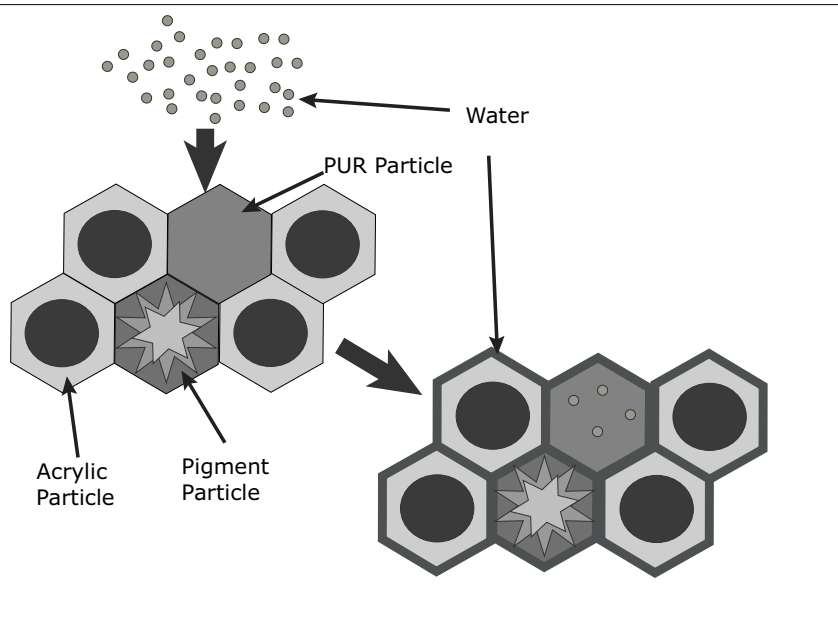
Fig. 5.10: Schematic picture of water uptake. Water is attracted by the hydrophilic elements of the polymer (e.g. hydrophilic shell of acrylic particles and polymeric dispersant), and occupies space between the particles. A large fraction of the water molecules migrate into the dispersant resulting in plasticization of the dispersant material.

that consisted of a highly crosslinked solventborne top coat and a waterborne base coat was studied. The relaxation analysis enabled to identify water and different polymeric compounds in the base coat.

The plasticization of the polymeric dispersant by water was observed, as the mobility of its ^{1}H nuclei increased. A significant number ^{1}H nuclei of the dispersant was mobilized during uptake. While this amount was plasticized within 4 hours, the mobility of these plasticized domains was still increasing during 30 hours.

In the considered systems, the self-diffusion coefficient of water in the base coat was estimated. When the base coat was partially saturated, the self-diffusion coefficient was about $0.5 \times 10^{-10}\,\mathrm{m^2/s}$, whereas in the fully saturated state the self-diffusion coefficient was $1.8 \times 10^{-10}\,\mathrm{m^2/s}$. This high value proves that water is highly mobile in the fully saturated base coat, whereas at lower concentrations water is stronger bonded to the polymer matrix of the base coat.

It is concluded that initially water is attracted by hydrophilic areas of the polymer

matrix, like the shell of the acrylic particles and hydrophilic PEO/PPO hairs of the disper-
sant. When the water content increases, water becomes mostly located in the hydrophilic
part of the dispersant and causes its plasticization and swelling. Thus, the sorption of wa-
ter in the base coat is mainly hydrogel formation of water with the polymeric dispersant.

Appendix: Benchmarking the Fit Procedure

To validate the fitting procedure, we have investigated the stability of the RILT fit with
respect to the signal-to-noise ratio (SNR) variations.
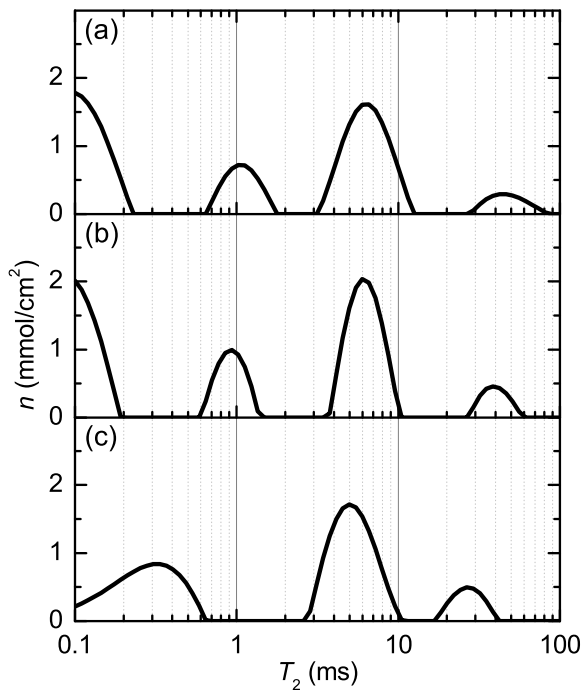
Fig. 5.11: The spectra of a wet base coat of the primary BC/TC sample for the original
data measured with 8192 averages (a), and the same data with artificial noise
added, (the SNR decreased by a factor of 3 (b) and 5 (c)).

Artificial noise was added to the original data, which decreases the SNR by factors
3 and 5. The spectra were obtained and compared with the original spectrum of the

sample, see Figure 5.11. A decrease of the SNR by a factor of three does not significantly change the number, positions and amplitudes of the T_2 components. If the SNR is five times smaller than in the original data, two components merge to one.

Note, that in this study relaxation measurements were performed with 8192 averages and uptake experiments with 2048, Figure 5.11a. Therefore, uptake experiments were performed with SNR, which is a factor of two lower than SNR in relaxation measurements. Our stability analysis indicates that the SNR during the uptake measurements is suitable for a proper resolution of the T_2 spectra.

6. Modeling Water Transport Kinetics

6.1 Introduction

In the previous chapters an empirical basis for understanding water uptake in a specific base coat/top coat systems has been obtained. It was found that water redistributes in the base coat instantly, i.e. becomes homogeneously distributed much quicker than the time resolution of the measurements. It was concluded that the rate of water transport is limited by penetration through the barrier, i.e. the top coat. Finally, it was concluded that the polymeric dispersant in the base coat plays a key role in water uptake by the coatings. The next step in the study of water uptake by two-layered systems is to develop a theoretical model connecting the properties of the sample and water transport kinetics. Presently, published studies have mostly focused on modeling water transport in single layer coatings.

This chapter introduces a model for water transport in the base coat/top coat systems. The presented theory describes the process as Fickian diffusion with constant diffusivity through the top coat to the base coat. The latter acts as an instantaneous reservoir. The chapter starts with a description of the conceptual model for water transport. The model includes the barrier properties of the top coat, which define the timescale of the process, and the base coat sorption isotherm, which defines the actual transport kinetics. The chapter proceeds with an investigation of the barrier properties of the top coat and verifies their relation with the timescale of the process. Further, the sorption isotherm of the base coat is studied on the basis of gravimetry. This compared with the isotherm, extracted from the uptake data via the model to confirm its role in defining the driving force of water transport. The state of water in the base coat, reflected by the shape of the isotherm is discussed. Finally, the ability of the model to predict water transport is verified by a comparison of water transport, simulated via the model, with the experimental data.

6.2 Experimental Details

6.2.1 Samples

The investigated polymeric systems are two-layered base coat/top coat systems. For a detailed description of the samples we refer to Section 4.2 in Chapter 4. Here, we

briefly summarize the sample composition and the sample preparation for the experiments. The base coats are waterborne physically dried systems which consists of 40% w/w acrylic particles, 20% w/w polyurethane (PUR) particles, 30% w/w DPP (di-keto-pyrrolo-pyrrole) pigment particles and 10% w/w polymeric dispersant in the sample. The acrylic particles have a glass transition temperature of ca. 25 °C and the glass transition temperature of the PUR particles is approximately equal to 0 °C.

The top coat is a 2-component solvent borne polyurethane coating with a glass transition temperature of approximately 60 °C. Experiments were performed at 25 °C. Consequently, the top coat is still in the glassy state, the acrylic particles of the base coat are at the transition between the rubbery and the glassy state, and PUR particles are in the rubbery state.

The coatings were prepared on glass slides of $18 \times 18 \, \text{mm}^2$ with various base coat and top coat thicknesses. An overview of studied samples is given in Table 6.1, in which BC and TC refer to the base coat and top coat, respectively. The numbers after BC or TC indicate the layer thicknesses in μm. The lateral dimensions of the films are equal to approximately $16 \times 16 \, \text{mm}^2$.

To place liquid in contact with the samples, a glass tube with a diameter of 1.1 cm was glued on the top of the coating/film (Figure 6.1). A marker at the bottom of the substrate was placed to trace deflections of the substrate and fluctuations due to instabilities of the setup.

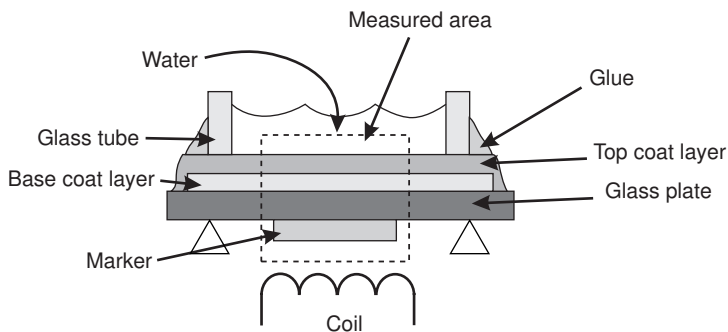*Fig. 6.1:* Schematic representation of the experimental set-up used for water uptake experiments.

6.2.2   NMR Measurements of Water in Coatings

In order to measure water content of the samples during water transport, high resolution imaging, based on the GARField approach [43] was used. The total amount of water in the base coat was estimated by integration over the base coat of water distribution profiles

Sample	BC thickness, (μm)	TC thickness, (μm)
BC25TC57	25	57
BC50TC23	50	23
BC50TC64	50	64
BC50TC73	50	73
BC50TC102	50	102

Tab. 6.1: The list of samples used in experiments. The letters BC and TC refer to the base coat and top coat, respectively. The numbers added to BC and TC represent the thickness of the layers in μm

measured by NMR imaging. For a detailed discussion of the signal analysis we refer to Section 4.4 and to our work [19]. In the measurements of water transport we have used the same settings as in Chapter 4. Water transport was measured as a function of the water activity in the environment. To vary the water activity experiments were performed with water, dry air and PEG (polyethylene glycol) aqueous solutions. With PEG the water activity of an aqueous solution can be regulated very accurately according to Ninni[69]. In case of pure liquid water, the water activity equals one, whereas with PEG solutions it can be set to lower values. For dry air, the water activity equals zero. Additionally, a dependency of water self-diffusion coefficient from the water activity was measured with NMR diffusometry. For the details of the procedure of water self-diffusion coefficient evaluation and the settings of NMR experiments we refer to Section 5.3.2 and our work [20].

6.3   Theory

6.3.1   Model

This section introduces a model for water transport in two-layered base coat/top coat systems, where the hydrophobic top coat has a barrier function and the hydrophilic base coat is an instantaneous reservoir. The latter means that water redistributes instantaneously in the base coat upon entering the layer.

The state of water can be described in terms of the chemical potential μ [J/mol] and the activity a, which are related as

$$\mu = \mu^+ + RT \ln a, \tag{6.1}$$

where μ^+ [J/mol] is the standard chemical potential. The description of the state of water requires knowledge of chemical potentials and activities in the environment a_{ex}, in the top coat a_{TC} and in the base coat a_{BC}. Water in the environment can be present as liquid, i.e.

either pure water ($a = 1$) or an aqueous solution ($a < 1$), or as vapour ($a < 1$). In the case of a vapour phase the activity is directly linked to the relative humidity: $RH = a \times 100\%$.

The top coat will act as a barrier only when it absorbs water in negligible quantities and water has a low diffusion constant in the top coat. Thus, water in the top coat is diluted, behaves ideally and the chemical potential of water $\mu_{TC}(x)$ [J/mol] at depth x [m] in the top coat can be related to its concentration $\rho(x)$ [mol/m^3] by the following expression

$$\mu_{TC}(x) = \mu^{+} + RT \ln \rho(x)/\rho_S , \tag{6.2}$$

where ρ_S [mol/m^3] is the maximal concentration of water in the top coat, when it is in contact with pure liquid water. Therefore, the activity of water in the top coat reads

$$a_{TC}(x) = \rho(x)/\rho_S . \tag{6.3}$$
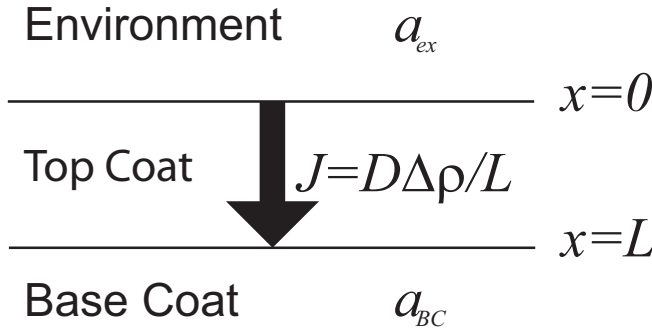
Fig. 6.2: A schematic of the 2-layered system with water on top of it. a_{ex} and a_{BC} are water activities in the environment and the base coat, respectively. J denote the water flux through the top coat, D is diffusivity of water in the top coat and L is the top coat thickness. $\triangle\rho$ is difference between the concentration at the top coat/environment interface and the top coat/base coat interface. x is the position in the top coat, which is distance from the top coat/environment interface.

As water behaves ideally the water flux J [mol/m^{2}s] is described by Fick's law with a constant diffusivity and the flux of water through the top coat reads

$$J = \frac{D}{L} \left[\rho(0) - \rho(L) \right] . \tag{6.4}$$

With the relationship in Eq. 6.3 means that flux in Eq. 6.4 can be rewritten as

$$J = \frac{D\rho_s}{L} \left[a_{TC}(0) - a_{TC}(L) \right] . \tag{6.5}$$

When the base coat acts as an instantaneous reservoir the water concentration and the water activity in the base coat are homogeneous during the water transport. This implies that the water activity is a unique function of the total water content in the base coat

$$a_{BC} \equiv a_{BC}(n/n_{max}) \tag{6.6}$$

where $n\,[\text{mol}]$ and $n_{max}\,[\text{mol}]$ are the total amount of water and the water uptake capacity of the base coat, respectively.

We assume that water instantaneously equilibrates at the interfaces. This implies the following boundary conditions: $a_{TC}(0) = a_{ex}$ for the TC/environment interface and $a_{TC}(L) = a_{BC}(n/n_{max})$ for the BC/TC interface.

The rate of change in the total amount of water in the base coat follows from the conservation law

$$\frac{dn}{dt} = AJ, \tag{6.7}$$

where $A\,[\text{m}^2]$ is the area of penetration

The combination of Eq. 6.5 and Eq. 6.7 results in the equation for water content in the base coat during water transport

$$\frac{dn/n_{max}}{dt} = \frac{1}{\tau}\left[a_{ex} - a_{BC}(n/n_{max})\right], \tag{6.8}$$

where the timescale τ assimilates both characteristics of the top coat (D, ρ_S, L) and the base coat (n_{max})

$$\tau = \frac{Ln_{max}}{AD\rho_s} \tag{6.9}$$

Note, that $D\rho_S$ equals the permeability [12] of the top coat to water.

According to the model, water uptake in the systems of interest is governed by two system-related parameters: the timescale τ, which is determined by the barrier properties of the top coat and the capacity of the base coat (Eq. 6.9) and the inverse sorption isotherm of the base coat $a_{BC}(n/n_{max})$. The way, how the parameter τ is present in the transport equation (Eq. 6.8), implies that it defines the timescale of the process. The inverse isotherm $a_{BC}(n/n_{max})$ defines the transport process kinetics (i.e. time dependency of the water content $n(t/\tau)$), in particular the sorption and desorption kinetics.

6.3.2 Influence Sorption Isotherms on Water Transport Kinetics

To explore how the shape of the sorption isotherms influences the transport kinetics, typical isotherms for polymeric materials, were used to simulate uptake ($a_{ex} = 1$) and drying
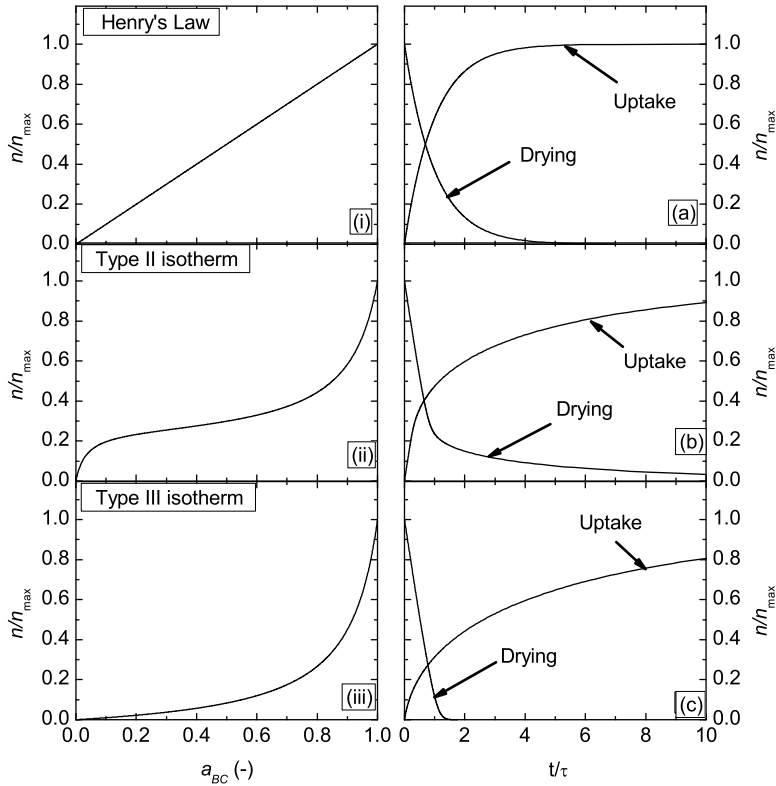
Fig. 6.3: Left side: The sorption isotherms typically observed for polymeric materials: linear isotherm, described by Henry's law (i), Type II (ii) and Type III (iii) isotherms, according to BET classification [21]. Right side: Uptake and drying kinetics, simulated by the model for systems with linear (a), Type II (b) and Type III (c) isotherms. τ is the timescale of the process (Eq. 6.9), introduced by the model. Note, that the drying occurs at much faster rate than the uptake for the systems with the non-linear isotherms.

$(a_{ex} = 0)$: ideal, Type II and Type III isotherms. For a detailed discussion of the physics of the isotherm types we refer to Section 2.2. Eq. 6.8 was integrated numerically to obtain

n/n_{max} as a function of t/τ for each isotherm (Figure 6.3).

For the ideal case, Henry's law, the sorption and desorption kinetics are symmetric. Type II and III isotherms result in slow uptake and fast drying. The drying process for system with Type II isotherm features a slow rate later stage, which is absent in Type III systems. This is due to the fact that in case of Type II isotherm drying is slow at low water activities as the shape of the isotherm at low activities result in much smaller driving force then for Type III isotherm.

The slow uptake rates in Type II and Type III systems are a result of the low driving force at high water activities, combined with the large amount of water. The fast drying rate is because high driving force is maintained during a major part of the drying process. Note, that hydrophilic polymers usually have Type II or Type III isotherms.

6.3.3 Measuring the Barrier: D_2O/H_2O exchange

The permeability of the top coat in a two-layered system can be measured with a D_2O/H_2O exchange experiment. This section discusses the theory behind this experiment, based on the model, formulated in Section 6.3.1.

In the D_2O/H_2O exchange experiment a sample is saturated with water and then is placed in a liquid environment with heavy water. The water exchanges with heavy water through the top coat between the saturated heavy water environment and mixture of H_2O and D_2O in the base coat. When Fickian diffusion with a constant diffusivity of water in the top coat is assumed, this process can described with Eq. 6.8. If water and heavy water behave identically in the base coat, the energy of water molecules in the mixture is independent on proportions of H_2O and D_2O. This means that H_2O/D_2O mixture in the base coat is an ideal mixture [73]. As a result, the water activity in this mixture is linear with water content: $a_{BC} = n/n_{max}$.

As the environment considered to be an infinite reservoir of heavy water, its water activity $a_{ex} = 0$. Thus, the solution of Eq. 6.8 for the system, initially saturated by water ($n(0) = n_{max}$) and subsequently exposed to heavy water, reads

$$n \equiv n_{max} \exp\left(-\frac{t}{\tau}\right) , \qquad (6.10)$$

where τ is the timescale for water transport (Eq. 6.9).

The amount of water can be measured with NMR. Due to the fact that protons and deuterons have significantly different NMR frequencies, only water is probed in such experiment.

6.4   Results

6.4.1   Barrier Properties of the Top Coat

Understanding water transport in the top coat requires knowledge about the effect of top coat properties on water diffusion in the film. In this section water permeation through the top coat and the barrier properties of the top coat is investigated at room temperature.

First, the water permeability of the top coat is investigated with wet cup measurements on a free film. Glass cups with an area $A = 0.95\,\text{cm}^2$ were filled with water and sealed with top coat free films of various thicknesses. The cups were exposed to environments with various water activities a_{ex}. Saturated aqueous solutions of various salts were used to create the proper environments with respect to the relative humidity. The mass change $\triangle m$ was measured with a Mettler-Toledo AX205DR analytical balance after exposure of the cups to a specific environment with a duration of $\triangle t$. The typical durations of the exposure $\triangle t$ were in the order of few days. The flux of water $J = \triangle m \triangle t^{-1} A^{-1} M^{-1}$ was measured as a function of difference of water activities over the films (where $M = 18\,\text{g/mol}$ is the molar mass of water). In the case of Fickian permeation through the film with a constant diffusivity, the flux reads

$$J = \frac{D\rho_S}{L}\triangle a, \tag{6.11}$$

where $\triangle a$ is the difference of water activity over the film. Note, that there is a unit activity, i.e. $a = 1$ inside the cups.

Figure 6.4 shows the measured fluxes for different samples as a function of the water activity difference in the wet cup experiments. Linear relationships are observed for all samples, proving that water permeates through the top coats via Fickian diffusion with a constant diffusion coefficient. From the slopes of the lines, permeabilities of the top coats can be estimated via Eq. 6.11: $D\rho_S \simeq (1.2 \pm 0.3) \times 10^{-9}\,\text{mol}\,\text{m}^{-1}\text{s}^{-1}$.

Further, to investigate how the presence of the base coat influences the top coat properties, the wet cup experiment were also performed on a BC50TC64 free film, see Figure 6.4. The film was fixed with the top coat facing the cup. It is assumed that the base coat permeability is much higher than of the top coat and the flux is determined by the permeability of the top coat.

The permeability of the top coat in BC50TC64 $D\rho_S$ equals $5 \times 10^{-9}\,\text{mol}\,\text{m}^{-1}\text{s}^{-1}$. Note, that this value is significantly higher than the permeability of free film top coats. This indicates that there is an interaction between the layers which results in the weaker barrier properties of the top coat when it is applied over the base coat in the two-layered systems. A possible explanation can be a crosslinker migration from the top coat to the base coat, which is known for this type of systems [74]. The loss of the crosslinker by the top coat results in its higher permeability.

As water transports in the top coats via Fickian diffusion with a constant diffusiv-
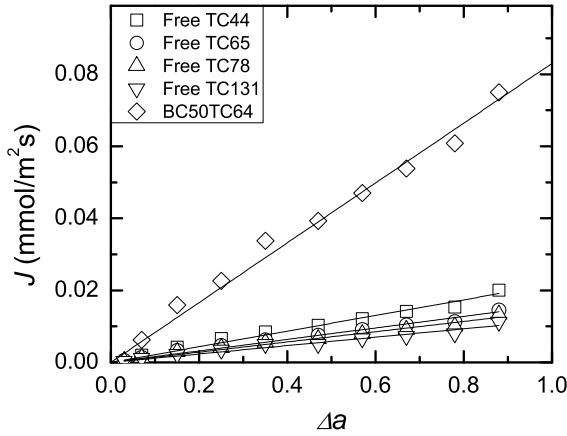
Fig. 6.4: Flux through the top coat as a function of water activity difference over the free film top coats and the free film two-layered system. The abbreviations BC and TC mean base coat and top coat, respectively. The numbers after the abbreviations denote the layer thickness in μm. It is assumed that the flux through the BC50TC64 free film is determined by the permeation through the top coat only, as water diffuses in the base coat much faster, than in the top coat. Note, that the flux through the top coat in BC50TC64 is much higher than the flux in the free film top coats of a comparable thicknesses.

ity, the barrier properties and timescale of water transport can be assessed via D_2O/H_2O exchange experiment. The amount of water in the base coats was measured for every base coat/top coat sample during the exchange. Figure 6.5 shows the total amount of water in the base coat as a function of time as measured by NMR imaging.

Sample	$\tau\,(\mathrm{h})$	$n_{max}/A\,(\mathrm{mmol/cm^2})$	f
BC25TC57	1.56	0.031	0.9
BC50TC23	1.77	0.086	0.96
BC50TC64	3.38	0.077	0.93
BC50TC73	3.47	0.068	0.93
BC50TC102	3.75	0.054	0.88

Tab. 6.2: The timescales of water transport τ, uptake capacities n_{max} of the base coats and the parameter f, which characterize the difference between water in the base coat and liquid water. The parameter f is discussed in the next section.
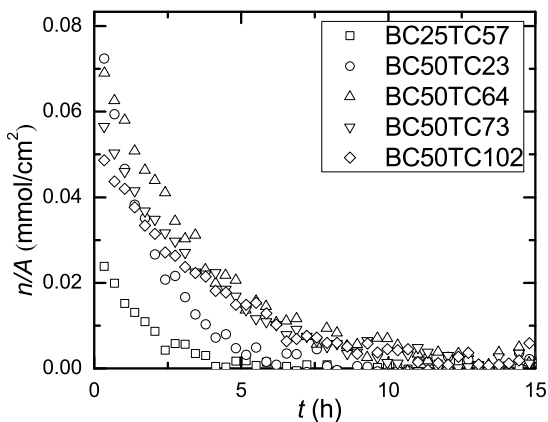
Fig. 6.5: The water content in a base coat n/A as a function of time t during H_2O/D_2O exchange experiments for different BC/TC systems.

Fig. 6.6: The product of parameters $\tau A/n_{max}$ of the samples as a function of the top coat thickness. The linear dependency verifies the relation in Eq. 6.9. From the slope the permeability of the top coat can be estimated.

By fitting this data with Eq. 6.10, values for τ and n_{max} are obtained (Table 6.2). The ratio τ/n_{max} appears to be proportional to L (Figure 6.6), which confirms Eq. 6.9. This

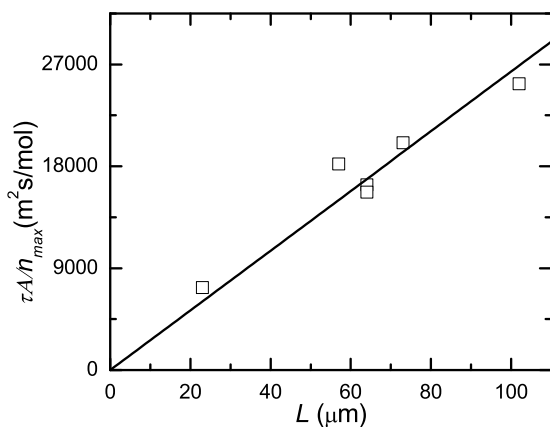means that the permeability of the top coats in two-layered systems does not varies much between the various samples and top coat thicknesses. From the linear fit of these values in Figure 6.6 the permeability $D\rho_S$ is estimated via Eq. 6.9: $4 \pm 1.6 \times 10^{-9}\,\text{gm}^{-1}\text{s}^{-1}$. This value is in line with the permeability, estimated from the wet cup experiment with the sample BC50TC64. A clear advantage of D_2O/H_2O exchange method over wet cup experiment is the time needed for the experiment: hours for the exchange vs. days for the wet cup measurements.

Both the wet cup experiments and the D_2O/H_2O exchange experiments show that the top coats in two-layered samples have significantly higher permeabilities than the free films top coats. The higher permeability of the top coat layers can be a result of crosslinker migration to the base coat [74]. As a result the crosslink density in a free film top coat is higher than in the top coat in the base coat/top coat film, resulting in higher permeability of the latter one.

6.4.2   Sorption Isotherms of the Base Coat

Understanding the water transport kinetics requires the knowledge of the sorption isotherms of the base coats. The shape of the sorption isotherm reflects how water is present in the system. In this section the sorption isotherms of the base coats are studied with the help of gravimetry and NMR uptake measurements.

We start with the sorption isotherm of the base coat in the two-layered system BC50TC64. The sorption isotherm of this sample was obtained gravimetrically, by measuring its mass under equilibrium at various water activities. The contribution of water in the top coat to the mass change was neglected, as most of the water is absorbed by the base coat. The measurements were performed with a Mettler-Toledo AX205DR analytical balance. Figure 6.7 shows the desorption and sorption isotherms of BC50TC64. Their shape is close to one other, therefore it is concluded that there is no significant hysteresis between sorption and desorption. Their shape is typical for Type III isotherms according to the B.E.T. classification [21] and reflects a process of water clusters formation in the base coat. Note, that while the small plateau in the data points at low water activities is typical for Type II isotherms, we do not consider it as significant as it less than the experimental error. Type III isotherms can be described by the so-called Guggenheim-Anderson-De Boer (GAB) expression [75, 76]. We adopt the isotherm model under the assumption that there is no difference between initially absorbed water and water in clusters

$$\frac{n}{n_{max}} = \frac{1-f}{f}\frac{f \cdot a_{BC}}{1 - f \cdot a_{BC}} \tag{6.12}$$

where f refers to the difference between clustered water in polymer and liquid water $f = \exp\left[(\triangle g)/RT\right]$, where $\triangle g\,[\text{J/mol}]$ describes the difference between of the free energies per molecule, when it is absorbed to a cluster or when it condenses in liquid water. Note,
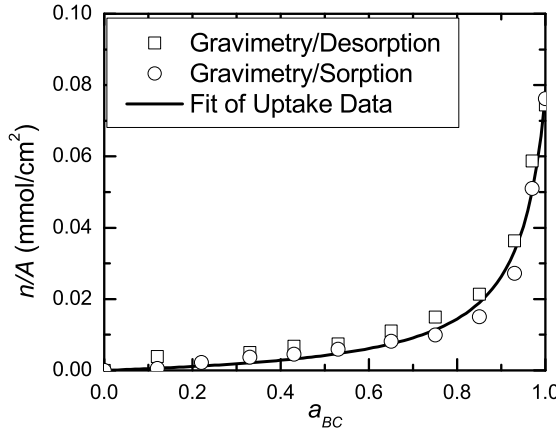
Fig. 6.7: Sorption (circles) and desorption (squares) isotherms of BC50/TC64 obtained by gravimetry and by fitting analytical solution (Eq. 6.14)the uptake data. There is no significant hysteresis between sorption and desorption isotherms. The shape of the isotherm is typical for Type III isotherm, indicating clustering of water in the base coat.

that when $f = 1$, there is unlimited amount of water in the sample at $a = 1$, resulting in infinite dilution of the base coat. When f is less than one, water sorption is limited by various processes, e.g. by swelling stress: $\triangle g = \sigma v_1$ where σ is the stress generated by polymer as a response to the creation of extra volume v_1 when a new water molecule enters the polymer.

When the sorption isotherm is described by Eq. 6.12, Eq. 6.8 can be solved analytically for water transport. The solution for the initial condition $n(0) = n_0$ reads

$$\frac{t}{\tau} = -\frac{f}{1 - f \cdot a_{ex}} \left[\frac{n - n_0}{n_{max}} + \frac{1 - f}{f} \frac{1}{1 - f \cdot a_{ex}} \right.$$
$$\left. \times \ln \frac{a_{ex}(1 - f[1 - n/n_{max}]) - n/n_{max}}{a_{ex}(1 - f[1 - n_0/n_{max}]) - n_0/n_{max}} \right] \tag{6.13}$$

For water uptake ($n(0) = 0$, $a_{ex} = 1$) the solution reads

$$\frac{t}{\tau} = -\frac{1}{1/f - 1} \left[n/n_{max} + 1/f \ln(1 - n/n_{max}) \right] \tag{6.14}$$

By fitting this solution to the water uptake data in Chapter 4 (Figure 4.7) the parameter f can be retrieved and isotherms can be recovered. The isotherm of BC50TC64,
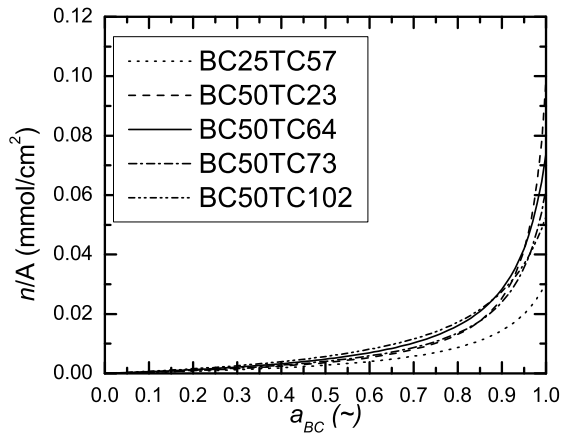
Fig. 6.8: The sorption isotherms for all samples as described by Eq. 6.12 with parameters obtained from the uptake data. There is no significant variation in the shapes of the isotherms of the different samples.

obtained via fitting Eq. 6.14 to the water uptake data, is shown by the solid line in Figure 6.7. It is in a good agreement with the gravimetric isotherm. This confirms that the driving force for uptake is determined purely by the sorption isotherm.

The results of the fit for all other samples are shown by Figure 6.8. The f parameter for the isotherms varies between 0.88 and 0.96, which are typical values for water in polymers [77, 78, 27]. The parameters are listed in Table 6.2 and point to difference between water in the base coats and liquid water. Note, that while there is a tendency of decrease of f for the samples with thicker top coats. While the accuracy of the fit does not allow to conclude about this trend, the possible explanation can be bigger stresses exerted on clusters in the samples with thicker top coats.

The combination of the observed isotherms and concentration dependence of the self-diffusion coefficient, reported in Section 5.3.2, supports the conclusion that water is present as clusters in the polymer matrix of the base coat. An increase of the cluster size results in an increase of the self-diffusion coefficient, since water has more mobility in bigger clusters. The maximal water content in the base coat is limited, probably by the stress induced by the polymer matrix on growing clusters.

6.4.3   Prediction of Transport

To verify the ability of the model to predict water transport, the water transport in the sample BC50TC64 at different external water activities is measured with NMR and simulated with Eq. 6.8 on the basis of the sorption isotherm in Figure 6.7. The fitted sorption has been used in the simulations, which were performed with analytical solution for water transport (Eq. 6.13).

First, a drying experiment is performed with $a_{ex} = 0$ (RH$\simeq$ 0%). Initially, the base coat is fully saturated. The amount of water in the base coat during drying is shown in Figure 6.9. The rate of drying is much faster than the uptake rate: a few hours for drying compared to several days for uptake. This asymmetry is due to the non-linear shape of the sorption isotherm. Additionally, the response of the sample on a switch of water activity

Before experiment	During experiment
1	0.95
0.95	0.9
0.9	0.8
1	0

Tab. 6.3: Water activities before and during the experiment and in simulations.

was simulated and measured with NMR imaging. The water activity was adjusted by using aqueous PEG solutions. The changes of water activities in the various experiments are shown in Table 6.3. The results are shown in Figure 6.9. The simulated curves are in good agreement with the experimental data, proving that the model put forward in this chapter is correct and can predict the transient water content of the base coat under various conditions on the basis of the top coat barrier properties and the base coat sorption isotherm.

6.5   Conclusions

This chapter has shown that water transport in two-layered organic coatings, composed of hydrophilic base coats and hydrophobic top coats, can be understood on the basis of the top coat permeability and the base coat sorption isotherms. A theoretical model for water transport in the considered systems was introduced and verified. The model described the relation between the top coat permeability to water, the base coat sorption isotherm and water transport kinetics. In this model, the top coat permeability determines the transport timescale and the base coat sorption isotherm defines the driving force of transport, and thus the water content in the base coat as function of time.

It was shown that polymeric systems with a non-linear base coat sorption isotherms will have a faster drying rate than the uptake rate. In contrast, systems with linear sorption
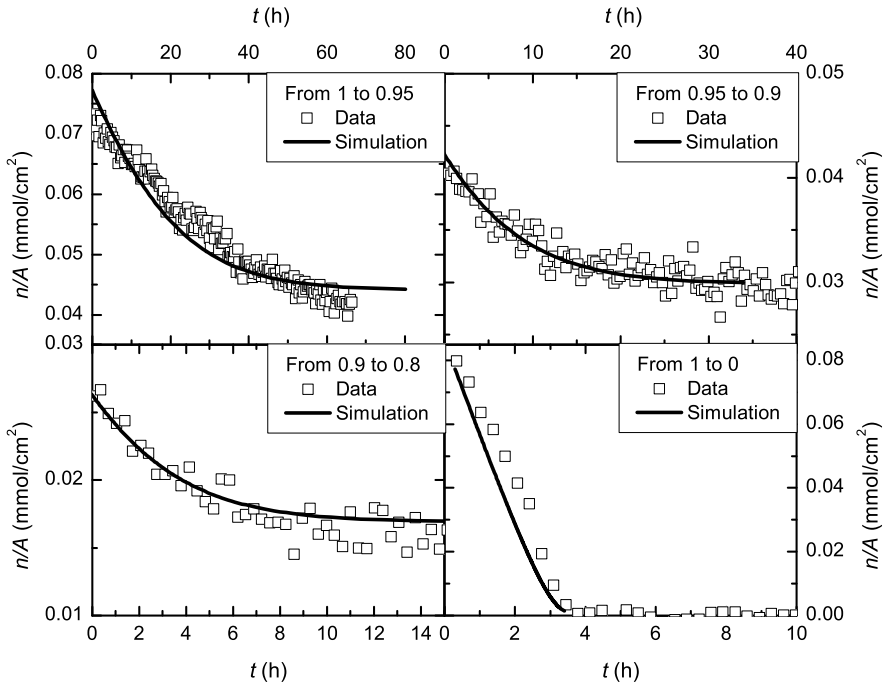
Fig. 6.9: Amount of water in the base coat of BC50TC64 during desorption processes. The results of the simulations with the model are shown with solid lines, whereas the NMR data is shown by squares.

isotherms, which obey Henry's lay, show a symmetry between the time dependencies of uptake and drying.

It was found in the study of the top coat barrier properties that the interplay between the layers results in reduction of the top coat barrier properties. The permeability to water of the top coat in two-layered systems was approximately 4 times higher that of free film top coats. Additionally, the introduced D_2O/H_2O experiment proved to be a fast method to estimate the top coat permeabilities.

The study of sorption isotherms of the base coats in the systems of interest has shown that water absorption is a process of water clustering in the base coats. This conclusion is supported by the concentration dependency of water self-diffusion coefficient in the base coat, which was measured in Chapter 5.

Practically, these findings mean that to understand water transport kinetics in the

considered of two-layered coating systems, it is sufficient to measure the top coat permeability to water and the sorption isotherm of the system. The introduced model can be used to predict water transport kinetics on the basis of these parameters, which are easy to measure with balance and wet cup experiments. This is an important result, because it enables an efficient screening of the water uptake properties in practice.

7. Water Transport and Humidity Fluctuations

7.1   Introduction

Coatings are frequently applied in multiple layers with distinct properties to meet the required specifications. During their service these systems are exposed to UV light, humidity and heat, resulting in weathering and reduction of their lifetime[79, 80]. The failure of systems subjected to weathering occurs as a result of a complex interplay of UV exposure, temperature and humidity. Water can be present in the form of water vapor or liquid, e.g. rain or dew, and can promote deterioration of coatings, both as a single factor and in combination with UV light and heat. Carfagna et al. [81] showed how hygrothermal aging affects mechanical properties of epoxy-based coatings. Martin et al. [82] and Nguyen et al. [83, 84, 85] concluded that water damages acrylic melamine coatings both alone and in combination with UV light and heat during artificial and natural weathering.

Natural, accelerated and artificial weathering exposures are standard durability tests for polymeric materials [79, 80, 86]. Natural weathering means that samples are subjected to natural conditions, i.e. direct sunlight, ambient outdoor temperature and moisture. Accelerated and artificial weathering are applied to perform durability tests in a shorter time than in natural weathering tests. Accelerated weathering tests are performed outdoor, like natural weathering tests, with the sole difference that the timescale of exposure is accelerated by concentrating natural sunlight and by applying artificial heating and cooling, wetting and drying of the samples. Artificial weathering tests are performed under laboratory exposure of the samples to artificial UV light, heat and water. Natural weathering includes a broad range of timescales, e.g. rainfall and day/night cycles introduce typical timescales in the order of hours and days, while humidity variations due to seasonal change have timescales in the order of months. In accelerated and artificial weathering, typical timescales are usually in the order of hours [80, 87]. Shi et al. [88] pointed out that results from accelerated tests may differ from natural weathering if the exposure cycles to water in accelerated tests become shorter than the drying timescale. In such case water accumulates in the sample, which would not occur in natural weathering conditions. Since moisture significantly contributes to weathering, understanding how the frequency of ambient humidity fluctuations influences the water migration in multilayer coatings is crucial.

This thesis is mostly focused on water transport in hydrophilic base coat/hydrophobic

top coat systems. In Chapter 4 it was found that the transport rate is limited by the penetration rate through the top coat and that water causes significant swelling of the base coat. Chapter 5 has shown that polymeric dispersant in the base coat plays a key role in promoting water uptake. Water plasticizes the dispersant and forms a hydrogel with the dispersant. Chapter 6 proved that in this type of multilayer coating can be described on the sole basis of the top coat permeability and the base coat sorption isotherm, accordingly to an introduced theoretical model. The top coat permeability determines the typical timescale of water transport and the sorption isotherm defines the process kinetics. This theoretical model can be used to investigate the response of the systems of interest to ambient time-dependent humidity fluctuations.

The present chapter aims to gain insight in the influence of the layer properties of base coat/top coat systems on the multilayer coating response to humidity fluctuations. A basic description of the fluctuations is introduced in the model, in which the fluctuations are considered as harmonic oscillations of water activity. Special attention will be paid to the influence of the shape of the base coat sorption isotherm on the response to fluctuations. In order to understand the physics of the response, a linear model will be discussed, which is applicable in case that the sorption isotherm is linear or the amplitude of the humidity fluctuations is small. Second, a full non-linear model will be studied to understand its consequences on the response.

7.2   Theory

7.2.1   Model

The aim of this section is to formulate a model for water transport in 2-layered coatings with hydrophilic base coats and hydrophobic top coats that are subjected to time-dependent humidity fluctuations. Specifically, the water content of the base coat $\theta \equiv n/n_{max}$ is considered, where $n\,[\text{mol}]$ and $n_{max}\,[\text{mol}]$ are the actual amount of water in the base coat and the water uptake capacity of the base coat, respectively. The rate of change of the water content in the base coat can be connected with the difference in water activity in the environment a_{ex} and in the base coat a_{BC}, see Eq. 6.8. The time-dependency of the water activity is taken into account by making a_{ex} in Eq. 6.8 time dependent:

$$\frac{d\theta}{dt} = \frac{1}{\tau}\left[a_{ex}(t) - a_{BC}(\theta)\right],\tag{7.1}$$

where $a_{BC}(\theta)$ is the inverse sorption isotherm of the base coat and $\tau \equiv n_{max}L/AD\rho_S$ is the timescale of water transport, see Eq. 6.9. $L\,[\text{m}]$ is the thickness of the top coat, $A\,[\text{m}^2]$ is area of water penetration and $D\rho_S\,[\text{mol}\cdot\text{m}^{-1}\text{s}^{-1}]$ is the permeability to water of the top coat.

In this study the fluctuations of water activity in the environment are modeled as harmonic oscillations

$$a_{ex}(t) = a_0 + \triangle a \sin \omega t \,, \tag{7.2}$$

where a_0 is the average external water activity and $\triangle a$ and ω are the amplitude and radial frequency of the water activity fluctuations, respectively. Note, that the activity varies by definition between 0 and 1. Consequently, this restricts the parameters: $\triangle a \leq a_0$ and $\triangle a \leq 1 - a_0$. Fluctuations in the water activity can be characterized by the average water activity a_0, the activity range $2\triangle a$ and their period $2\pi/\omega$. It is to be mentioned that every fluctuation can be decomposed in harmonic functions of the type of Eq. 7.2.

7.2.2 Systems with linearized sorption isotherms: Understanding the Response

First, to understand the physics of the response to the activity fluctuations, we investigate with linearized sorption isotherms. Linearizing the problem allows to obtain an analytical solution for water content of the base coat during fluctuations and to get insight into how the layers properties influence the response to the fluctuations.

A linear sorption isotherm can be written as follows

$$\theta = k a_{BC} \,, \tag{7.3}$$

where k is the solubility of water in the base coat. By combining Eq. 7.1, 7.2 and 7.3 the following expression for the water content oscillations are obtained

$$\theta(t) = \theta_0 + \frac{k\triangle a}{\sqrt{1 + \omega^2 \tau^2 k^2}} \sin\left(\omega t - \arctan \omega \tau k\right) \tag{7.4}$$

where $\theta_0 \equiv k a_0$ is the water content, when the system is in equilibrium with the average water activity a_0. The water content in the base coat varies as a sine function with a phase delay of $\phi = \arctan \omega \tau k$.

The amplitude of the oscillations is proportional to the amplitude of the activity fluctuations and the factor $1/\sqrt{1 + \omega^2 \tau^2 k^2}$ describes the damping of the oscillations, see Figure 7.1. Note that $k\triangle a$ equals the amplitude of the water content fluctuations solely when the base coat is able to responde instantly to the environment. The damping is due to the inertia of the system, which is determined by τk. Note the similarity with a RC-circuit, where the top coat has the role ofresistor and the base coat plays the role of capacitor. An increase of τ results in a higher inertia of the sample, since it takes longer for water to permeate through the top coat. An increase in the solubility in the base coat k leads to a decrease in the amplitude since more water has to be stored. When the radial frequency of the fluctuations becomes in order $1/\tau k$ a transition between damped and non-damped oscillations occurs and vice versa. Thus, the damping occurs for oscillations with periods much less than the transition point $T^* \equiv 2\pi \tau k$.
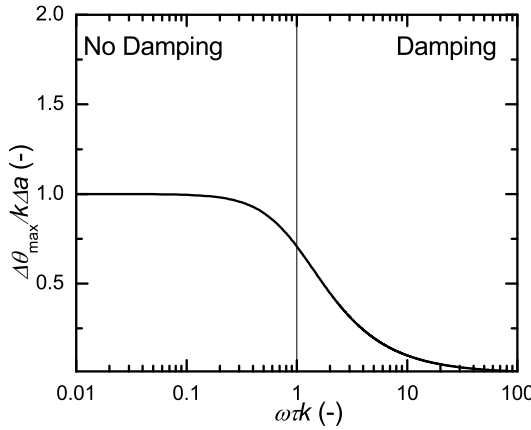
Fig. 7.1: The damping of the amplitude of water content oscillations for the sample with a linearized isotherm. The transition from the damping to no damping mode occurs when the radial frequency of the oscillations is in the order of $1/\tau k$, which is denoted by the vertical line. This means that the product of the timescale τ and the solubility k define the response time to the activity fluctuations of multilayer coatings.

7.2.3 Non-linear systems subjected to small fluctuations

Now, when the response of the base coat/top coat systems to the activity fluctuations with the linearized isotherm is understood and the role of the layers properties is established, the response of the systems with non-linear sorption isotherms to activity fluctuations with small amplitudes

For small water content fluctuations $\triangle\theta$, the inverse non-linear sorption isotherm $a_{BC}(\theta)$ can be written as follows

$$a_{BC} \simeq a_0 + \frac{1}{k'(a_0)}\triangle\theta - \frac{1}{2k'(a_0)^3}\frac{dk'(a_0)}{da_{BC}}\triangle\theta^2 + O(3) \tag{7.5}$$

where $k'(a_0) \equiv (d\theta/da_{BC})_{a_{BC}=a_0}$ is the differential solubility of water in the base coat at a certain water activity. A linear approximation for a non-linear isotherm can be used as long as the second order term can be neglected. Here, we introduce the relative error ε of the linear approximation, which is defined as the ratio of second and first order terms in Eq. 7.5

$$\varepsilon \equiv \frac{1}{2k'(a_0)^2}\left(\frac{dk'}{da_{BC}}\right)_{a_{BC}=a_0}|\triangle\theta| \tag{7.6}$$

By definition, this parameter should be small: $\varepsilon \ll 1$, implying that a linear approximation can be used, when there is little variation in the differential solubility in the considered activity range.

When the linear approximation holds, the fluctuations of water content can be described with Eq. 7.4, where the constant solubility k has to be replaced by the differential solubility $k'(a_0)$. Since the maximal amplitude of water content fluctuations $\triangle\theta_{max}$ for the linear solution reads $k'(a_0)\triangle a/\sqrt{1+\omega^2\tau^2 k'^2(a_0)}$, Eq. 7.6 can be used to formulate a criterion for judging whether the humidity fluctuations are small enough to use a linearized approach can be used

$$\frac{\triangle a}{\varepsilon} = 2k'(a_0)\left(\frac{dk'}{da_{BC}}\right)^{-1}_{a_{BC}/=a_0}\sqrt{(1+\omega^2\tau^2 k'(a_0)^2)}. \tag{7.7}$$

This condition defines what values of the activity amplitude $\triangle a_0$ are acceptable for using the linear approximation. The condition is visualized in Figure 7.2, where the shaded region shows the amplitude values $\triangle a$ as a function of the radial frequency, which result in a relative error less than ε in case of using the linear approximation. The linear approximation can always be used for damped oscillations, because the water content variation in the sample becomes smaller at higher frequencies leading to a smaller relative error. If the solubility varies little with water activity, thus the plateau $2k'(a_0)\left(dk'/da_{BC}\right)^{-1}_{a_{BC}=a_0}$ will have higher values allowing to use linear solution at a broader range of values for humidity fluctuations amplitude.

Regarding the frequency dependence, there are two modes of oscillations: damped and non-damped. The damped mode occurs at high frequencies, for $\omega \gg 1/\tau k'(a_0)$ the oscillations are damped. In this case the condition in Eq. 7.7 is met because the damping at high frequencies will result in small water content variations. In this case the solution for the water content is described by Eq. 7.4 with $k = k'(a_0)$. For low frequencies, $\omega \ll 1/\tau k'(a_0)$, when the period of humidity oscillations $2\pi/\omega$ is less than the response time $2\pi\tau k'(a_0)$, needed for the base coat to equilibrate with the environment, no damping will occur. In this case the solution for the water content reads

$$\theta(t) = \theta(a_{BC})|_{a_{BC}=a_{ex}(t)}. \tag{7.8}$$

7.3 Behavior of BC/TC systems

The aim of this section is to investigate how specific type of systems of interest, i.e. the base coat/top coat systems, respond to humidity fluctuations. First, a brief description of the samples is given. Further, the analysis, presented in the previous sections, is applied to the systems and the response of the samples when variation of differential solubility is significant.
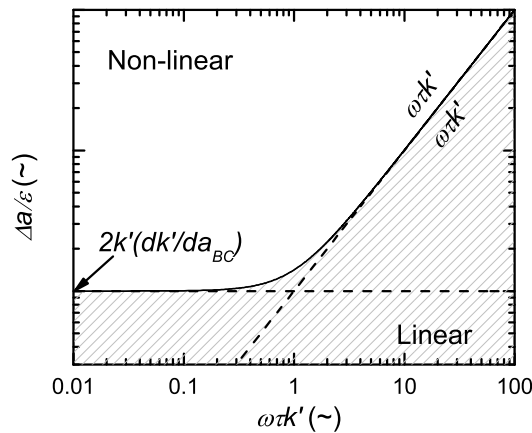
Fig. 7.2: The diagram showing whether values of external water activity fluctuation $\triangle a$ are small enough to use linear approximation is valid. ε defines the relative error of using the linearized approach. For example, if only 10% error is tolerated, $\varepsilon = 0.1$. The linear approach can be used only if $\triangle a/\varepsilon$ is in the shaded area under the solid line. The increase of the tolerated values of $\triangle a$ with the frequency means that due to damping, linear solution can be used for the high frequency fluctuations.

7.3.1 Sample Description

Although this chapter is devoted to a theoretical analysis, the theory will be applied on the systems of interest in this thesis, i.e. a two-layered hydrophilic base coat/hydrophobic top coat systems. Therefore, the most important features of these systems are briefly summarized. For a more detailed description of the composition of these samples, we refer to Section 4.2 of the thesis. The base coat of the considered systems is a waterborne physically dried system, consisting of 40% w/w acrylic particles, 20% w/w polyurethane (PUR) particles, 30% w/w DPP (di-keto-pyrrolo-pyrrole) pigment particles and 10% w/w polymeric dispersant in the sample. The glass transition temperatures are 25 °C and 0 °C for acrylic and PUR particles, respectively. The top coat is a solventborne highly crosslinked acrylic PUR layer with a glass transition temperature of ca. 60 °C.

In this chapter we focus on one specific sample to demonstrate how the results of the investigation apply to a practical reals system, BC50TC64. For the numerical simulations the parameters of the sample were used, see Table 7.1. In this table BC and TC refer to base coat and top coat, respectively and the numbers after BC or TC are the layer thicknesses in μm.

For the systems of interest, it was found that the sorption isotherm of the base coat is of Type III, implying that water sorption in the base coat is the consequence of water clusters formation. This sorption isotherm can be described by the Guggenheim-Anderson-De Boer equation [75, 76]

$$\theta \equiv \frac{n}{n_{max}} = (1/f - 1)\frac{f \cdot a_{BC}}{1 - f \cdot a_{BC}}, \tag{7.9}$$

where θ is the water content in the base coat, $n\,[\text{mg}]$ is the actual amount of water in the base coat and n_{max} is the maximal amount of water that the base coat can absorb. Further, a_{BC} is the water activity in the base coat and f is a parameter, characterizing the difference between water in the base coat and liquid water. It was observed and predicted by the model for the sample BC50TC64, that water uptake by the sample lasts approximately 3 days while drying occurs less than in 5 hours.

Parameter	value
f	0.93
τ	3.4 h
n_{max}/A	1.39 mg/cm^2
L	64 μm
L_{BC}	50 μm

Tab. 7.1: The list of parameters of the sample BC50TC64. f characterizes the difference between water in the base coat and liquid water. τ is the timescale of water transport from Eq. 6.9 and n_{max} is water uptake capacity of the base coat. A is contact area with water. L and L_{BC} are thicknesses of the top coat and of the base coat layers, respectively.

7.3.2 The Response to Humidity Fluctuations

First, we study when the oscillations in water content occur in damped or non-damped mode. The key parameters for this are the timescale τ and the differential solubility of the base coat $k'(a_0)$. Since the sorption isotherm of the base coat is of Type III, the expression for the differential solubility can be derived from the Guggenheim-Anderson-De Boer relation (Eq. 7.9).

The transition from the sorption mode to the damping mode occurs at a period $T^* \equiv 2\pi\tau k'(a_0)$. In Figure 7.3 the different modes of the fluctuations are shown for the sample BC50TC64. The solid line denotes the period T^* as a function of water activity. When the period of the fluctuations becomes in order of T^*, the transition from the damping to the no-damping regime happens. Important to note that the period increases at higher water
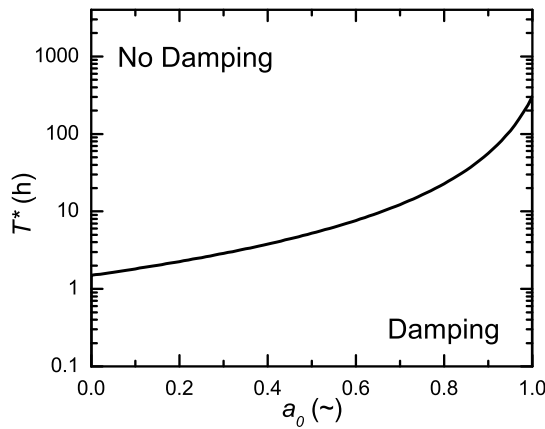
Fig. 7.3: The transition line $T^* \equiv 2\pi\tau k'$ for the sample BC50TC64. This line does not define sharp transition, rather damping occurs when the periods of the fluctuations are much less than T^* and no damping happens when the period is bigger than the T^* value. Important to note, that the increase of T^* with the water activity means that at high humidities fluctuations with periods in the order of days will have non-damped response in the water content.

activities. The values for the transition point T^* at low relative humidity are less than several hours when the RH is less than 50%. This means that fluctuations are not damped at this humidity range, except for the fluctuations with timescales less than few hours.

As the most of humidity fluctuations have timescales starting from few hours, most of realistic humidity fluctuations are not damped. In contrast, for humidities above 50% the fluctuations with the periods more than a day are not damped.

The conclusion that at high humidities only slow humidity fluctuations, i.e. with the periods in the order of days or weeks, are not damped at high humidities is valid for the majority of polymeric systems. It is known that sorption isotherms of hydrophilic polymeric materials have either Type II or Type III shape. In these cases , the differential solubility k' increases with increasing activity, leading to a shift of the value of T^*.

To illustrate the response of the base coat/top coat systems in water content to fluctuations with large amplitudes, i.e. when the linear approach does not work, the numerical solutions for water content in the base coat of a specific sample, BC50TC64, were calculated. The solutions were obtained for low, high and full humidity range, i.e for activity variations between 0 and 0.5, between 0.5 and 1 and between 0 and one, respectively. The whole activity range is considered to study how variation of the differential solubility

influences the response of the samples. The low activity range mimics natural conditions of the desert in Arizona. The high activity range refers to tropical regions such as Florida.

The solutions for the response in water content in the BC50TC64 for activity variations between 0 and 0.5, between 0.5 and 1 and the whole activity range, are shown in Figure 7.4a, b and c, respectively. Note, the values of transition period T^* are 3.3 hours for the case with $a_0 = 0.25$, 6.5 hours for $a_0 = 0.5$ and 19 hours for $a_0 = 0.75$, which is consistent with the obtained solutions: the fluctuations with oscillation periods less than T^* are damped and the slower humidity fluctuations induce bigger water content variations. The narrow 'hills' in the oscillations and broad 'valleys' for the high and whole humidity ranges (Figure 7.4b and Figure 7.4c, respectively) are the consequence of the asymmetry between uptake and drying for these samples. The drying of the samples takes hours while days are needed to equilibrate the sample with high humidity.

7.4 Conclusions

In this chapter it was shown that the response of two-layered hydrophilic base coat/hydrophobic top coat systems to humidity fluctuations can be damped. The response time is determined by the product of the timescale of permeation through top coats and solubility of the base coat and draws the borderline between regimes of damped and non-damped oscillations. Humidity fluctuations with timescales less than the response time are damped.

The response time depends on the considered humidity range for systems with nonlinear sorption isotherms, as water solubility varies with the water activity. For polymeric systems with non-linear sorption isotherms this means that at high humidity range (RH>50%) only humidity fluctuations with timescales in order of days or weeks will have an non-damped response. Particularly for the specific systems of interest, studied in this thesis, only humidity fluctuations with periods more than a day, will result in a significant variations of water content in the coating. In contrast, for low humidity range, i.e. with RH less than 50%, the most of fluctuations are non-damped.

The practical outcome of this investigation is that at high humidity range, only slow humidity fluctuations, i.e. with a timescale of days or weeks, will result in significant water content variations and hygroscopic stresses for the systems of interest. This applies to the majority of two-layered systems with hydrophilic base coats: hydrophilic polymers normally have Type II or III isotherms, thus their differential solubilities increase with water activity.

The damping of short timescale humidity oscillations, i.e. with periods less than a day, implies that a most of the humidity fluctuations in accelerated/artificial weathering will have limited influence on the water content in the samples due to damping. As a consequence, accelerated or artificial weathering does not represent natural weathering in terms of moisture exposure, especially at the high humidity range.
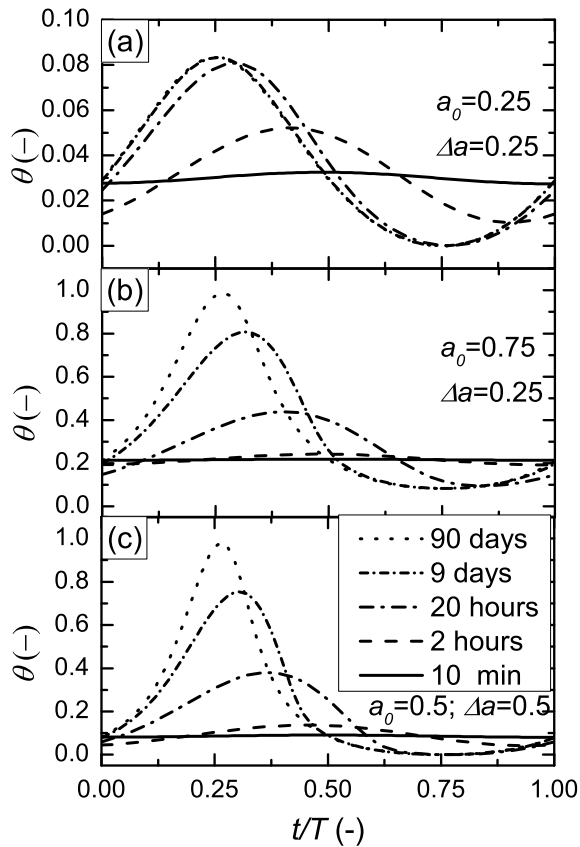
Fig. 7.4: Response in water content of the base coats during humidity oscillations at low
(a), high (b) and whole activity ranges (c), on the basis of numerical simulation.
T is the activity oscillation period, which values are shown in the legend.

8. Plasticizer in Top Coats: Influence of Stress Relaxation on Transport

8.1 Introduction

Penetration of hydraulic fluids in multilayer coatings, used in aerospace applications, promotes deterioration of these systems. Presently, phosphate-ester based hydraulic fluids are commonly used in aircrafts, for example Skydrol[TM], and dominate the market. It is known that the exposure to Skydrol fluids results in plasticization and deterioration even of highly crosslinked systems, like aerospace top coats [89]. Immersion in Skydrol is a standard test for paints and coatings, described by ISO 2812 and ASTM D1308-02. Furthermore, it is known that Skydrol absorption can result in a depression of the glass transition temperature of polymers[90]. It acts as an organic solvent [91] and causes a decrease in mechanical performance [92].

Little is known about how Skydrol penetrates into organic coatings.The main component of Skydrol fluids is TBP (tri-butyl phosphate), which constitute more than 60% w/w in the latest generations. TBP is a plasticizer and an organic solvent, and it is expected that it plays a key role in Skydrol absorption. Therefore, TBP uptake by coatings is one of the first steps in understanding Skydrol uptake.

It is well known that solvent penetration in polymeric systems is accompanied by structural relaxation processes, this may result in non-Fickian kinetics of the process [93, 94, 33]. A notable example of diffusion in presence of relaxation processes is Case II diffusion [34]. Since the top coat can be plasticized by the forementioned type of penetrants, TBP uptake by multilayer coatings differs from the water uptake by multilayer systems with hydrophobic top coats considered in the previous chapters. Therefore, the investigation of TBP penetration in multilayer coatings starts from understanding TBP uptake by the top coat layers only.

This chapter aims to understand the TBP penetration into a highly crosslinked top coat and to investigate how relaxation processes influence the uptake kinetics. The penetration is studied at a temperature near the glass transition temperature of the coating as an extreme case with the faster uptake. A combination high resolution NMR imaging and NMR relaxometry was used to measure TBP uptake. TBP redistribution in the coating, kinetics of uptake, swelling and plasticization of the coating were studied.

8.2   Experimental Details

8.2.1   Samples

The studied system is a highly crosslinked polyurethane top coat. The top coat is a 2-component, ambient curing coating, based on a polyester polyol with an OH number of 250 mgr/KOH solids and glass transition temperature of $34\,^{\circ}$C and a methylene bis-cyclohexylisocyanate based polyisocyanate with isocyanate equivalent weight of 191 on solids. The glass transition temperature of the cured coating is $77\,^{\circ}$C.

        The samples were sprayed in a single application on square glass slides with thickness of $150\,\mu$m and side of 18 mm. After spraying samples were stored for a week at room temperature and then cured at $80\,^{\circ}$C during 3 days. The dry film had a thickness of ca. $120\,\mu$m.

        To place TBP in contact with the film, a glass tube with a diameter of 11 mm was glued on top of the sample. Silicon glue was used to fix the tube. On the bottom of the glass slide, a marker was attached to trace fluctuations and sample bending. A schematic picture of the experimental setup is shown in Figure 8.1.
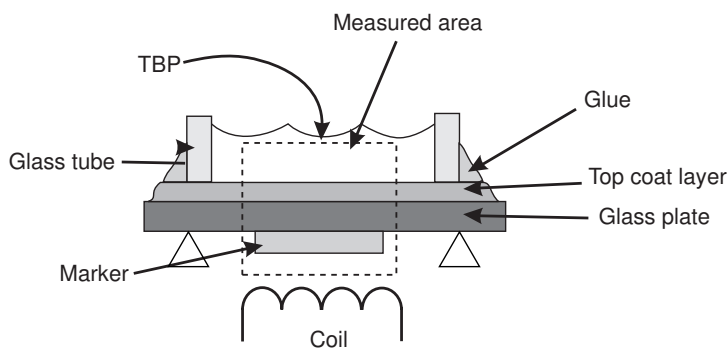

Fig. 8.1: Schematic representation of the experimental set-up used for TBP uptake experiments. The coating has a thickness of $120\,\mu$m. The glass tube has a diameter of 11 mm. The glass plate has a thickness of $150\,\mu$m and a side of 18 mm.

        As the process was measured at a temperature of $80\,^{\circ}$C, a special designed chamber was used to host the RF coil and the sample. The chamber was heated with hot water and the temperature was monitored with a thermocouple installed inside the chamber. The temperature fluctuations during the measurement were less than $0.5\,^{\circ}$C.

8.2.2   NMR Experiment

In order to measure the process of TBP penetration into the coating, an Ostroff-Waugh pulse sequence[54] was used with a flipping angles nominally equal to $90\,^{\circ}$C. A detailed

description of NMR settings and equipment is given in Chapter 4. Below, the key experimental settings are summarized. NMR signals were measured with $t_e = 0.1$ ms and 1024 echoes were recorded. An acquisition time equal to 0.09 ms was used, which corresponds to a spatial resolution of ca. 5μm. The signals were averaged 1024 times with a repetition time of 1 s. Thus, the time between the two subsequent measurements was approximately 20 minutes.

The recorded signals were treated with the procedure, described in Chapter 4, using CuSO4 0.01 M aqueous solution as a reference. As a result, the following signal for the n-th echo was obtained

$$S_n(x) = \frac{\rho(x)}{\rho_w} \left[1 - \exp(-t_r/T_1)\right] \exp(-nt_e/T_2), \tag{8.1}$$

where $\rho \, [\text{mol/m}^3]$ is the actual concentration of probed ^{1}H nuclei, $\rho_w \, [\text{mol/m}^3]$ is the density of ^{1}H nuclei in liquid water, $t_r \, [\text{s}]$ is the repetition time, $T_1 \, [\text{s}]$ is the longitudinal relaxation time, $t_e \, [\text{s}]$ is the echo time, $T_2 \, [\text{s}]$ is the transversal relaxation time and n is the number of spin-echo.

The T_1 values were as follows: about 2 s for TBP and ca. 0.3 s for the coating and for the coating with TBP inside. This means that the T_1 term in Eq. 8.1 can be neglected for the signal of the sample. Regarding the TBP signal, it loses about 60% of the intensity due to T_1 factor at the used settings.

8.2.3 Data processing

During the process of TBP penetration, three regions in the sample: liquid TBP on top of the sample, dry coating and coating, which has absorbed some TBP. In order to understand the process, TBP distributions are evaluated, swelling of the sample is considered as well as plasticization of the coating by TBP. This is done on the basis of the measured spin echoes of liquid TBP, dry top coat and top coat with TBP, which are shown in Figure 8.2. In order to determine swelling and TBP front position, the liquid TBP/coating interface and coating with TBP/dry coating interface have to be traced. The position of the TBP front is traced on the basis of the first echo, since there is sufficient contrast between the signals of coating with TBP and the dry top coat. Tracing the liquid TBP/top coat interface is not possible on the basis of the first echo due to lack of the contrast, therefore the 20th spin echo was used as it provides sufficient contrast between the two regions. To assess plasticization of the sample, T_2 relaxation analysis was performed: T_2 spectra of total signal of the coating were obtained with regularized inverse Laplace transform [68]. The details of the procedure are given in Section 5.2.2.
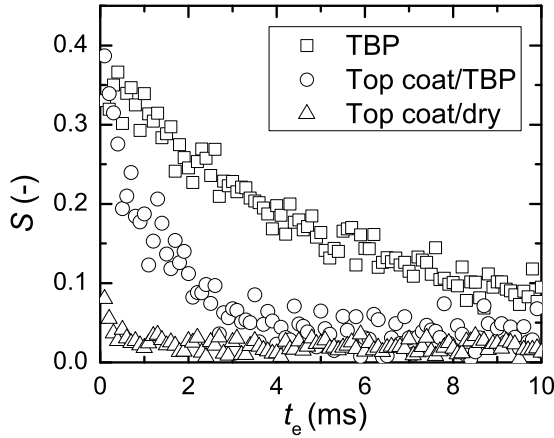
Fig. 8.2: T_2 relaxation decays of NMR signals of liquid TBP (squares), the top coat with TBP (circles) and the dry top coat (triangles). The vertical line marks the position of the 20th echo, which is used to locate the interface between liquid TBP and coating, which has absorbed TBP.

8.3   Theory

The aim of this section is to discuss how relaxation processes can affect the kinetics of solvent uptake in polymeric materials. The problem is considered to be one-dimensional since during the uptake by coatings penetration in the direction, perpendicular to the coating plane, is much faster than redistribution in the coating plane.

When penetration into the polymer causes swelling of the sample, it can be considered as a strain ε of the material. In one-dimensional case of swelling, the strain of the material is connected to the penetrant volume fraction ϕ and its concentration $\rho \, [mol/m^3]$

$$\varepsilon = \phi = \rho v \tag{8.2}$$

where $v \, [\mathrm{m^3/mol}]$ is molar volume of the penetrant. This relation is valid if the swelling of the material is only due to the volume of the penetrant.

It is known that stresses in polymeric materials, induced by strain, can experience relaxation, which is associated with the viscosity of the material. The stress relaxation of a material with a strain ε can be described by the Maxwell relationship

$$\frac{\partial \varepsilon}{\partial t} = \frac{\sigma}{\eta} + \frac{1}{E} \frac{\partial \sigma}{\partial t} \tag{8.3}$$

where σ [Pa] is stress in the material, η [Pa·s] and E [Pa] are viscosity and Young's modulus of the material, respectively. This model introduces a relaxation timescale τ_R [s], which characterizes the time needed for stresses to relax in the material under a constant strain.

$$\tau_R \sim \frac{\eta}{E} \tag{8.4}$$

Fast relaxation is usually observed for rubbery systems, whereas glassy polymers have a slow relaxation stress relaxation. In case of relaxation processes induced by penetration, the relaxation timescales should be compared with the diffusion timescale $\tau_D \sim L^2/D$. The ratio between the relaxation and diffusion timescales is called the Deborah number for solvent diffusion in polymers [32]

$$De = \frac{\eta D}{EL^2} \tag{8.5}$$

Thus, diffusion in glassy polymers is usually characterized by $De \gg 1$, whereas diffusion in rubbery systems occurs with $De \ll 1$.

To illustrate the influence of stress relaxation on diffusion, its contribution in the process is considered. The stresses in the polymer increase the chemical potential $\mu_0(\rho)$ [J/mol] of the penetrant by σv

$$\mu = \mu_0 + \sigma v \tag{8.6}$$

Then, the flux of the penetrant J [molm^{-2}s^{-1}] can be described as follows

$$J = -\frac{D_0}{RT}\frac{\partial \mu}{\partial x} = -\frac{D_0}{RT}\left[\frac{\partial \mu_0}{\partial x} + v\frac{\partial \sigma}{\partial x}\right] \tag{8.7}$$

where D_0 [m^2/s] is the self-diffusion coefficient of the penetrant.

When $De \ll 1$, the stresses will relax fast compared to diffusion and there will be no stress term in the flux, and $\mu = \mu_0(\rho)$.

The case $De \gg 1$, means that the viscous term of Maxwell relation in Eq. 8.3 can be neglected. In this case only elastic stress is present, which is a unique function of the penetrant concentration $\sigma = E\rho v$.

Both in the cases when $De \ll 1$ and $De \gg 1$ the chemical potential is a unique function of penetrant concentration. This allows to rewrite flux Eq. 8.7 as

$$J = -\frac{D_0}{RT}\left[\frac{\partial \mu_0}{\partial \rho} + Ev^2\right]\frac{\partial \rho}{\partial x} \tag{8.8}$$

where in case of $De \ll 1$ the elastic modulus should be taken as zero, $E = 0$. Note, that this flux is in fact the Fick's first law $J = -D(\rho)\partial \rho/\partial x$ with a concentration dependent diffusion coefficient

$$D(\rho) = \frac{D_0(\rho)}{RT}\frac{\partial \mu_0}{\partial \rho} + Ev^2 \tag{8.9}$$

Therefore, when the stress relaxation term can be neglected or the relaxation process happens much faster than diffusion, Fickian kinetics of the process will be observed. This implies that in these extreme cases the concentration profiles should be a function of $x/t^{1/2}$, where x is the distance from the solvent/coating interface.

The situations, when $De \sim 1$, the relaxation of the stress, has to be taken into account. In general, analytical solution for the stress of Eq. 8.3 reads

$$
\begin{aligned}
\sigma(x,t) \;=\;& \exp\left(-\frac{E(\rho(x,t)t)}{\eta(\rho(x,t))}\right) \\
&\times\; \int_0^t E(\rho(x,t'))v\partial\rho/\partial t' \exp\left(\frac{E(\rho(x,t')t')}{\eta(\rho(x,t'))}\right) dt'
\end{aligned}
\tag{8.10}
$$

Note, that the stress includes history term.

Substituting this stress into the flux in Eq. 8.7 will cause its modification. The resulting flux will not be invariant to Fick's law, and consequently, the uptake kinetics will differ from Fickian kinetics.

8.4   Results

The aim of this section is to get an insight into TBP penetration in the coating. This is done with high resolution NMR imaging, which is used to assess TBP distributions and swelling during the process. Additionally, T_2 relaxation analysis is performed to evaluate mobilities of TBP and polymer chains of the coating.

First, to assess the TBP penetration, signal profiles of the sample during the uptake were measured, see Figure 8.3. The interface between liquid TBP and and the top coat was set at $0\,\mu$m by repositioning the profiles and is denoted by the vertical line. The time between the two subsequent profiles is approximately 20 minutes. The light grey lines are the profiles during the first 50 hours of the uptake and the dark grey profiles were measured beyond 50 hours. For $t < 50\,$h a sharp progressing front is observed, denoted by the upper horizontal arrow. Further, little signal variation is observed behind the front, while it moves through the sample. After the front has reached the substrate ($t > 50\,$h), the signal increase is observed everywhere in the sample, which is shown by the vertical arrow. Swelling occurs during the whole uptake, and is denoted by the lower horizontal arrow.

To evaluate the kinetics of the uptake, the front position is analyzed. The position of the front $f\,[\mu$m$]$ is estimated as the distance of this front to the TBP/coating interface, see Figure 8.4. The front progresses into the sample, until it reaches the substrate at ca. 50 hours. The observed front position is compared with the two extreme cases of penetration kinetics: Fickian diffusion ($f \sim t^{1/2}$) and Case II diffusion ($f \sim t$) [34]. Apparently, the
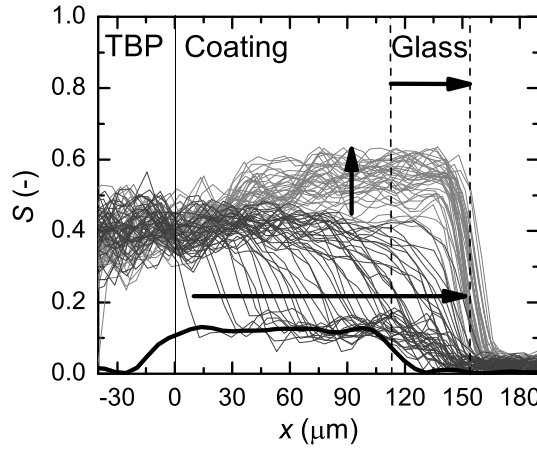
Fig. 8.3: Signal profiles of the coating during the TBP penetration. The bold line shows the signal profile of the dry coating. The signal profiles during the first 50 hours of the uptake are shown by dark grey lines and the dark grey lines show signal profiles after 50 hours. The time between two subsequent profiles is 2.5 hours. The arrows denote the TBP fronts progression during the first 50 hours (upper horizontal arrow), swelling (lower horizontal arrow) and the signal increase in the sample after 50 hours (vertical arrow). The vertical line denote the position of liquid TBP/top coat interface.

front progression rate is between these two extremes. By fitting a power law, it has been found that power equals 0.63, i.e. $f \sim t^{0.63}$. Therefore, it is concluded that the uptake rate has non-Fickian kinetics.

In order to evaluate the amount of absorbed TBP and its influence on the sample, the swelling of the sample during the penetration is estimated, see Figure 8.5. The swelling was estimated from the change in the distance between the marker and the TBP/coating interface. The swelling increases until 70 hours and its end value is ca. 35 μm, which is 29% of the initial thickness of the sample. The amount of absorbed TBP, n_{TBP} [mol], is calculated as follows

$$n_{TBP}/A = 27 \times \frac{\triangle H}{v_{TBP}}, \tag{8.11}$$

where $\triangle H$ [m] is swelling of the coating, $v_{TBP} = 274 \, \text{cm}^3/\text{mol}$ is molar volume of liquid TBP and A [m] is the area of TBP penetration. The number 27 is the number of protons in a single TBP molecule. In the calculation it is assumed that the extra volume of the
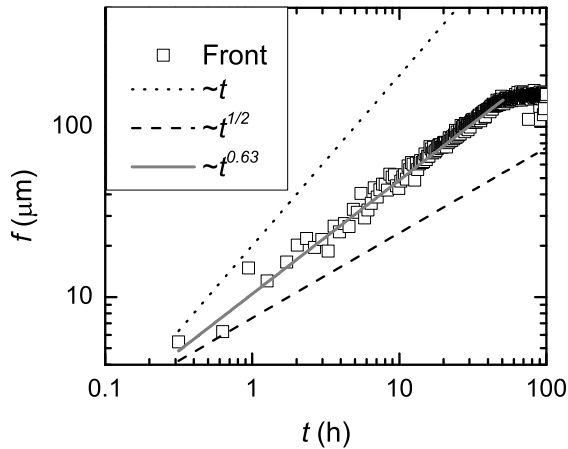
Fig. 8.4: The position of TBP front f in the sample as a function of time. Note that the front position is defined as a distance between the TBP front and the liquid TBP/coating interface.

sample gained during swelling equals the volume of TBP, absorbed by the coating, i.e. the TBP molar volume equals molar volume of liquid TBP.

The right y-scale in Figure 8.5 shows an estimate of the number of TBP protons n_{TBP} [mol/m^2] in the sample.

To evaluate the plasticization of the sample, the mobilities of the protons in the coating are assessed via their T_2 values during uptake. Figure 8.6 shows the T_2 relaxation spectra, obtained from the total signal of the coating during TBP penetration. When $t < 50$ h, low mobility protons are observed with $T_2 \simeq 0.1$ ms and highly mobile protons with T_2 values between 0.9 and 2 ms. For $t > 50$ h an extra population of protons with intermediate mobility appear with T_2 values between 0.3 ms and 0.8 ms. Further, an increase of the mobility of the highly mobile protons is observed, indicated by increase of their T_2 values to the value of ca. 4 ms. To quantify the amount of the observed protons, the total intensity of the spectrum of protons with the low and intermediate mobility (0.1 ms $\leq T_2 \leq$ 0.8 ms) protons was calculated as well as the total intensity of highly mobile protons ($T_2 > 0.8$ ms). Figure 8.7a shows the number of protons with low and intermediate mobilities and the number of highly mobile protons are shown by Figure 8.7b. The number of visible protons is presented as a function of number of TBP protons, absorbed by the coating. The number of low/intermediate mobility protons stays nearly constant until the number of TBP protons reaches the value of ca. 0.3 mmol/cm^2, which corresponds to approximately 50 hours of uptake. After this their number increases with
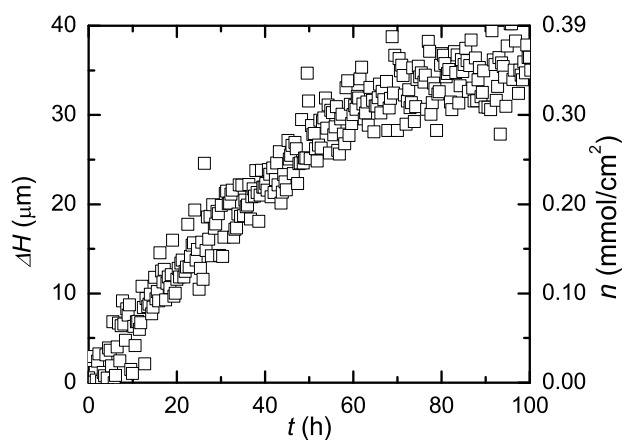
Fig. 8.5: The swelling of the coating as a function of time. The right axis shows the estimate of TBP protons, corresponding to the swelling values. The estimation is based on the assumption that TBP in the coating has the same molar volume as liquid TBP. The vertical line marks the moment the TBP front reaches the substrate.
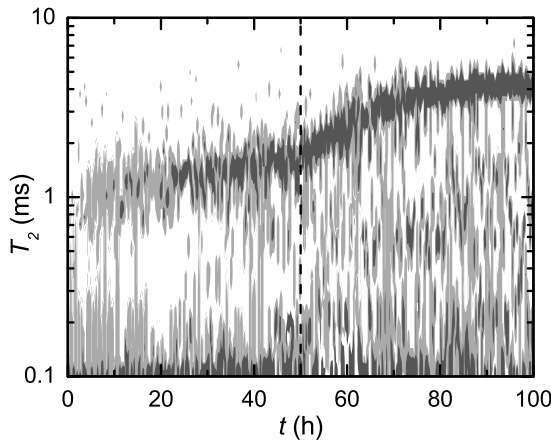
Fig. 8.6: T_2 relaxation spectra of the total signal of the top coat during TBP uptake. Several spectral components indicate several proton species with different mobilities. Before 50 hours, two spectral components are observed: at $T_2 \sim 0.1$ ms and in the range $T_2 \sim 2$ ms. After 50 hours some scattered spectral components appear between these two. Note the increase in T_2 after 50 hours, when the front reaches the substrate.

the amount of TBP and time. The slope of the increase equals approximately 1, when compared to number of protons in absorbed TBP, however with a poor accuracy. The number of highly mobile protons is linear with swelling and there are 1.5 highly mobile protons per absorbed TBP proton in the coating. This means that one TBP molecules mobilize about 40 protons of the coating, of which 13 are highly mobile and ca. 27 have a low or intermediate mobility. It is important to note, that the number highly mobile protons increases linearly with the swelling during the whole uptake and the protons of intermediate mobility appear only after 50 hours.

8.5   Discussion

The previously described observations suggest that the following processes occur during penetration,

First, the sharp fronts of TBP indicate a steep dependency of diffusion coefficient from the TBP concentration. The timescale of TBP diffusion in the unplasticized system is $\tau_D \sim 50$ h, being the time, needed for the TBP front to reach the substrate. Behind the front, the coating is plasticized and TBP will have a significantly higher diffusion coeffi-
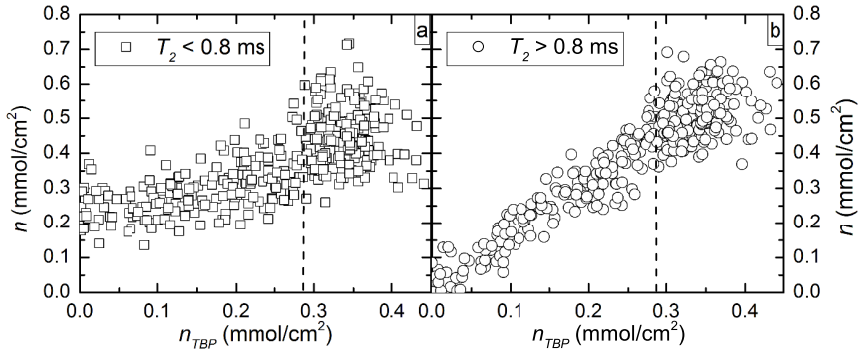
Fig. 8.7: Amount of visible protons originating from TBP and coating of high ($T_2 >$ 0.8 ms, triangles) and low ($T_2 < 0.8$ ms, circles) mobilities as a function of amount of TBP in the sample.

cient. As little signal variation is observed behind the fronts, this means that the diffusion timescale in plasticized coating is less than the time for measurement of NMR signal profile, i.e. 20 minutes. This implies that the diffusion coefficient in plasticized coating is at least 100 times bigger than the diffusivity of TBP in the unplasticized coating. Note, that this is the increase of intrinsic diffusion coefficient, implying that the differences of self-diffusion coefficient of TBP in the coating faces at least a similar increase.

From the front progression rate, the TBP penetration exhibits non-Fickian kinetics, i.e. the front position moves in the coating proportionally to $t^{0.63}$. The possible reason for the deviation from Fickian kinetics can be stress relaxation process in the coating. The typical stress relaxation time in this type of coatings can be estimated from the typical elastic modulus of glassy polymers, which is in order of 10^9 Pa and typical values of viscosities of such systems, which lie in the range of $10^{13} - 10^{15}$ Pa $\cdot$ s ([95, 96]). Consequently, the relaxation times in the system of interest in the glassy state lie in the range of ca. $3 - 300$ h. Combined with the diffusion timescale of about 50 h, we get that the Deborah number for TBP uptake in the top coat is between 0.1 and 10. This implies that the stress relaxation affects the uptake kinetics.

Finally, the mobility increase of the polymeric chains combined with the increased permeability of the coating indicate that the coating is significantly plasticized. It is known that solvents can cause depression of glass transition temperature [97]. Consequently, knowing that the temperature during the studied case was close to the glass transition temperature, the plasticized coating can appear in the rubbery state.

8.6   Conclusions

In this study it was found that relaxation of stress due to swelling by TBP (tributyl phosphate) plays a key role in the uptake by highly crosslinked top coat, resulting in non-Fickian kinetics of penetration. The stress relaxation time is comparable to TBP diffusion timescales, resulting in modification of driving force in such a way, that it departs from Fickian diffusion.

Further, it was concluded that TBP absorption significantly increases the permeability of the top coat. The possible implications of are that the top coat becomes prone to other penetrants and cannot perform well as a barrier in multilayer coating when exposed to hydraulic fluids, which comprise TBP in significant quantities.

Finally, it was concluded that the presence of TBP forces the top coat to appear in rubbery state due to depression of glass transition temperature. This can result in degradation of the mechanical properties of the systems and loss of protective properties of the top coat.

9. Conclusions and Outlook

9.1 Conclusions

In this thesis it has been shown that for understanding water transport in a hydrophilic base coat/hydrophobic top coat system, knowledge of the sorption isotherm of the base coat and of the permeability of the top coat is sufficient. The permeability of the top coat determines the timescale of the transport, whereas the sorption isotherm of the base coat defines the driving force of water transport and the details of the time-dependency of the process.

Practically, this implies that quantitative, simple and cost-efficient tests of water transport in such type of multilayer coatings can be performed by gravimetric measurements of the base coat sorption isotherm and the top coat permeability and by using these parameters to estimate the water content of the sample as a function of time.

It was found that two-layered polymeric systems with non-linear base coat sorption isotherms (i.e. Type II or Type III) dry much faster than they take up water. This implies that mostly incidental penetration of water will have little consequences in terms of presence of water in the coating, as water will rapidly escape the sample when drying starts.

A theoretical investigation showed that in most of the considered systems subjected to humidity fluctuations, the response time is in the order of days for high humidities and has values of a few hours at low humidities. The response time is determined by the product of the timescale of penetration through the top coat and the differential solubility of the base coat. This means that most two-layered polymeric base coat/top coat systems with hydrophilic base coats are relatively inert to most humidity fluctuations, as the response in terms of water content will be damped. As accelerated and artificial weathering tests include only humidity fluctuations with typical timescales less than a day, this raises concerns if these tests can be compared to natural moisture exposure.

Furthermore, it was found that the polymeric dispersant in the base coat is a key contributor to the water uptake. Water absorption by the base coat is mainly a process of hydrogel formation of water with the dispersant in the base coat. This indicates that water soluble and hydrophilic components of the base coat are promoters for water absorption.

Finally, it was shown that stress relaxation is a key contributor to the driving force

of the penetration of a plasticizer into a highly crosslinked top coat, resulting in non-Fickian kinetics of the uptake process. The plasticizer, which is tributyl phosphate, causes a steep increase in the permeability of the film and may cause degradation of mechanical properties of the coating. This implies that, practically, tributyl phosphate (the main component of common aerospace hydraulic fluids) makes multilayer protective coatings more permeable and causes significant stresses in the system.

9.2 Outlook

The study presented in this thesis has answered some of the scientific questions about transport phenomena in multilayer coatings. Still, a number of problems has to addressed. Some of these problems have to be discussed to complete the picture, obtained in this study. Other problems are considered as a logical follow-up to the main findings of in this work.

9.2.1 Water Redistribution: Lateral Transport

The starting point of one-dimensional water transport in multilayer coatings may not always be valid. Typical examples of deviating geometries are when the water contact area with the coating is smaller than the coating surface area, see Figure 9.1a, when the layer thicknesses vary in the plane of a coating, see Figure 9.1b, or when a localized damage is present, e.g. due to stone chips or cracks, see Figure 9.1c.

       In such cases, a profound investigation of the redistribution of water in the plane of the coating is needed. Furthermore, consequent hygroscopic stresses, which may occur as a result of different water redistribution rates and swelling rations of the layers, have to be understood. This requires measurements of water redistribution in the plane of the coating and understanding stresses in the system.

       Measurements of such water redistributions can be achieved via a modification of GARField high resolution NMR imaging in terms of the ability to measure in a second dimension. A possible approach can be the addition of secondary field gradients to a primary static gradient to measure in an additional dimension, such used by Godward et al. [98] to enhance the stray-field imaging technique, or implemented by Casanova and Blumich [99] for the modification of the mobile NMR. For this kind of problem, an imaging in the second dimension in the order of millimeters is sufficient. Regarding the stresses, their evaluation will require a detailed study of stress-strain relationships of individual layers, as well as of the whole multilayer coating.
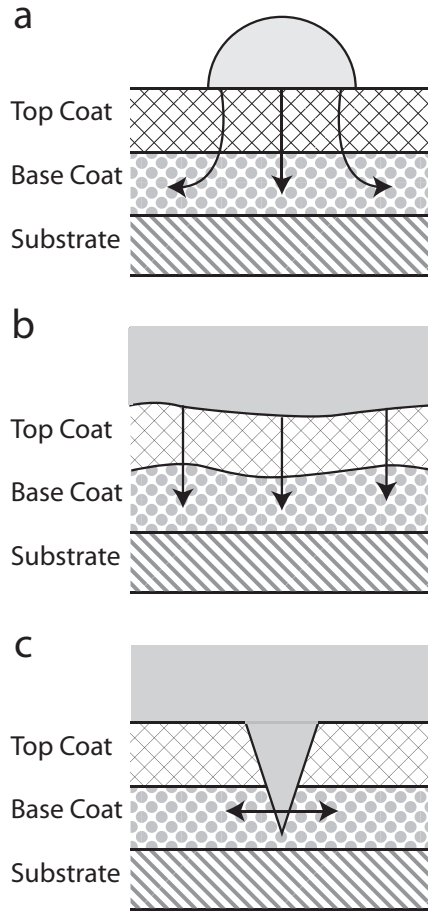
Fig. 9.1: A schematic pictures of situations when lateral redistribution of water may play a role: (a) limited contact area with water, (b) significant variations of the layers thicknesses and (c) presence of localized damage.

9.2.2 Water Redistribution: Hampered Behind the Barrier

Another challenge in multilayer coatings is when instant redistribution of water in the layer beneath the barrier is fully hampered. This situation is met, when the layer under the top coat is has low permeability. A related topic is water transport through coating on permeable media, such as wood, bricks or concrete. The instant redistribution in these cases does not occur due to the size of the material.

In such cases, understanding the redistribution of water beneath the barrier, as wa-

ter is associated with various damage mechanisms in coatings and porous media. Furthermore, the failure mechanisms of the barrier layer in such systems have to be studied. When coated porous media are concerned, it is known that blister formation or adhesion loss are frequent failure phenomena. The redistribution in multilayer coatings can be studied with high resolution NMR imaging, used in this thesis, while coated bulk media can be assessed with NMR imaging with resolution of millimeters [65].

9.2.3 Behind the Sorption Isotherm: The Influence of the Composition

Knowing that the sorption isotherm of the base coat is a key feature that determines the response of multilayer coatings to moisture, the obvious research challenge is to determine how the sorption isotherm depends on the composition. This knowledge is important for further development of coatings with respect to their water resistance.

Regarding the cases, when base coats comprise multiple polymer phases, the first step should be studying sorption isotherms of the individual phases. A next step addresses the question how sorption isotherms of the single phases result in sorption isotherm of a multiphase layer. Note that hygroscopic stresses can result in complex interactions between multiple polymer phases, since water induced swelling of one phase can induce stress on other phases, influencing their water sorption. It is known that the stresses can significantly influence sorption in composites of multiple polymer phases [100, 101]. Thus, one of the key challenges is to verify to what extent interaction between coating layers occurs, and to determine interactions between polymer phases of multiphase layers. The objective is verifying if there is an interaction between the layers of the coating and to determine the nature of interactions between the polymer phases of multiphase layers.

Such investigation requires accurate measurements and modeling of the water sorption isotherm for each polymer phase. Furthermore, this study may benefit from studying enthalpy and entropy of sorption, which can be performed with sorption calorimetry [102]. Knowledge of these parameters is an important empirical basis for modeling the isotherms.

9.2.4 The Temperature: Key Parameter in Transport

The present study was done under isothermal conditions at room temperature. It is known that temperature strongly influence the rates of transport, the absorption capacities and even water-polymer interactions. Therefore, evident follow-up is concern the role of the temperature. The aim of such study is understanding temperature dependency of water transport, the combination of temperature variations in time and water water transport, and the response of multilayer coatings to a combination of temperature and humidity fluctuations.

The temperature dependency of water transport is most evident in the potential effect on the top coat permeability and the base coat water absorption. The model intro-

duced in Chapter 6 should be verified over a wider temperature range, i.e. if the diffusivity of water in the top coat remains constant at all temperatures. The question to consider is whether supersaturation of water can occur in the sample, e.g. as a consequence of temperature decrease of a coating saturated with water, and its consequences for multilayer coatings. Consequently, measurements of top coat permeabilities and the base coat sorption isotherms have to be performed at different temperatures. Further, a model for the hygrothermal response of multilayer coatings has to be developed.

9.2.5 Ion Transport in Multilayer Coatings: The Influence of Water

Water in coatings can facilitate ion transport to the substrate. This process can be critical for the coating performance, since the presence of ions is an important ingredient of corrosion mechanism. Obvious follow-up of the present study is to answer the question how ions migrate in multilayer coatings in the presence of water.

Furthermore, it should be evaluated if ions can accumulate in multilayer coatings due to trapping of permeated ions during drying.

9.2.6 Plasticizer Ingress in Multilayer Coatings and Composites: Effects of Stress Relaxation

This thesis presented a study of the penetration of phosphate-ester hydraulic fluids penetrate into multilayer coatings. There is still a number of open questions to be answered.

First, to understand the transport it should be known how TBP (tributyl phosphate) is present in the polymeric material and how does it interact with the coating. This will require evaluation of TBP sorption isotherms, TBP self-diffusion coefficients and an analysis of the dependency of the viscoelastic properties of the material as a function of the TBP content. The self-diffusion coefficients can be measured with NMR, whereas the viscoelastic properties, i.e. elastic modulus and Maxwell's relaxation time can be analyzed with DMA (dynamic mechanical analysis). Measurements of sorption isotherms is an experimental challenge as the TBP vapor pressure is low. It makes difficult to control its activity.

Second, follow-up should address non-isothermal conditions, i.e. determining how temperature influences transport of plasticizer. Such study should include the investigation how temperature regulates diffusion and the stress relaxation rates.

Third, the present study has only considered the top coat layer. Even when the plasticizer migration in the top coat is fully understood, an open question is how plasticizer will penetrate into a multilayer coating. One of the key questions then concerns the effect of stress relaxation in multilayered structure.

Bibliography

[1] R.J. Irwin, M. VanMouwerik, L. Stevens, M.D. Seese, and W. Basham. *Environmental Contaminants Encyclopedia*. National Park Service, Water Resources Division, Fort Collins, Colorado, Distributed within the federal government as electronic document, 1997.

[2] E. Brodkin, R. Copes, A. Mattman, J. Kennedy, R. Kling, and A. Yassi. Lead and mercury exposures: interpretation and action. *Canadian Medical Association journal*, 176:59–63, 2007.

[3] V.L.D. Badisa, L.M. Latinwo, C.O. Odewumi, C.O. Ikediobi, R.B. Badisa, L.T. Ayuk-Takem, Jude Nwoga, and John West. Mechanism of DNA damage by cadmium and interplay of antioxidant enzymes and agents. *Environmental toxicology*, 22:144–151, 2007.

[4] Jie Liu, Wei Qu, and M.B. Kadiiska. Role of oxidative stress in cadmium toxicity and carcinogenesis. *Toxicology and applied pharmacology*, 238:209–14, 2009.

[5] P.J. Lioy. Exposure science: a view of the past and milestones for the future. *Environmental health perspectives*, 118:1081–90, 2010.

[6] B. Turpin, R. Saxena, and E. Andrews. Measuring and simulating particulate organics in the atmosphere: problems and prospects. *Atmospheric Environment*, 34:2983–3013, 2000.

[7] H.R. Cheng, H. Guo, S.M. Saunders, S.H.M. Lam, F. Jiang, X.M. Wang, I.J. Simpson, D.R. Blake, P.K.K. Louie, and T.J. Wang. Assessing photochemical ozone formation in the Pearl River Delta with a photochemical trajectory model. *Atmospheric Environment*, 44:4199–4208, 2010.

[8] J. Fenger. Air pollution in the last 50 years From local to global. *Atmospheric Environment*, 43:13–22, 2009.

[9] EU RoHs. Directive 2002/95/Ec Of The European Parliament and of the Council of 27 January 2003 on the restriction of the use of certain hazardous substances in

electrical and electronic equipment. *Official Journal of the European Union*, pages 6–10, 2003.

[10] Commission European Communities (CEC). Regulation (EC) No 1907/2006 of the European Parliament and of the Council. *Official Journal of the European Union*, 396:1–849, 2006.

[11] R Lambourne and TA Strivens, editors. *Paint and Surface Coatings: Theory and practice*. Woodhead Publishing Ltd, 1999.

[12] R. Blahnik. Problems of Measuring Water Sorption in Organic Coatings and Films, and Calculations of Complicated Instances of Moistening. *Progress in organic coatings*, 11:353–392, 1983.

[13] M. Hulden and C.M. Hansen. Water permeation in coatings. *Progress in Organic Coatings*, 13:171–194, 1985.

[14] G. van Der Wel and O.C.G. Adan. Moisture in organic coatings: A review. *Progress in Organic Coatings*, 37:1–14, 1999.

[15] P. Carbonini, T. Monetta, L. Nicodemo, P. Mastronardi, B. Scatteia, and F. Belucci. Electrochemical Characterization of Multilayer Organic Coatings. *Progress in Organic Coatings*, 29:13–20, 1996.

[16] J.H. Park, G.D. Lee, H. Ooshige, A. Nishikata, and T. Tsuru. Monitoring of water uptake in organic coatings under cyclic wetdry condition. *Corrosion Science*, 45:1881–1894, 2003.

[17] S. Devasahayam. Effect of moisture-ingress on adhesion energy in a metal oxide-polymer system. *Journal of Applied Polymer Science*, 99:2052–2061, 2006.

[18] K.N. Allahar, B.R. Hinderliter, D.E. Tallman, and G.P. Bierwagen. Water Transport in Multilayer Organic Coatings. *Journal of The Electrochemical Society*, 155(8):F201–F208, 2008.

[19] V. Baukh, H.P. Huinink, O.C.G. Adan, S.J.F. Erich, and L.G.J. van der Ven. NMR Imaging of Water Uptake in Multilayer Polymeric Films: Stressing the Role of Mechanical Stress. *Macromolecules*, 43:3882–3889, 2010.

[20] V. Baukh, H.P. Huinink, O.C.G. Adan, S.J.F. Erich, and L.G.J. van der Ven. Water-Polymer Interaction during Water Uptake. *Macromolecules*, 44:4863–4871, 2011.

[21] S. Brunauer, L.S. Deming, W.E. Deming, and E. Teller. On a theory of the van der Waals adsorption of gases. *Journal of the American Chemical Society*, 62:1723–1732, 1940.

[22] J.A. Barrie. *Diffusion in Polymers*, chapter 8. Academic Press, London, 1968.

[23] H. Yasuda. Permeation, solution, and diffusion of water in some high polymers. *Journal of Polymer Science*, 57:907–923, 1962.

[24] P.M. Jacobs and F.R. Jones. Diffusion of moisture into two-phase polymers. *Journal of Materials Science*, 24:2343–2347, 1989.

[25] V. Detallante, D. Langevin, C. Chappey, M. Metayer, R. Mercier, and M. Pin. Water vapor sorption in naphthalenic sulfonated polyimide membranes. *Journal of Membrane Science*, 190:227–241, 2001.

[26] S.D. Gurumayum Sharma, D. Moreton, and B. Vincent. Adsorption isotherm and atomic force microscopy studies of the interactions between polymers and surfactants on steel surfaces in hydrocarbon media. *Journal of Colloid and Interface Science*, 263:343–349, 2003.

[27] H. Bahaj, M. Bakass, C. Bayane, J. P. Bellat, M. Benchanaa, and G. Bertrand. Modeling of water vapor adsorption isotherms onto polyacrylic polymer. *Journal of Thermal Analysis and Calorimetry*, 103:117–123, 2011.

[28] O. Rodríguez, F. Fornasiero, A. Arce, C.J. Radke, and J.M. Prausnitz. Solubilities and diffusivities of water vapor in poly(methylmethacrylate), poly(2-hydroxyethylmethacrylate), poly(N-vinyl-2-pyrrolidone) and poly(acrylonitrile). *Polymer*, 44:6323–6333, 2003.

[29] N. Dolmaire, E. Espuche, F. Mechin, and J.-P. Pascault. Water transport properties of thermoplastic polyurethane films. *Journal of Polymer Science Part B: Polymer Physics*, 42:473–492, 2004.

[30] L. Perrin, Q.T. Nguyen, D. Sacco, and P. Lochon. Experimental Studies and Modelling of Sorption and Diffusion of Water and Alcohols in Cellulose Acetate. *Polymer International*, 42:9–16, 1997.

[31] J. Crank. chapter 1. Oxford: Oxford University Press, 2nd edition, 1975.

[32] J. S. Vrentas, C.M. Jarzebski, and J.L. Duda. A Deborah number for diffusion in polymer-solvent systems. *AIChE Journal*, 21:894–901, 1975.

[33] D. Vesely. Diffusion of liquids in polymers. *International Materials Reviews*, 53, 2009.

[34] N.L. Thomas and A.H. Windle. A theory of case II diffusion. *Polymer*, 23:529–542, 1982.

[35] A. Arce, F. Fornasiero, O. Rodriguez, C.J. Radke, and J.M. Prausnitz. Sorption and transport of water vapor in thin polymer films at 35°C. *Physical Chemistry Chemical Physics*, 6:103, 2004.

[36] M. Giacomelli Penon, S.J. Picken, M. Wubbenhorst, and J. van Turnhout. Vapor diffusion in porous/nonporous polymer coatings by dielectric sorption analysis. *Journal of Applied Polymer Science*, 105:1471–1479, 2007.

[37] T. Nguyen, E. Byrd, D. Bentz, and C. Lin. In situ measurement of water at the organic coating/substrate interface. *Progress in organic coatings*, 27:181.

[38] K. Wapner and G. Grundmeier. Spatially resolved measurements of the diffusion of water in a model adhesive/silicon lap joint using FTIR-transmission-microscopy. *International Journal of Adhesion and Adhesives*, 24:193–200, 2004.

[39] K. Wapner, M. Stratmann, and G. Grundmeier. In situ infrared spectroscopic and scanning Kelvin probe measurements of water and ion transport at polymer/metal interfaces. *Electrochimica Acta*, 51:3303–3315, 2006.

[40] P. Bosch, A. Fernandez, E.F. Salvador, T. Corrales, F. Catalina, and C. Peinado. Polyurethane-acrylate based films as humidity sensors. *Polymer*, 46:12200–12209, 2005.

[41] P.R. Laity, P.M. Glover, J. Godward, P.J. Mcdonald, and J.N. Hay. Structural studies and diffusion measurements of water-swollen cellophane by NMR. *Cellulose*, page 227.

[42] Wei Wang, Ying Jin, and Zhaohui Su. Spectroscopic study on water diffusion in poly(ester urethane) block copolymer matrix. *The Journal of Physical Chemistry. B*, 113:15742–15746, 2009.

[43] P.M. Glover, P.S. Aptaker, J.R. Bowler, E. Ciampi, and P.J. McDonald. A novel high-gradient permanent magnet for the profiling of planar films and coatings. *Journal of Magnetic Resonance*, 139:90–97, 1999.

[44] J.P. Gorce, D. Bovey, P.J. Mcdonald, P. Palasz, D. Taylor, and J.L. Keddie. Vertical water distribution during the drying of polymer films cast from aqueous emulsions. *The European physical journal. E, Soft matter*, 8:421–9, 2002.

[45] G. Bennett, J.P. Gorce, J.L. Keddie, P.J. Mcdonald, and H. Berglind. Magnetic resonance profiling studies of the drying of film-forming aqueous dispersions and glue layers. *Magnetic Resonance Imaging*, 21:235–241, 2003.

[46] J. Mallégol, G. Bennett, P.J. Mcdonald, J.L. Keddie, and O. Dupont. Skin Development during the Film Formation of Waterborne Acrylic Pressure-Sensitive Adhesives Containing Tackifying Resin. *The Journal of Adhesion*, 82:217–238, 2006.

[47] S. J. F. Erich, O. C. G. Adan, L. Pel, H. P. Huinink, and K. Kopinga. NMR Imaging of Coatings on Porous Substrates. *Chemistry of Materials*, 18:4500–4504, 2006.

[48] S.J.F. Erich, J. Laven, L. Pel, H.P. Huinink, and K. Kopinga. Dynamics of cross linking fronts in alkyd coatings. *Applied Physics Letters*, 86:134105, 2005.

[49] A.C. Hellgren, M Wallin, P. K. Weissenborn, Peter J. Mcdonald, P. M. Glover, and J.L. Keddie. New techniques for determining the extent of crosslinking in coatings. *Progress in organic coatings*, 43:85–98, 2001.

[50] Charles P. Slichter. *Principles of magnetic resonance*. Berlin : Springer, 3rd enl. and upd. ed. edition, 1990.

[51] F. Bloch, W.W. Hansen, and M. Packard. The nuclear induction experiment. *Physical Review*, 70:474–485, 1946.

[52] G. Eidmann, R. Savelsberg, P. Blumler, and B. Blumich. The NMR MOUSE, a mobile universal surface explorer. *Journal of Magnetic Resonance*, 122:104–109, 1996.

[53] P.J. Mcdonald. Stray field magnetic resonance imaging. *Progress in Nuclear Magnetic Resonance Spectroscopy*, 30:69–99, 1997.

[54] E.D. Ostroff and J.S. Waugh. Multiple spin echoes and spin locking in solids. *Physical Review Letters*, 16:1097.

[55] J.L. Markley, W.J. Horsley, and M.P. Klein. Spin-Lattice Relaxation Measurements in Slowly Relaxing Complex Spectra. *The Journal of Chemical Physics*, 55:3604, 1971.

[56] G. Mcdonald and J. Leigh. A new method for measuring longitudinal relaxation times. *Journal of Magnetic Resonance*, 9:358–362, 1973.

[57] W. Grunder, H. Schmiedel, and D. Freude. Eine neue Methode zur Messung von Korrelationszeiten mit Hilfe von NMR-Impulsverfahren. *Annalen der Physik*, 482:409–416, 1972.

[58] R. Kimmich and N. Fatkullin. Polymer chain dynamics and NMR. *NMR. 3D Analysis. Photopolymerization*, 170:1–113, 2004.

[59] P. Sotta, C. Fülber, D.E. Demco, B. Blümich, and H.W. Spiess. Effect of Residual Dipolar Interactions on the NMR Relaxation in Cross-Linked Elastomers. *Macromolecules*, 29:6222–6230, 1996.

[60] H.Y. Carr and E.M. Purcell. Effects of diffusion on free precession in nuclear magnetic resonance experiments. *Physical Review*, 94, 1954.

[61] M.D. Hürlimann. Diffusion and relaxation effects in general stray field NMR experiments. *Journal of magnetic resonance*, 148:367–78, 2001.

[62] J.H. Van Vleck. The dipolar broadening of magnetic resonance lines in crystals. *Phys. Rev Phys Rev*, 74:1168, 1948.

[63] J. Moos, J. van Diemen, and G. Broekroelofs. Aqueous coating composition comprising an addition polymer and a polyurethane, July Application Patent WO 01/48106 A1, 2001.

[64] K. Nachtkamp, J. Mosbach, K. Noll, H.G. Schmitz, and A. Sickert. Aqueous coating compositions containing water dispersible polyurethane polyureas as binders and the coatings produced therefrom, August US Patent 5141987, 1992.

[65] K. Kopinga and L. Pel. One-dimensional scanning of moisture in porous materials with NMR. *Review of Scientific Instruments*, 65:3673–3681, 1994.

[66] S. Popineau, C. Rondeau-Mouro, C. Sulpice-Gaillet, and M.E.R. Shanahan. Free/bound water absorption in an epoxy adhesive. *Polymer*, 46:10733–10740, 2005.

[67] D. W. Drew, A. S. Clough, P. M. Jenneson, T. E. Shearmur, M. G. D. van der Grinten, and P. Riggs. Water diffusion at short times in hydrophilic polymer studied by an ion beam analysis technique. *Nuclear Instruments and Methods in Physics Research Section B: Beam Interactions with Materials and Atoms*, 119:429–432, 1996.

[68] L. Venkataramanan, Y.Q Song, and M.D. Hurlimann. Solving Fredholm integrals of the first kind with tensor product structure in 2 and 2.5 dimensions. *IEEE Transactions on Signal Processing*, 50:1017–1026, 2002.

[69] L. Ninni. Water activity in poly(ethylene glycol) aqueous solutions. *Thermochimica Acta*, 328:169–176, 1999.

[70] H.R. Pruppacher. Self-Diffusion Coefficient of Supercooled Water. *The Journal of Chemical Physics*, 56:101–107, 1972.

[71] J.R. Zimmerman and W.E. Brittin. Nuclear magnetic resonance studies in multiple phase systems: lifetime of a water molecule in an adsorbing phase on silica gel. *J. Phys. Chem.*, 61:1328–1333, 1957.

[72] Hao Ju, A.C. Sagle, B.D. Freeman, J.I. Mardel, and A.J. Hill. Characterization of sodium chloride and water transport in crosslinked poly(ethylene oxide) hydrogels. *Journal of Membrane Science*, 358:131–141, 2010.

[73] P. Atkins and J. De Paula. *Atkins' Physical Chemistry*, chapter 5. W. H. Freeman, 8 edition, 2006.

[74] L.G.J. van der Ven, R.T.M. Leijzer, K.J. van Den Berg, P. Ganguli, and R. Lagendijk. Interactions between basecoats and clearcoats in car refinish systems. *Progress in Organic Coatings*, 58:117–121, 2007.

[75] Ernesto O. Timmermann. A B. E. T.-like three sorption stage isotherm. *Journal of the Chemical Society, Faraday Transactions 1*, 85:1631, 1989.

[76] M. Monleón Pradas, M. Salmerón Sánchez, G. Gallego Ferrer, and J.L. Gómez Ribelles. Thermodynamics and statistical mechanics of multilayer adsorption. *The Journal of chemical physics*, 121:8524–31, 2004.

[77] C. Pérez-Alonso, C.I. Beristain, C. Lobato-Calleros, M.E. Rodríguez-Huezo, and E.J. Vernon-Carter. Thermodynamic analysis of the sorption isotherms of pure and blended carbohydrate polymers. *Journal of Food Engineering*, 77:753–760, 2006.

[78] H. Feng. Modeling of vapor sorption in glassy polymers using a new dual mode sorption model based on multilayer sorption theory. *Polymer*, 48:2988–3002, 2007.

[79] D. Kockott. Natural and artificial weathering of polymers. *Polymer Degradation and Stability*, 25:181–208, 1989.

[80] L.F.E. Jacques. Accelerated and outdoor/natural exposure testing of coatings. *Progress in polymer science*, 25:1337–1362, 2000.

[81] C. Carfagna, P. Mastronardi, and L. Nicolais. Hygrothermal ageing of epoxy based coatings. *Journal of Materials Science*, 17:2239–2244, 1982.

[82] J.W. Martin, T. Nguyen, E. Byrd, B. Dickens, and N. Embree. Relating laboratory and outdoor exposures of acrylic melamine coatings:: I. Cumulative damage model and laboratory exposure apparatus. *Polymer degradation and stability*, 75:193–210, 2002.

[83] T. Nguyen, J.W. Martin, E. Byrd, and N. Embree. Relating laboratory and outdoor exposure of coatings: II. *Journal of Coatings Technology*, 74:65–80, 2002.

[84] T. Nguyen, J.W. Martin, E. Byrd, and N. Embree. Relating laboratory and outdoor exposure of coatings III . Effect of relative humidity on moisture-enhanced photolysis of acrylic-melamine coatings. *Polymer Degradation and Stability*, 77:1–16, 2002.

[85] T. Nguyen, J. Martin, and E. Byrd. Relating laboratory and outdoor exposure of coatings: IV. Mode and mechanism for hydrolytic degradation of acrylic-melamine coatings exposed to water vapor in the. *Journal of Coatings Technology*, 75, 2003.

[86] S.H. Hamid and M.B. Amin. Lifetime prediction of polymers. *Journal of applied polymer science*, 55:1385–1394, 1995.

[87] E. Mathieu and J.L. Laurent. Comparison of two instruments for accelerated weathering tests on plasticized PVC. *Polymer degradation and stability*, 51:77–81, 1996.

[88] X. Shi, B.R. Hinderliter, and S.G. Croll. Environmental and time dependence of moisture transportation in an epoxy coating and its significance for accelerated weathering. *Journal of Coatings Technology and Research*, 7:419–430, August 2009.

[89] D.J. Swanberg. Water-Reducible Polyurethane Enamels: Candidate Low VOC Aerospace Topcoat Formulations. *SOLVENT SUBSTITUTION*, page 229, 1990.

[90] M. Buggy and K. O'Byrne. Effects of skydrol (a hydraulic fluid) on the network structure of TGDDM/DDS-based resins. *Journal of Applied Polymer Science*, 65:2025–2030, 1997.

[91] E. M. Gutman, a. Grinberg, E.A. Ribak, and I. Petronius. Environmental effects on the static strength and stress relaxation of a quartz fabric-reinforced, cyanate resin-matrix composite. *Polymer Composites*, 18:561–565, 1997.

[92] G. Sala. Composite degradation due to fluid absorption. *Composites Part B: Engineering*, 31:357–373, 2000.

[93] J. Crank and G.S. Park. Diffusion in high polymers: some anomalies and their significance. *Transactions of the Faraday Society*, 47:1072–1084, 1951.

[94] J. S. Vrentas and C. M. Vrentas. Viscoelastic diffusion. *Journal of Polymer Science Part B: Polymer Physics*, 39:1529–1547, 2001.

[95] S Turner. *Physics of Glassy Polymers*. Applied Science Publishers, London, 1973.

[96] R.N. Ogorkiewicz. *Engineering Properties of Thermoplastics*. Wiley, London, 1970.

[97] A.F. Ismail and W. Lorna. Penetrant-induced plasticization phenomenon in glassy polymers for gas separation membrane. *Separation and purification technology*, 27:173–194, 2002.

[98] J. Godward, E. Ciampi, M. Cifelli, and P.J. McDonald. Multidimensional imaging using combined stray field and pulsed gradients. *Journal of magnetic resonance*, 155:92–99, 2002.

[99] F. Casanova and B. Blümich. Two-dimensional imaging with a single-sided NMR probe. *Journal of Magnetic Resonance*, 163:38–45, 2003.

[100] K. Derrien and P. Gilormini. The effect of moisture-induced swelling on the absorption capacity of transversely isotropic elastic polymermatrix composites. *International Journal of Solids and Structures*, 46:1547–1553, 2009.

[101] A.L. Volynskii, I.A. Barvinskii, L.I. Lopatina, A.V. Volkov, and N.F. Bakeyev. Features of the sorption properties of polymer-polymer composites obtained by polymerization of methylmethacrylate in the isotactic polypropylene matrix. *Polymer Science*, 29:1518–1525, 1987.

[102] J. Van Bokhoven. A method to measure the net heat of adsorption and the adsorption isotherm simultaneously. *Thermochimica Acta*, 34:109–126, 1979.

Summary

Coatings form the interface between structures and the environment in many application domains. They play a crucial role in providing protection, e.g. against corrosion, they form a barrier against an aggressive environment and they create the aesthetic appearance. To fulfill such functionalities, coatings are often composed of multiple layers, wherein each layer is designed to add a specific feature to the coating. The top coat serves as a barrier, whereas a base coat provides color and primers secure a good adhesion and corrosion protection. Nowadays, it is common that most objects are protected and decorated by coatings.

Water penetration often forms a key factor in deterioration of a coating and its substrate. For example, water penetration may contribute to blister formation, leeching of water soluble components, hygroscopic stresses or freeze-thaw damages. Furthermore, water may act as a solvent or an electrolyte carrier, and may promote biodegradation. Consequently, a profound understanding of water penetration into (multilayer) coatings lays the foundation for improved product durability. Such a fundamental approach includes water penetration kinetics, water induced structural changes in coatings and clarification of the state of water in coatings.

Most of the published studies are devoted to single layer coatings and only little is known about the water penetration in multilayer systems. Investigation of water transport in multilayer systems requires experimental techniques that measure transient water distributions and evaluate water-polymer interactions. The only technique combining these features is high resolution NMR (nuclear magnetic resonance) imaging.

This thesis presents a study into water transport in multilayer coatings. This investigation was performed in two ways: experimentally with high resolution NMR imaging, combined with relaxometry and theoretically with an introduction and verification of a model for water transport.

The thesis starts with an overview of knowledge about water in coatings in Chapter 2. This chapter focuses on water in polymers, since in organic coatings water mainly permeates in polymeric binder. The relation between the state of water in the polymer matrix and equilibrium sorption is addressed and the mechanisms of water transport kinetics are discussed.

Further, the thesis proceeds with a description of NMR principles in Chapter 3. It discusses the NMR basics, principles of imaging and how information about molecular

motions of the measured species is present in the NMR signal.

The key results of the study are presented in the Chapters 4-8.

First, water uptake was studied in two-layer systems consisting of hydrophilic base coats and hydrophobic top coats. The base coat consisted of acrylic, polyurethane and pigment particles and the formulation included a polymeric pigment dispersant.

Chapter 4 presents the results of visualization of water transport in the two-layered systems on the basis of high resolution NMR imaging. The water transport rate in the studied systems appeared to be barrier limited. Mainly the base coat absorbed water, where it quickly redistributed. The swelling of the base coat showed to be linearly related with the absorbed water quantity.

Further, Chapter 5 presents the results of a relaxation analysis of the NMR signal, which was introduced to identify water and polymeric phases in the base coat. Polymeric dispersant plasticization was observed. This polymeric dispersant appeared to be a major contributor to the water uptake capacity of the base coat. It was found with NMR diffusometry that high water mobility occurred under saturated conditions, whereas in partially saturated systems water mobility decreased and bonding to the polymer played a key role.

In Chapter 6 a theoretical model was formulated for the transport in multilayer coatings, composed of a hydrophobic top coat and a hydrophilic base coat. This model basically assumed instantaneous equilibration of water in the base coat and Fickian water transport in the top coat. According to the model, the sorption isotherm of the base coat is the driving force of the process and the top coat permeability to water determines the timescale of transport. The asymmetry of the observed uptake/drying rates appeared to be due to the non-linear sorption isotherm of the base coat. Furthermore, top coats applied on base coats showed a higher permeability than free films and water uptake capacities of base coats decreased, when thicker top coats were applied. The ability of the model to predict water transport using the base coat sorption isotherm and the top coat permeability was validated experimentally. ***Practically, it is sufficient to measure the base coat sorption isotherm and the top coat permeability to understand water transport. This enables design of a simple and efficient procedure to test water resistance of this type of coatings. Such procedure will include only basic and cost-efficient equipment, like balances for gravimetric measurements of sorption isotherms and permeability.***

In the next step, the model was used for a theoretical investigation of the response of multilayer coatings to relative humidity fluctuations, which is presented in Chapter 7. The theoretical investigation showed that in most of the considered systems the response time is in the order of days for high humidities and has values of a few hours at low humidities. The response time is determined by the product of the timescale of penetration through the top coat and the differential solubility of the base coat. This means that most two-layer polymeric base coat/top coat systems with hydrophilic base coats are relatively inert to most humidity fluctuations, as the response in terms of water content will be damped. As accelerated and artificial weathering tests include only humidity fluctuations with typical

timescales less than a day, this raises concerns if these tests can be compared to natural moisture exposure. Finally, the thesis addresses migration of plasticizer into a top coat. It was found that stress relaxation results in non-Fickian kinetics of the uptake process. The plasticizer, which is tributyl phosphate, causes a steep increase in the permeability of the film and may cause degradation of mechanical properties of the coating. This implies that, practically, that tributyl phosphate (the main component of common aerospace hydraulic fluids) makes multilayer protective coatings more permeable and causes significant stresses in the system.

List of publications

- V. Baukh, H.P. Huinink, O.C.G. Adan, S.J.F. Erich, and L.G.J. van der Ven. NMR Imaging of Water Uptake in Multilayer Polymeric Films: Stressing the Role of Mechanical Stress. *Macromolecules*, 43:3882-3889, 2010.

- V. Baukh, H.P. Huinink, O.C.G. Adan, S.J.F. Erich, and L.G.J. van der Ven. Water-Polymer Interaction during Water Uptake. *Macromolecules*, 44:4863-4871, 2011.

- H. Zhu, H.P. Huinink, S.J.F. Erich, V. Baukh, O.C.G. Adan, K. Kopinga. High spatial resolution NMR imaging of polymer layers on metallic substrates. *Journal of Magnetic Resonance, 214:227–236*

- V. Baukh, H.P. Huinink, O.C.G. Adan, S.J.F. Erich and L. van der Ven. Predicting Water Transport in Multilayer Coatings
  submitted to *Macromolecules*

- V. Baukh, H.P. Huinink, O.C.G. Adan, S.J.F. Erich and L. van der Ven. Influence of Water Activity Fluctuations on Multilayer Coatings
  in preparation

- V. Baukh, H.P. Huinink, O.C.G. Adan, S.J.F. Erich and L. van der Ven. Plasticizer in Top Coats: Influence of Stress Relaxation on Transport
  in preparation

Dankwoord

Tackling the challenges related to this PhD project has required significant collaborative efforts. First of all, I want to praise and thank the God for making these efforts successful.

Henk, thank you for your supervision. Your example has helped me to make a big step forward towards being a scientist and a better person.

Olaf, I appreciate your supervision and guidance. Each meeting with you had a huge impact on my perception of things, not only related to the work itself. Thank you.

Peter McDonald, I am grateful for your commitment as my second supervisor. Discussions with you and your feedback were very important for me.

Bart, thank you for your assistance and guidance and showing good examples. From the beginning of my PhD you became a role model for me as an innovator in science and technology.

Leo, I thank you for your contribution to my study during our meetings. Furthermore, your efforts as a representative of and contact in AkzoNobel have allowed tackling many problems I met.

Klaas, we were rarely interacting during the project, but those few interactions has really helped to reach certain milestones. I would like to express my gratitudes to you.

Leo, sometimes I dropped in your room, getting valuable advices, when I had questions. Thank you for this and your questions during my reports at Group Meetings.

I also thank my committee members, Bert de With, Hans de Wit and Manuel Monleon Pradas for devoting their time and efforts to reading and evaluating my thesis and for agreeing to participate in my defence.

Peter Geurink, thank you for your invaluable help and efforts, which helped to initiate this project, your participation in meetings and discussions and your work to promote our collaborative efforts.

Hans, your commitment and enthusiasm in helping me were always amazing. Many things would have been more difficult, if even possible to achieve, without your assistance. Thank you.

Jef, thank you for your help with electronic equipment. Furthermore, I am grateful for your always optimistic attitude - it really inspires.

I want to thank Taco Scherer and Ruud van Overbeek from AkzoNobel Automotive & Aerospace Coatings for the useful discussions and Kenny Raghosing and Fred Rous from AkzoNobel Automotive & Aerospace Coatings for samples preparation. Also I

Curriculum vitae

Viktor Baukh was born on 10th of March, 1983, in Komsomolsk on Amur, Russia. After the graduation in 2000 from Secondary School 25 in Odessa, Ukraine, he started his study in Department of Physics in Odessa National University, Ukraine. In 2005 he has obtained Master degree in theoretical physics under supervision of Alexander Zhuk. During the master studentship he was performing a theoretical study of accelerated expansion of multidimensional universe with compacticified extra dimensions. In 2007 Viktor has started a PhD project at the Eindhoven University of Technology in the group Transport in Permeable Media. The PhD project aimed to investigate a water transport phenomenon in multilayer coatings.